Top seal variability of potential CO_2 storage sites on the northern Horda Platform

Jørgen Kalaoja

Master Thesis in Geosciences

Structural Geology and Tectonics

60 Credits

Department of Geosciences

Faculty of Mathematics and Natural Sciences

University of Oslo

Spring 2023

©Jørgen Kalaoja, 2023

Top seal variability of potential CO_2 storage sites on the northern Horda Platform

Supervisors: Alvar Braathen and Rikke Bruhn

This work is published digitally through DUO – Digitale Utgivelser ved UiO

http://www.duo.uio.no/

Printed: Reprosentralen, Universitet i Oslo

Acknowledgements

I would like to thank Alvar Braathen (Main Supervisor) and Rikke Bruhn (Co-supervisor) for their guidance and insight throughout my project. Their thorough help and motivation during my final year at the institute have been a blessing and have kept me motivated to consistently work on this project.

I would like to thank the people at Midgard for their constructive feedback and informal discussions at Bifrost this final semester. I would also like to thank CGG for granting me the opportunity to work with their seismic data and making this research possible.

My fellow B.Sc. and M.Sc. students will always have a special place in my heart. Our fun chats and social gatherings have been crucial for motivating me through these five years at GEO, and especially this final year.

Jørgen Kalaoja

Oslo, Norway, May 14th, 2023

Preface

This master's thesis (ECTS 60) is submitted to the Department of Geosciences, University of Oslo (UiO), in the candidacy for the Master of Science program Structural Geology and Tectonics (ECTS 120). The main supervisor is Professor Alvar Braathen and Associate Professor Rikke Bruhn (UiO, Nautilus).

This thesis is a contribution to the University of Oslo and the Norwegian CCS Research Center (NCCS). Seismic data is courtesy of CGG and well data are courtesy of the NPD Diskos archive and the Northern Lights project (Total E&P Norge AS, Equinor, and A/S Norske Shell). Software is courtesy of Schlumberger (Petrel E&P Software Platform).

Abstract

The concentration of CO_2 in the atmosphere is a big problem and has received much attention recently. Reducing CO_2 emissions is critical to prevent Earth from rapid global warming, and the green transition is therefore urgent. Reducing CO_2 emissions while retaining high energy production requires new and expensive technology, and a smooth transition from fossil fuels to renewable energy is needed. Carbon capture and storage (CCS) is a method to reduce emissions by capturing CO_2 from a point source, transporting it to a repository, and storing it permanently underground in geological formation. The northern Horda Platform in the northern North Sea has achieved attention as a future CO_2 storage site. The CO_2 requires storage in an aquifer with sufficient top seal to prevent the CO_2 from migration back to surface. In this study, I investigated the Middle Jurassic to Lower Cretaceous successions, which have been proposed as the potential top seal for CO_2 storage sites on the northern Horda Platform. I did this research using 3D seismic interpretation to map the top seal of the area of interest. The seismic interpretation was used to create attribute maps to observe the study area further. My results indicate a series of N-S striking thick-skinned faults and a north-westwards thinning of the top seal related to tectonic activity in the area, which occurred during deposition of the sedimentary units. I divided the Cromer Knoll Gp. into three units to analyze the sealing capacities within the group, and concluded, based on the gamma-ray values of each unit, that the sealing properties reduce upwards in the stratigraphy. I investigated how the northwards thinning of the seal affected the top seal quality, and I proposed two potential storage sites based on my research. However, there are uncertainties related to my studies based on the detail of data acquisition, the aquifer, and potential migration pathways.

Table of Contents

1 Introduction

Global warming is a problem that has received much attention in recent years and is a problem that will only increase. There are different factors behind an increase in global temperature, but the most important one is the increase of CO_2 in the atmosphere. In 2019, the CO_2 concentration was at its highest in over 2 million years, and research shows that the CO_2 concentration has increased drastically since the industrial revolution (IPCC, 2021). 193 parties of the Paris Agreement strategy for 2050 agreed to limit the increase in global temperature to 2.0 ^oC of pre-industrial revolution levels and keep the temperature increase below 1.5 ^oC of pre-industrial revolution levels (Paris Agreement, 2020). Global industrial energy consumption increased by 61% from 1990 to 2019, and according to the international energy Agency (IEA), 78.8% of the OECD energy supply in 2019 originated from coal, oil, and natural gas (IEA, 2020). Although the share of fossil fuels is decreasing, reaching the Paris Agreement goals for 2050 could prove difficult, as the target set by the Norwegian government is a reduction of greenhouse gas emissions at 90-95% compared to 1990 (Paris Agreement, 2020). There is still much work left, as Norwegian greenhouse gas emissions have only had a reduction of 4.2% from 1990 to 2020 (SSB, 2021). Changing to more renewable power generation methods will lower CO_2 emissions, although this requires revolutionary new and expensive technology. Another method is to find a way to capture and store the CO_2, thus preventing it from emitting into the atmosphere. This process is called Carbon Capture Storage (CCS).

1.1 Carbon Capture Storage

CCS consists of three phases (Fig. 1.1): 1) capture of CO2 from an industrial area, e.g., from hydrocarbon combustion, the production of cement or steel, 2) compress the gas to a liquid form and transport it to a storage site with ships and pipelines, 3) inject the liquid CO_2 deep underground under high pressure into a reservoir, (Northern Lights, 2021). The CO_2 needs a burial depth >800 m. That burial depth is to keep the CO_2 above its supercritical temperature (Fig. 1.2). At this depth, the CO_2 will stay in the liquid phase at normal surface pressure and require over 300 times less space than as a gas. (CO2CRC, 2008).

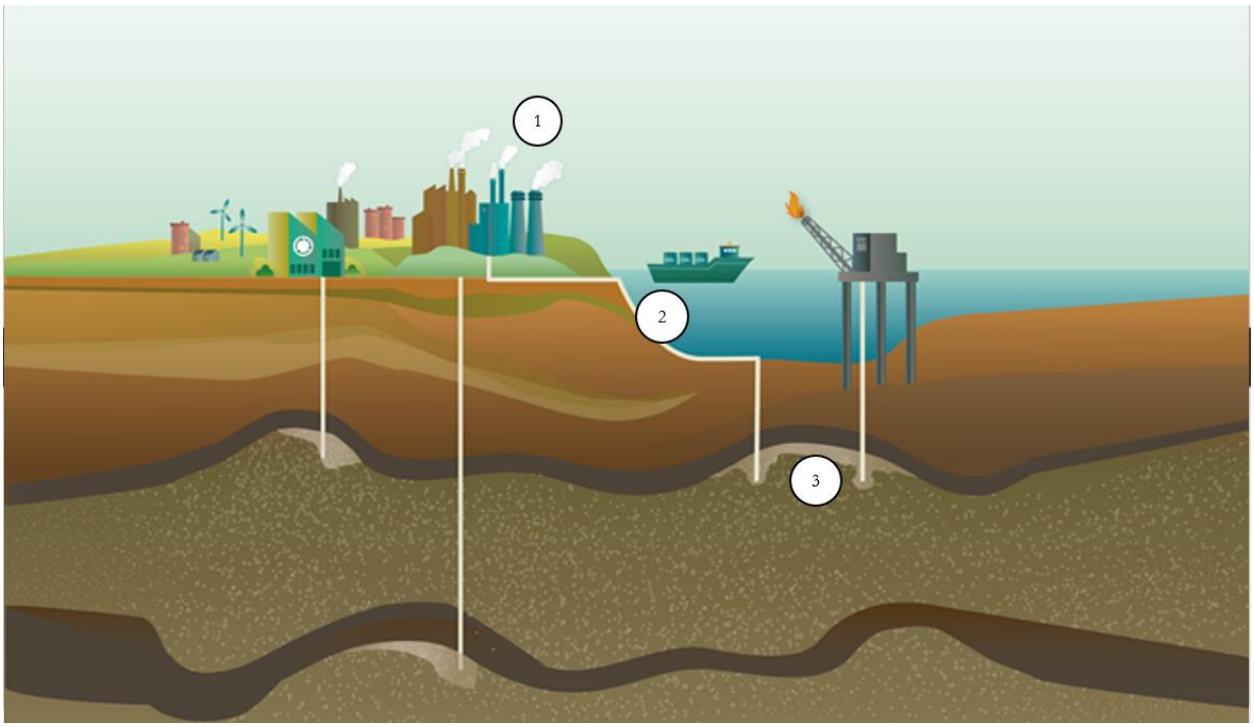

Figure 1.1: The principles of CCS: 1) Capture of CO2 from point source, 2) Transport to storage site, 3) Store the CO2 deep underground, (Geoviden 2020, GEUS).

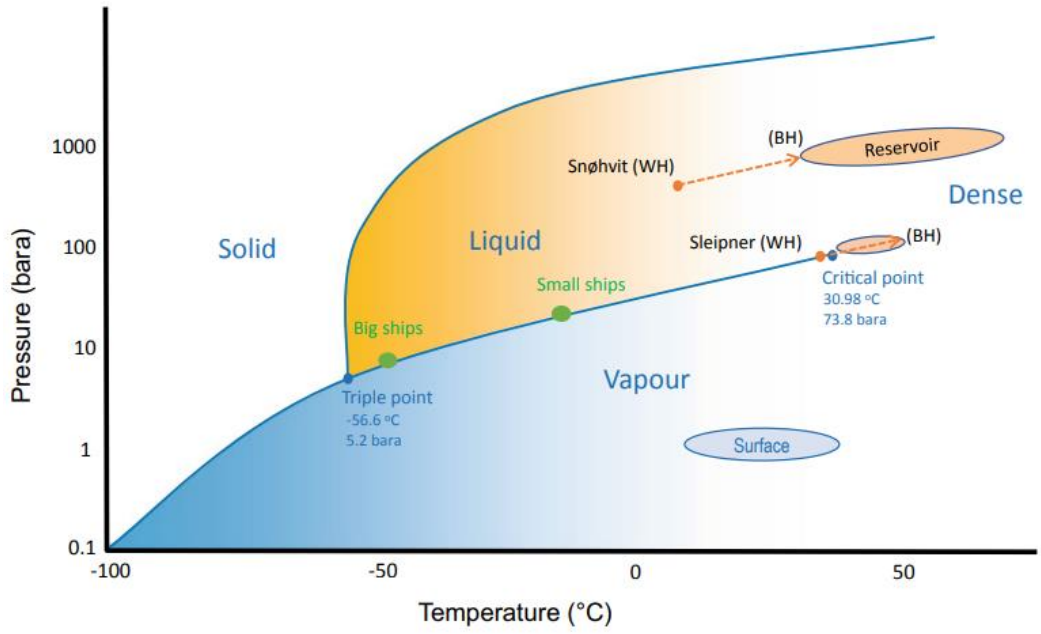

Figure 1.2: Temperature vs pressure phase diagram of CO_2. The figure also shows the temperature and pressure values of the Sleipner and Snøhvit fields (CO2CRC, 2008).

The properties of geological reservoirs for CCS are similar to those of hydrocarbon fields: a reservoir with high porosity and permeability to store the CO_2, usually sandstone or limestone. Furthermore, a low permeability cap rock prevents CO_2 from leaking, usually shale or salt

(Grunau, 1987). CO_2 migration is driven by the buoyancy of the CO_2 relative to the ambient aquifer, and good traps are needed. There are four different geological methods for CO_2 trapping (stratigraphic and structural, residual, solubility, and mineral trapping) (Fig. 1.3) (IPCC, 2005). Stratigraphic and structural trapping of CO_2 includes the cap rock, faulting, and how the seal folds (Færseth, Johnsen and Sperrevik, 2007). Different factors control the sealing capacity of a cap rock, such as the pressure applied on the weakest point of the seal, its thickness, the minimum effective stress, and the degree of overpressure. Fault-related factors controlling the seal are cataclasis (crushed grains), clay smear (clay/shale smeared into the fault plane), cementation of permeable rocks, and juxtaposition of low-permeable rocks (Watts, 1987).

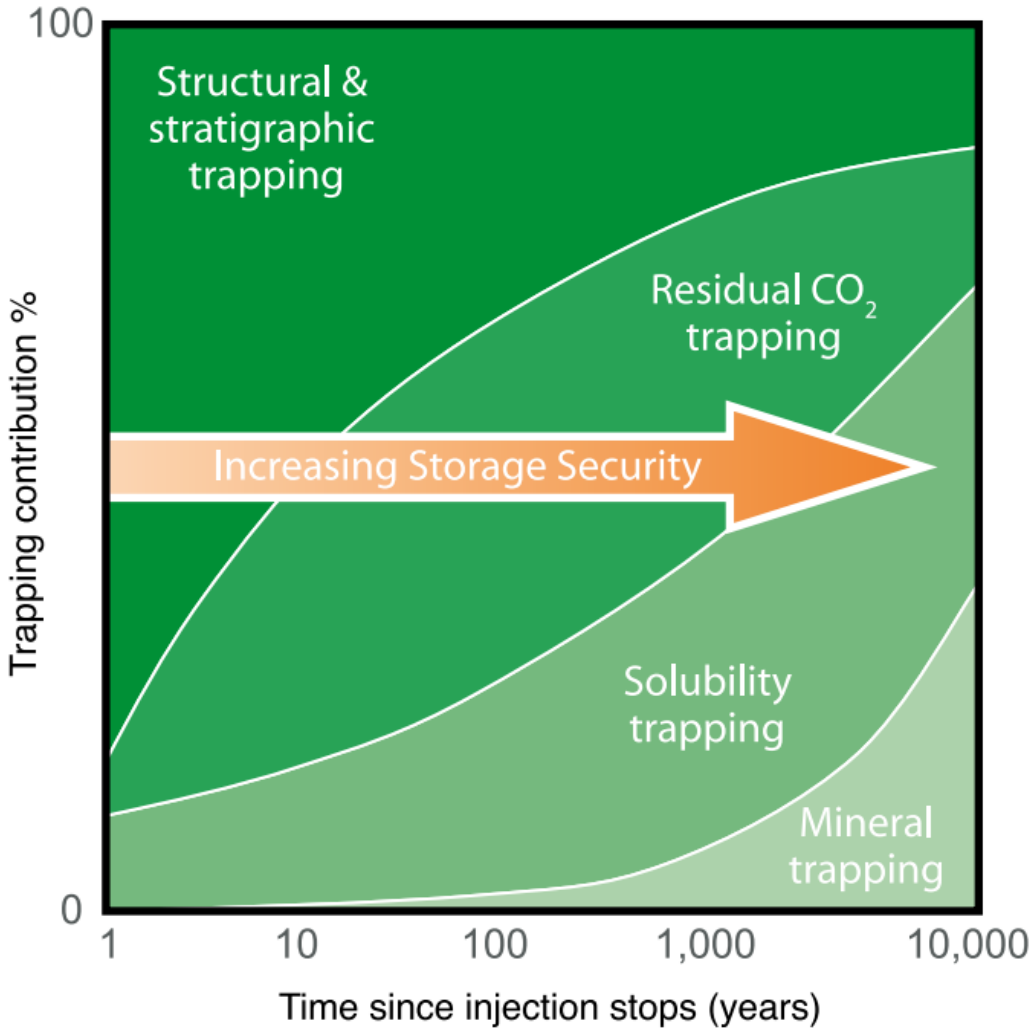

Figure 1.3: This figure shows carbon storage over time (horizontal axis) vs trapping contribution (vertical axis) with increased storage security towards the right. Structural and stratigraphic trapping are the main trapping mechanisms in the earlier stage of injection. With an increase in time residual and solubility trapping becomes more important, and after thousand(s) of years mineral trapping becomes the most permanent and secure trapping mechanism (Benson et al., 2005).

When the CO_2 migrates upwards due to buoyancy, some of the CO_2 is stuck inside the pore spaces of the reservoir, resulting in residual trapping (Bachu et al., 1994). Solubility trapping occurs when CO_2 dissolves in brine. As CO_2-saturated brine has a higher density than the brine that's not CO_2 saturated, the CO_2-saturated brine will sink to the bottom of the reservoir. Mineral trapping is considered the most permanent CO_2 trapping method. The dissolved CO_2 reacts with elements and precipitates as minerals. Mineral trapping is a slow process and is time-dependent, whether it precipitates as a carbonate (days) or a silicate (thousands of years) (Gunter et al., 1993).

Much research has been conducted on the potential use of CCS (e.g., Marchetti, 1977; Wu *et al.*, 2021…). However, it has never become common because it requires new technology with high associated risks. This has led to project shutdowns and some very high costs. The main economic driving force for CO_2 storage is carbon taxes. Carbon taxes forces emitters to pay a sum based on their greenhouse gas emissions (Durmaz, 2018). Another economic factor is the cost of CCS. The CO_2 first needs to be captured from an industrial area either onshore or from an offshore platform. This could be a long and expensive process if the CO_2 captured onshore is to be stored offshore. The CO_2 must be transported to a pier, where it will be stored temporarily before being loaded on a ship. The CO_2 will be transported to the offshore storage site by ship or pipeline from the shore. These processes are important steps in CCS which involve the cost of technology and the cost of storing the CO_2, as well as funding from investors.

Not surprisingly, the cost of renewables has an opposite economic effect on CCS than fossil fuels. If fossil fuel production costs are low, more fossil fuel will be produced, and the demand for CCS will also be higher. If renewables such as hydropower, solar, and wind cost are high. There will be a higher demand for fossil fuels as energy production. Therefore, more CCS, given that the energy is produced with CCS (Durmaz, 2018).

1.2 Background

The principles of CCS were first introduced by Marchetti in 1977. In the paper *On Geoengineering and the CO_2 Problem*, he proposed the terms of CO_2 collection, CO_2 transportation, and CO_2 disposal (Marchetti, 1977). As the climate problem became a more prominent political issue, CCS received more attention than before, which led to the initiation of the first CCS project in 1986 (Gough and Shackley, 2006).

In an attempt to reduce CO_2 emissions, Norway introduced CO_2 taxes in 1991 (Kasa, 2000). The introduction to CO_2 taxes resulted in the birth of the Sleipner CCS project in 1996, which became the first large-scale CCS project in the world. This project was initiated by Equinor and other license partners and has since the beginning captured and stored about 1 Mt CO_2 yearly. The Sleipner field is located in the North Sea, and the storage site places around 700 meters depth below the seafloor. The reservoir is sandstone with porosities of 35-40% and permeabilities above 1 Darcy. Below the CO_2 storage aquifer, there is a gas field reservoir.
Snøhvit is the second CO_2 storage site in Norway, situated in the Barents Sea, with the CO_2 storage placed at 2400 meters below the seafloor. Both reservoirs are sandstone, but Snøhvit, which places deeper, has lower porosities of 15-20% and permeabilities above 0.5 Darcy. The Snøhvit field has a thicker cap rock than Sleipner, and it also has a natural gas field located above the CO_2 storage site, (Eiken *et al.*, 2011).
In 2020, the Norwegian government proposed a large-scale CCS project called Langskip, led by a partnership of Equinor, Shell, and Total. The project predicts a cost of 25.1 billion NOK, and the Norwegian state expects to pay for 2/3 of the total cost. The Langskip project is planned to consist of two phases: Phase 1 has an expected capacity of storing 1.5 Mt CO_2 per year for 25 years. Phase 2 is expected to increase the capacity of storing 5.0 Mt CO_2 per year (Tangen *et al.*, 2021).
The Northern Horda platform has received attention as a potential storage site for the Langskip project and a future cluster for CO_2 storage sites. Research shows that due to fault juxtaposition and high clay content in the cap rock, the seal at the Northern Horda Platform represents a low risk of leakage (Wu *et al.*, 2021). Due to oil and gas production at the Troll field west of the area, an estimation of the reservoir's storage capacity is difficult because of pressure conditions (Lauritsen *et al.*, 2018). However, the reservoir has high porosity and permeability self-juxtaposition sandstones, indicating a good reservoir (Wu *et al.*, 2021). Self-juxtaposition makes the same stratigraphy appear across faults, which could lead to good CO_2 migration in the case of a reservoir rock (Urban S. Allan (2), 1989).

1.3 Aim of Thesis

My thesis aims to better understand the spatial and temporal development of the latest Jurassic to middle Cretaceous depositional systems, and the potential implications for top seal integrity at

potential future CO_2 storage sites on the northeastern Horda platform. This region contains a northward thinning of the Cromer Knoll Gp. deposited during peak rifting in the early Cretaceous, which is essential in the secondary seal of potential CO_2 storage sites. Tectonic activity and the composition of the Cromer Knoll Gp. could significantly impact its sealing capacities and should be further investigated. I hypothesize that the northwards thinning and increase in tectonic activity will reduce the sealing capacities. Based on these results, I will evaluate if the studied area on the northern Horda Platform is sufficient for CO_2 storage.

The key objectives of the project are:

1. To establish detailed seismic stratigraphy for the uppermost Jurassic and Cretaceous successions, using a continuous coverage broadband survey tied to wells with key stratigraphic information and good stratigraphic control on the Horda Platform in the outlined area of interest.
2. To interpret key horizons, with a focus on key horizons in the Upper Jurassic and Lower Cretaceous in the area of interest.
3. Map the correlation of time and lithology in selected wells to establish an understanding of the development of unconformities.
4. Interpret key faults to understand the fault development in the area.

2 Geological Setting

This chapter will cover the geological evolution of the Northern North Sea. I will first write about the North Sea's geological structures, then zoom into the more specific research locality in the Northern North Sea. I will also discuss the geological evolution of the area, starting from Pre-Permian until the Quaternary. The area has been subjected to various events of syn-rift (rift phase 1 in the Permo-Triassic and rift phase 2 in the Late Jurassic to Early Cretaceous), followed by post-rift subsidence, uplift, and erosion, which I will examine in further detail.

2.1 Structure

The Norwegian Continental Shelf (NCS) is located west of the Norwegian mainland. It comprises mainly the North Sea in the south, the Mid-Norwegian continental margin, and the Western Barents Sea (Faleide, Bjørlykke and Gabrielsen, 2015). The North Sea is an extensional sedimentary intracratonic (located on the continental crust) basin enclosed by South-Western Norway in the northeast, the United Kingdom in the west, Denmark in the southeast, and Germany, Netherlands, Belgium, and France in the south (Fig. 2.1) (e.g. Odinsen *et al.*, 2000; Faleide, Bjørlykke and Gabrielsen, 2015).

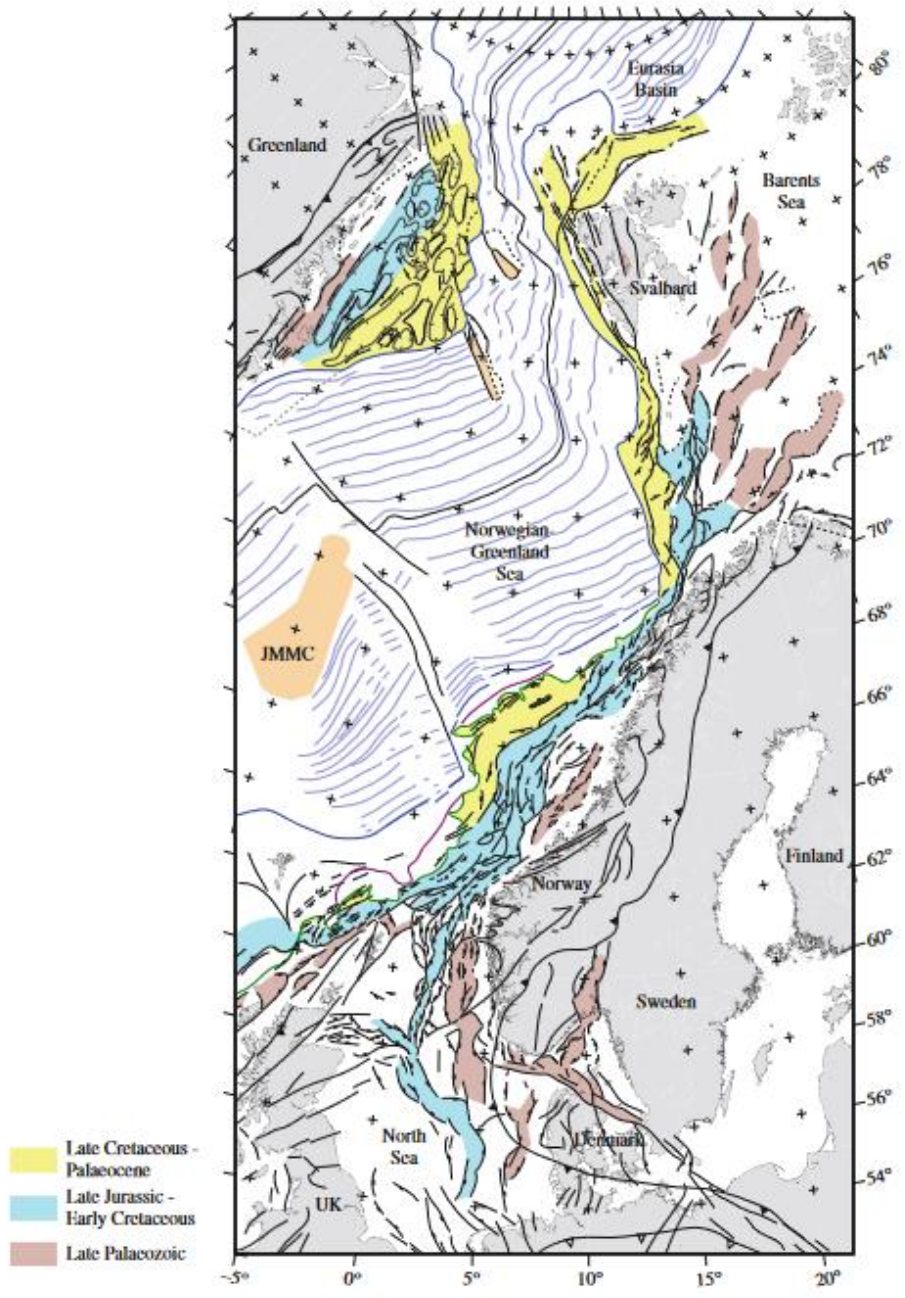

Figure 2.1: Map of the Norwegian continental shelf, which covers scope of rift phases occurring through three different Eras (Faleide, Bjørlykke and Gabrielsen, 2015).

The main structural element in the North Sea is the Jurassic triple rift system, comprising the Viking Graben, the Central Graben, and the Moray Firth Basin (Færseth, 1996). Research suggests an extensional dip-slip movement of faulting in the E-W direction and that it occurred in three phases. The N-S striking faults developed in the Late Bathonian to Early Callovian, the NE-SW

striking faults developed in the Oxfordian, and the NW-SE extensional faults developed in Kimmeridgian to Tithonian (Davies, Turner and Underhill, 2001). The main structures of the northern North Sea comprise from west to east of the East Shetland Platform, East Shetland Basin, Viking Graben, Horda Platform, and the Øygarden Fault Complex (Whipp *et al.*, 2014). s

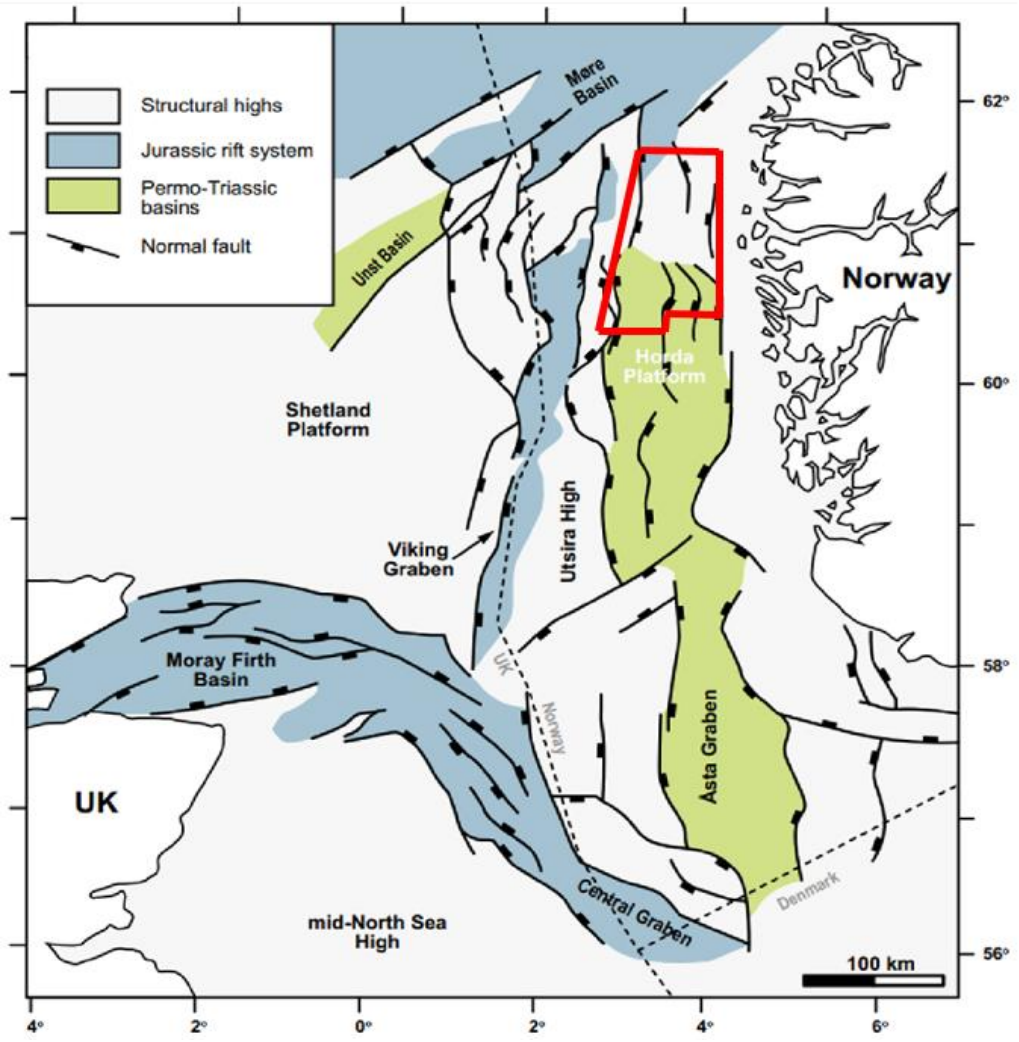

Figure 2.2: Map of the northern North Sea and its main structures with the research area marked by the red polygon (Modified from: Whipp et al., 2014).

The Horda Platform is located in the eastern part of the North Sea (Fig. 2.2). The Horda Platform bounds between the Viking Graben to the west and Øygarden Fault Complex to the east and is located at approximately 60° N. The structural high is ca. 300 km long, 50 km wide and consists of mainly N-S trending structures (e.g. Færseth, 1996; Whipp *et al.*, 2014; Duffy *et al.*, 2015). The main fault systems at the Horda Platform are the Troll Fault System, Svartalv Fault System,

Tusse Fault System, Vette Fault System, and the Øygarden Fault Complex (Fig. 2.3). These fault systems are N-S trending and were active during rift phase 1 (Permo – Triassic) and 2 (Late Jurassic – Early Cretaceous). At the northern Horda Platform, the N-S striking faults are more than 60 km long, have a throw of up to 5 km, and a dipping angle of around 40° (e.g. Færseth, 1996; Bell *et al.*, 2014; Whipp *et al.*, 2014). The N-S striking faults are thick-skinned, which means they involve displacement of the basement and have a 6 – 15 km spacing. The faulting has created some easterly dipping fault blocks (Vette, Tusse, Svartalv, and Troll). Up to 3 km of Permo-Triassic sediments fill these half-grabens (Badley *et al.*, 1988; Færseth, 1996).

Between the N-S faults are some NW-SE striking faults. These faults are smaller, less than 10 km long, less than 100 m of throw, and more closely spaced. These NW-SE striking faults are thin-skinned, which means they do not involve the basement and are restricted to post-Triassic successions (Whipp *et al.*, 2014).

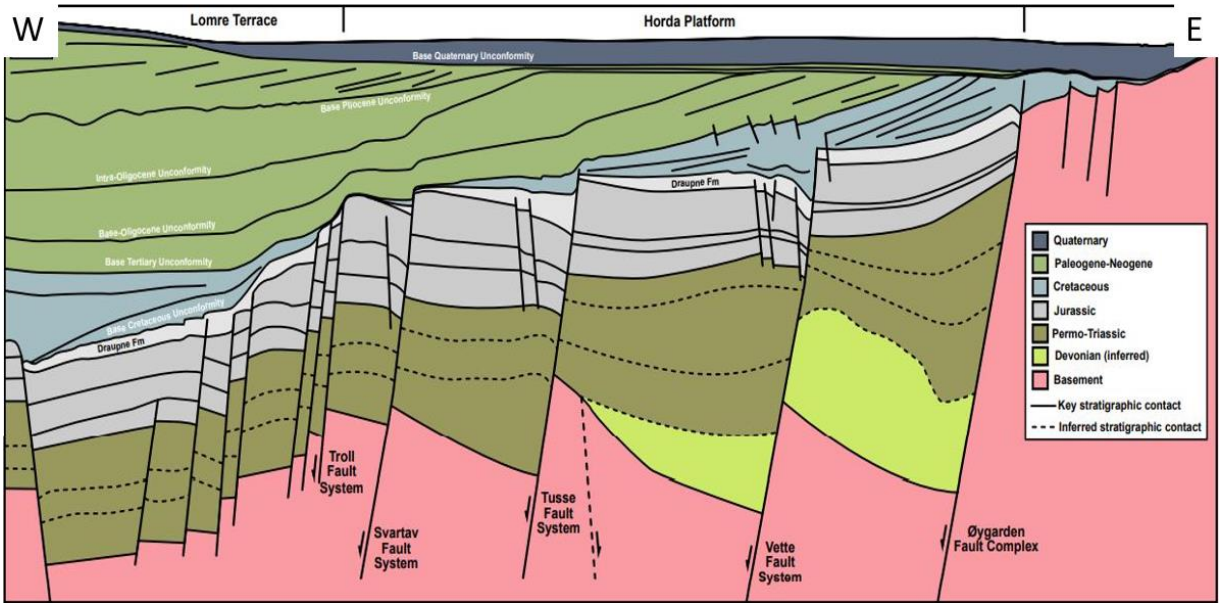

Figure 2.3: A cross section from W-E of the Horda Platform showing the successions and main structural features. (Modified from: Whipp et al., 2014).

2.2 Geological Evolution

2.2.1 Pre-Permian

The first stage in the tectonic development of the North Sea was the closing of the Iapetus Ocean, which led to the collision of Laurentia and Baltica (P. A. Ziegler (2), 1975). This closing

governed the development of the Caledonian orogeny during Middle Silurian at approximately 430 Ma (Corfu, Andersen and Gasser, 2014). The structure of the Caledonian orogeny comprised of thin-skinned thrust sheets in the foreland to the east (Baltica), and more thick-skinned tectonics towards the hinterland in western Norway. These allochthonous nappes divides into Lower- and Middle allochthon (continental origin) and Upper allochthon (oceanic origin). The Lower- and Middle allochthon are situated in the foreland, and the Upper allochthon is in the hinterland (Milnes *et al.*, 1997; Fazlikhani *et al.*, 2017).

The orogenic uplift was followed by extensional shear zones in the weak décollement and a reactivation of the thrust sheets. The extension occurred in two stages. The first mode (Mode I) of extension defines the reactivation of the Caledonian nappes with low-angle extensional shearing. The second mode (Mode II) defines the introduction of the Baltic Shield in extension, which means the shearing cuts through the weak décollement (Fossen, 1992).

The collapse led to the deposition of the Old Red Sandstone, which can be found in the Devonian basins in western Norway. These basins are filled with conglomerates (Seranne and Seguret, 1987). The Devonian basins include Hornelen, Hasteinen, Kamshesten, and Solund.
The conglomerates have later been metamorphosed and lost their porosity and permeability. The sediments have been detected in some wells in the northern North Sea, and are most likely present under the East Shetland Basin, the Viking Graben and the Horda Platform (Faleide, Bjørlykke and Gabrielsen, 2015). Large listric normal faults structurally characterize these, and the sediments preserve in half-grabens (Fazlikhani *et al.*, 2017). The climate became drier during the Carboniferous because the Northern North Sea was at the equator at the time (Faleide, Bjørlykke and Gabrielsen, 2015).

2.2.2 Permian – Triassic (Syn-rift 1)

The Northern North Sea moved further north during the Permian. This led to the Northern North Sea becoming more arid (Faleide, Bjørlykke and Gabrielsen, 2015).
Extensional rifting in the Northern North Sea divides into two rifting phases. Rift phase 1 was initiated during the Permo – Triassic (Fig. 2.4) due to the breaking-up of Pangea (Færseth, 1996; Wu *et al.*, 2021). The rifting occurred in the Late Permian – Early Triassic and lasted about 25

Myr (Ter Voorde et al., 2000). The rifting phase occurred in the E – W direction, which led to the development of N – S striking normal faults. These faults had a throw of 3 – 5 km and generally had a westward dip on the Horda Platform, which bound easterly rotated fault blocks (Færseth, 1996; Duffy *et al.*, 2015).

The crustal thickness of the northern North Sea during Pre-Permian is estimated to have been approximately 36 km, which has been estimated by using the crustal thickness of today's western Norway as a proxy. The extension has forced a thinning of the crust towards the west of western Norway. Below the Viking Graben the thickness is expected to be between 21-24 km below the axis of the Viking Graben (Christiansson, Faleide and Berge, 2000).

The climate in the Northern North Sea stayed arid during the Triassic, which led to new continental sandstone deposits called the New Red Sandstone (Similar to the Old Red Sandstone) (Faleide, Bjørlykke and Gabrielsen, 2015).

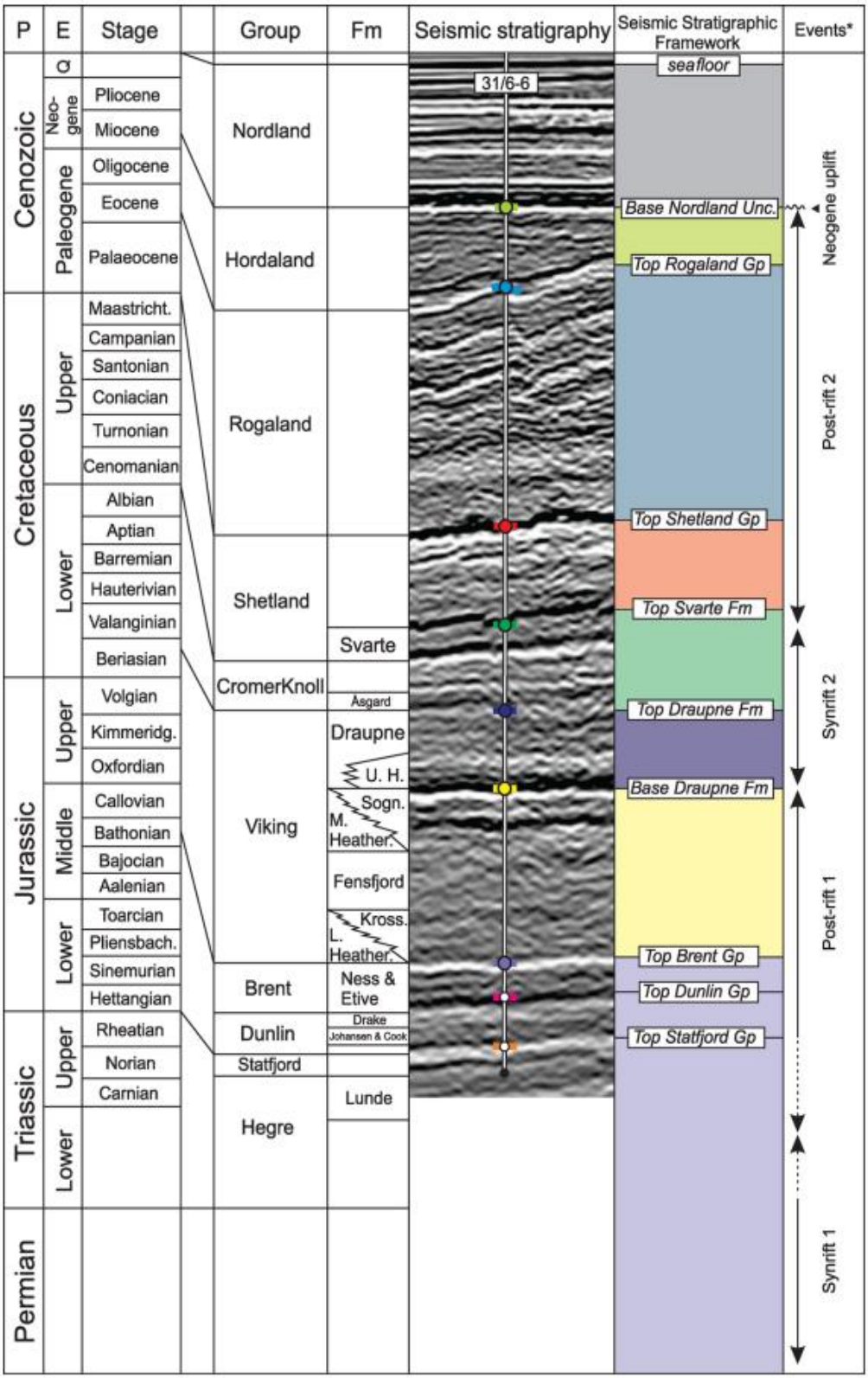

Figure 2.4: Geological time scale plotted with important lithostratigraphy on the Horda Platform. The figure includes a seismic section from the 31/6-6 well located in the Troll East field with key horizons (Wu et al., 2021).

2.2.3 Triassic – Jurassic (Post-rift 1)

Rift phase 1 was followed by a period of tectonic quiescence and thermal subsidence (e.g. Badley *et al.*, 1988; Roberts *et al.*, 1993; Duffy *et al.*, 2015). There was a high amount of sediment supply during the post-rift phase, which some places kept up with the subsidence rates. Combined with an uplift of Scandinavia, these factors were prominent in forming the basin geometry during the post-rift. The amount of sediment supply was crucial and lead to an alluvial to deltaic depositional environment rather than marine (Faleide, Bjørlykke and Gabrielsen, 2015).

The Statfjord Formation, Dunlin group, and Brent group were deposited during the post-rift thermal subsidence after Rift phase 1 (Fig. 2.4) (Helland-Hansen *et al.*, 1992). From Triassic to the Jurassic, the depositional environment changed from continental to shallow-marine. The climate also became more humid as the North Sea moved northwards towards a more humid climate zone (Faleide, Bjørlykke and Gabrielsen, 2015).

The Statfjord Formation overlays the Hegre Group (Which consists of the Teist-, Lomvi- and Lunde formations from bottom to top). The formation consists mainly of poorly sorted medium- to very coarse channel-fill sandstone bodies. It contains a 22 m thick sandstone succession with interbedded mudstones up to 12 m thick (Morton and Hurst, 1995). The mudstones are floodplain deposits that are grey to red in color (Høimyr, Kleppe and Nystuen, 1993).

The Dunlin Group consists of the Johansen, Amundsen, Burton, Cook, and Drake formations (Tihomir Marjanac and Ronald J. Steel, 1997), and it marks a change in depositional environment from alluvial (Statfjord Fm.) to deep marine (Amundsen Fm.) (Chamock *et al.*, 2001). The Johansen Fm. consists of fine-grained sandstones to siltstones in grain size. It results from an E-W prograding delta, which later changed deposition to the N-S direction (Sundal *et al.*, 2016). The formation has been considered a good reservoir for CO_2 storage and is therefore set to be used as the storage site for the Eos injection well in the Northern Lights project. Later, the area experienced a rising sea level, which gave birth to the Amundsen and Burton formations. The sea level rise reduced sediments' grain size and led to shale deposition.

Further up in the stratigraphy, the Cook Fm. is considered an estuarine sandstone deposit (Tihomir Marjanac and Ronald J. Steel, 1997). *Estuaries* are defined as a basin with a partial connection to the sea, as it is simultaneously filled with fresh water from a river (Pritchard, 1967). The Drake Fm. covers the Dunlin group at the top, these shales are deposited in a high-stand environment (Tihomir Marjanac and Ronald J. Steel, 1997). The thickness of the Dunlin Gp. varies from 10 – 100 m throughout the northern North Sea (Chamock *et al.*, 2001).

The Brent group consists of heterogeneous sandstones and is an important reservoir rock in the North Sea (Bjorlykke and Nedkvitne, 1992). It divides into the Broom/Oseberg, Rannoch, Etive, Ness, and Tarbert formations (Richards, 1992). Broom is the definition of the formation west of Viking Graben. Whereas on the eastern side, it often defines as the Oseberg Fm. The Broom Fm. is ca. 48 m thick and is an easterly thinning succession. The formation usually interprets as an easterly propagating fan delta due to an increase in deeper marine deposits towards the east. East of the Viking Graben, the Oseberg Fm. is interpreted as a westerly propagating fan delta (Richards, 1992). The Rannoch and Etive formations are regressive shoreface deposits (Bullimore and Helland-Hansen, 2009) and indicate a progradational phase of the Brent Delta (Richards, 1992). These formations are upwards-coarsening sandstones (Mitchener *et al.*, 1992) and the combined thickness in the UK sector is 154 m (Richards, 1992). The Ness Fm. consists of westerly thinning fluvial sandstones and comes in successions up to 180 m thick (Bjorlykke and Nedkvitne, 1992; Richards, 1992). The Tarbert Fm. consists of coarse to very coarse shoreface and coastal-plain sandstone deposits and indicates a transgressive environment (Richards, 1992; Bullimore and Helland-Hansen, 2009). The sandstones have an increase in cementation around the quartz grains with depth. Below 4 km depth, this significantly impacts the reduction of porosity and permeability (Bjorlykke and Nedkvitne, 1992).

2.2.4 Jurassic – Cretaceous (Syn-rift 2)

Rifting phase 2 started in the Middle Jurassic, after a tectonic quiescence of about 70 Ma (Duffy *et al.*, 2015). Subsidence during rift phase 2 led to a further increase in marine environment and the deposition of the Viking Group (Dreyer et al., 2005). Many authors discuss if the second rift phase was initiated by an Aalenian rise and a Middle- to Late Jurassic collapse of a Central North Sea thermal dome (Bell *et al.*, 2014), which developed the Trilete rift system (Davies, Turner and Underhill, 2001).

Rifting phases 1 and 2 had similar amounts of extension with stretching factors of 1.4 – 1.5 (β) (Roberts *et al.*, 1993), but the distribution of stretching changed between the phases. The amount of extension in rifting phase 1 was more evenly distributed from the East Shetland Basin in the west to the Horda Platform in the east (Bell *et al.*, 2014). Rifting phase 2 had the highest amount of extension in the Viking Graben and the Sogn Graben (Fig. 2.5), which was the only locality that received more stretching than the previous rifting phase (Færseth, 1996, Odinsen *et al.*, 2000). The Jurassic extension had a stretching factor of about 1.3 in the Viking Graben (Roberts *et al.*, 1993). As a collapse of a thermal dome most likely initiated the second rift phase, the brittle to ductile transition rose, which forced the strain to be more localized (Ziegler, 1992). The main difference between the two rift phases in the North Sea basin was the amount of stretching at the eastern Horda Platform. The eastern Horda Platform was the area that received the most amount of extension during the Permo – Triassic, contrary to the Jurassic extension, where the stretching at this area was negligible (β = 1.05). Rift phase 2 reactivated many of the faults initially created during the first rift phase, even though the dipping directions of the fault blocks sometimes changed (Roberts *et al.*, 1993; Færseth, 1996).

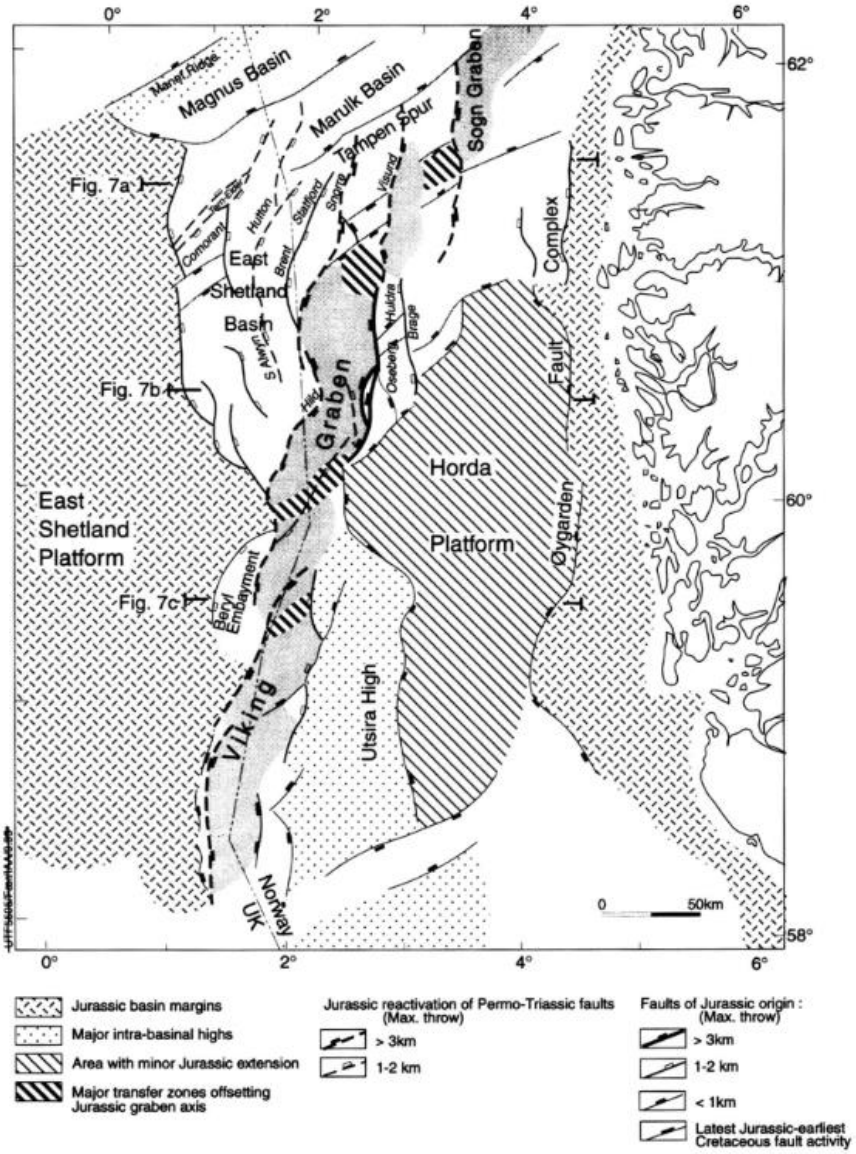

Figure 2.5: The Jurassic extension resulted in E-W extension, which was localized around the Viking and Sogn Grabens. The NE-SW structures north of the Viking graben were the youngest structures created from the Jurassic extension (Færseth, 1996).

The Middle-Upper Jurassic Viking Group comprises the Krossfjord, Fensfjord, Sognefjord, and Draupne formations (e.g. Bell *et al.*, 2014; Whipp *et al.*, 2014).

The three lowermost formations consist of well-sorted medium- to coarse-grained shallow-marine sandstones, with some interfingering from the west by the shallow-marine siltstone units of the Heather Formation (Dreyer *et al.*, 2005; Fawad, Rahman and Mondol, 2021). These three formations have higher contents of sandstone on the Horda Platform than elsewhere in the North

Sea (Dreyer *et al.*, 2005). Thus, the Krossfjord, Fensfjord and Sognefjord formations have received attention as potential reservoirs for CO_2 (Fawad, Rahman and Mondol, 2021). On the Horda Platform, this succession has a thickness of approximately 170 m.

The Draupne Fm. overlies the reservoir and was deposited during the Late Kimmeridgian to Late Berriasian (Whipp *et al.*, 2014). The North Sea was flooded in this period, and the lack of circulation in the water led to anoxic conditions. The lack of circulation governed the deposition of shales with high gamma-ray radioactivity caused by high organic content (up to 10-12%). The shaly units of the Heather and Draupne formations are used as the primary seals for the reservoir (Dreyer *et al.*, 2005; Fawad, Rahman and Mondol, 2021). The BCU (Base Cretaceous Unconformity) caps the top of The Viking Group. The BCU separates the syn-rift (Viking Group) from the post-rift (Cromer Knoll Gp.) and is detectable throughout most of the North Sea basin (Kyrkjebø, Gabrielsen and Faleide, 2004).

2.2.5 Cretaceous – Present (Post-rift 2 and uplift)

Rifting phase 2 was followed by a post-rift and thermal subsidence period that led to a deeper marine depositional environment (Odinsen *et al.*, 2000). The post-rift divides into three major stages. For the first stage, the sedimentation was highly influenced by the structural features from the syn-rift phase, which impacted the accommodation across the basin. In the second stage, the sedimentation rates were superior to the subsidence. The increase in sedimentation influenced the isostatic response. In the last stage, the subsidence stopped due to thermal equilibrium (Gabrielsen *et al.*, 2001).

The Cromer Knoll Group is located above the Draupne Fm. in the stratigraphy. This group consists of fine-grained deep-marine (low energy) clastics and carbonates with interbedded sandstones and was deposited during the lower Beriasian to upper Albian age (Gabrielsen *et al.*, 2001; Bell *et al.*, 2014). The group comprises the Åsgard, Tuxen, Mime, Sola, Rødby formations, and the Ran sandstone units. The group received various events of transgression and regression during the early Cretaceous. The Åsgard and Tuxen formations were deposited in open marine water, which resulted in dark grayish claystones and marlstones indicating low-energy deposition. The Åsgard Fm. is approximately 500 m thick in various reference wells around the central trough area and increases in thickness towards the Sogn Graben, where it is up

to 1200 m (Isaksen and Tonstad, 1989). The Tuxen Formation is thinner but increases in thickness up to 100 m in the basinal areas. After these formations' deposition, the area received a period of sea level rise and transgression. The transgression led to the deposition of the Mime Formation, a carbonific succession containing 5 to 20 meters of shallow marine limestones and marls. Regression happened around the Mid-Aptian age, and the marine environment became deeper marine. The Sola Formation consists of shales interbedded with carbonates and thickens towards the Viking Graben, where it is up to 200 m thick. The Ran sandstone units were deposited during the same period at the structural highs. The units grew up to about 100 m in some areas, and the sandstones varied from white to green to brown in color (Isaksen and Tonstad, 1989). Reddish marlstone with some siltstone at the base dominates The Rødby Formation. The formation is mostly about 15 to 30 meters thick, but the thickness increases towards the Viking Graben where it is about 210 m thick (Deegan and Scull, 1977). The Cromer Knoll Gp. varies vastly in thickness, up to 1400 m in the Sogn Graben, and it thins out towards the basin margins (Isaksen and Tonstad, 1989).

The Shetland Group locates above the Cromer Knoll Group in the stratigraphy. It comprises the Hidra, Hod, Tor, Ekofisk, Svarte, Blodøks, Tryggvason, Kyrre, Jorsalfare, and Hardråde formations (Isaksen and Tonstad, 1989). The lower four formations result from open marine conditions with debris infill during a sea level rise, which resulted in limestones, marls, mudstones, and shales. The Hidra Formation consists of a 30 to 70 meters thick succession of light-colored limestone considered an open marine deposit (Deegan and Scull, 1977). The depositional environment continued to be open marine, which led to the further deposition of limestone with periodite (minor cycles of limestone-marl deposition) sequences. The Hod Formation ranges in thickness from about 230 to 520 m (Deegan and Scull, 1977; Seilacher & Einsele, 1982; Isaksen and Tonstad, 1989). The Tor Formation has approximately the same thickness as the underlying formation and consists of fine-grained limestones (open marine). The formation separates from the Hod Fm., which has a slightly lower gamma-ray and higher velocity. Above the Tor Fm. is the Ekofisk Fm. where the gamma-ray is higher than the Hod Fm., and the velocity is lower. The formation consists of hard crystalline limestone about 100 m thick (Deegan and Scull, 1977). The Svarte Formation is constantly around 190 m thick and is dominated by light-colored mudstones with limestone and sandstone interbedding. The Svarte Fm. will be included as a part of

the Upper Cromer Knoll Gp. in this study, as it was previously reclassified on the northern Horda Platform due interpretation of new well data (Wu *et al.*, 2021; Osmond *et al.*, 2022).
The Blodøks Formation is a thin formation up to 20 m thick, consisting of black shales and mudstones. Therefore, it also has a higher gamma-ray value than the underlying formation. The overlying Tryggvason, Kyrre, Jorsalfare, and Hardråde formations are monotonous and comprise mudstones interbedded with limestones.
The upper six formations contain siliciclastic units of shales and mudstone, with some limestone interbedding, and are deposited in an open marine depositional environment. The group is up to 2000 m thick and thins towards the structural highs (Isaksen and Tonstad, 1989). The Cromer Knoll Gp. and Shetland Gp. are used as secondary and tertiary seals for the Troll Field, as the Draupne Fm. (primary seal) some places have been eroded (Osmond *et al.*, 2022).

The Rogaland group was deposited during Palaeocene to Eocene and lay above the Shetland group in the northern North Sea (Wu *et al.*, 2021). The group consists mainly of marlstones and mudstones (Deegan and Scull, 1977) and comprises the Våle, Lista, Sele and Balder formations (e.g. Isaksen and Tonstad, 1989; Schiøler *et al.*, 2007). The Våle Fm. consists of marl and claystone with some limestone interbedding. The formation is up to 100 m thick but thins out towards the Viking graben. The Lista Fm. ranges between 100 m and 200 m thickness in the Viking Graben and consists primarily of shales with limestone interbedding. It also contains some sandstone layers, but the amount of sandstone decreases upwards in the stratigraphy. The Sele Fm. overlies the Lista Fm., consists of Shales and Siltstones and is up to 90 m thick (Isaksen and Tonstad, 1989). The laminated shales of the Balder Fm. cap the top of the Rogaland Gp. (Schiøler *et al.*, 2007). The thickness varies vastly between 20 m and 100 m (Isaksen and Tonstad, 1989).

The Hordaland group contains fine-grained smectite-rich mudstones interbedded with sandstones (Løseth *et al.*, 2003) and was deposited from early Eocene to early Miocene (Wu *et al.*, 2021). The group varies in thickness across the Viking Graben, up to 1400 m, and thins out towards the north (Isaksen and Tonstad, 1989). During the Neogene, the northern North Sea experienced an uplift and erosion due to isostatic rebound from glacial erosion during the Quaternary (Japsen

and Chalmers, 2000). The glacial erosional surface set the boundary for the base Quaternary unconformity and the Nordland group (Wu *et al.*, 2021).

The Nordland group is the uppermost group in the Cenozoic succession, consisting of marine shales and clays. The group has a maximum thickness of approximately 1500 m and thins from the basin's center towards the east. The group contains the Utsira formation, comprising fine-grained marine sands and shales with an abundance of microfossils (Deegan and Scull, 1977). The group is capped by the seabed.

3 Theory

This chapter will cover the theoretical concept that my studies are based on.

3.1 Sequence stratigraphy

Sequence Stratigraphy is the study of sediments and sedimentary rocks concerning chronostratigraphy. The sea level, sedimentation, and accommodation vary over time and significantly impact the geology. A sequence divides into parasequences sets, depending on deposition and accommodation (Space available for deposition). The parasequence sets are progradational, retrogradational, and aggradational, which separate into individual parasequences (Fig. 3.1) (Wilgus *et al.*, 1988). This section will go through the different sequences, their definition, and how they identify.

$$Progradational: \frac{Deposition\ rate}{Accommodation\ rate} > 1$$

$$Retrogradational: \frac{Deposition\ rate}{Accommodation\ rate} < 1$$

$$Aggradational: \frac{Deposition\ rate}{Accommodation\ rate} = 1$$

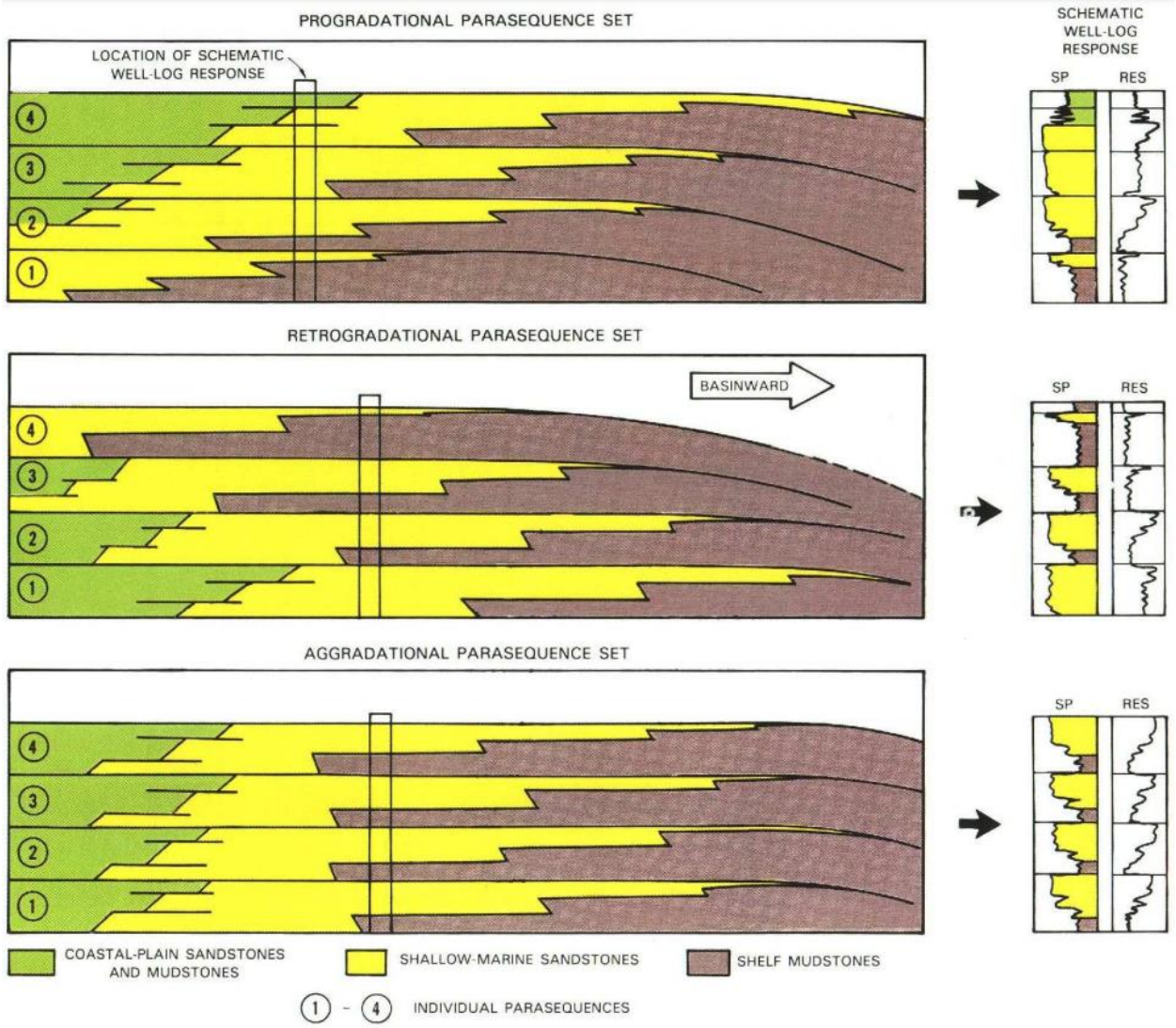

Figure 3.1: Three types of parasequence sets containing four parasequences (1-4) developing towards the right. Near-shore sandstones and mudstones are deposited closest to the shore. Furthermore, shallow-marine sandstones and shelf mudstones more distally. Well-log (Spontaneous potential and resistivity) responses to the parasequences are displayed to the right (Wilgus et al., 1988)

Progradational parasequence sets occur when the deposition rate is above the accommodation rate. There is insufficient space to accommodate all the sediments, resulting in an upwards shallowing trend. Retrogradational parasequence sets develop when the deposition rate is less than the accommodation rate. This results in an upwards deepening trend because there are not enough sediments to fill the accommodation. When the deposition rate is equal to the accommodation rate, there will not be a change in the deposition depth, which is called an aggradational

parasequence set. While the parasequence sets propagate differently, each parasequence is upward shallowing and bounds by a marine flooding surface. A marine flooding surface develops when there is an abrupt increase in water depth, which is often followed by stages of erosion (Wilgus *et al.*, 1988).

3.1.1 Systems tracts

The sequences divide into systems tracts based on their depositional systems (Fig. 3.2). The depositional systems change concerning sea level variations and can be separated into categories. A highstand systems tract (HST) occurs at the maximum sea level and lies directly above the maximum flooding surface in an aggradational to progradational parasequence set. A falling stage systems tract (FSST) results from a fall in sea level, resulting in a higher deposition rate than accommodation rate. There will be a forced regression, and the sediments will deposit on the shelf slope. The deposition continues on the shelf slope at the minimum sea level, called a lowstand systems tract (LST) (Fig. 3.2). Sediments will be deposited as submarine fans on the FSST surface, bounded by a regressive surface. During a sea level rise, the accommodation rate succeeds the deposition rates, and there will be a transgressive systems tract (TST) (Fig. 3.2). A transgressive systems tract occurs in an aggradational to retrogradational parasequence depending on deposition and accommodation, and the deposition moves closer to the shore upwards in stratigraphy (Wilgus *et al.*, 1988; Christie-Blick and Driscoll, 1995; Catuneanu, 2020).

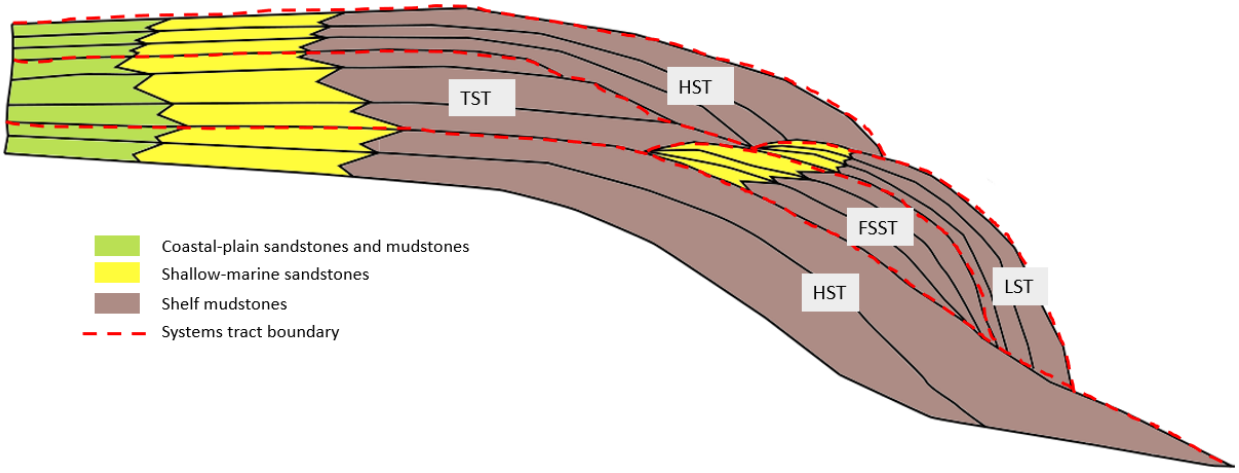

Figure 3.2: Systems tracts develop as a result of deposition and sea level variations. The systems tracts can be set into system to separate the depositional environments. Inspired by: (Wilgus et al., 1988).

3.1.2 Unconformity and conformities

Unconformities and conformities bound older and younger stratigraphic units. An unconformity separates the stratigraphic units as an erosional surface, which has led to a hiatus in the stratigraphy. It is restricted to surfaces lowering the deposition level, meaning geological processes such as dune development and point bars are not included (e.g. Vail and Mitchum, 1977; Wilgus *et al.*, 1988; Christie-Blick and Driscoll, 1995). Conformity separates older and younger stratigraphy without the signs of erosion and hiatuses. An example are surfaces where the deposition rate significantly drops, leading to a stratigraphic boundary (Wilgus *et al.*, 1988).

3.1.3 Stratal terminations

Stratal terminations identify system tracts and paleo-environments and divide into upper and lower boundary terminations. The upper boundary terminations are truncation, toplap, and offlap (Fig. 3.3). Truncations appear as the strata terminate towards an unconformity developed due to erosion. It is usually viewed as an angular unconformity. Toplap is an upper boundary termination with no signs of erosion and hiatuses in the stratigraphy. They appear as clinoforms towards the overlying stratigraphy and often appear as progradation of fluvial deposits (Fig. 3.3). Offlap appears because of forced regression during sea-level fall. Older strata terminate towards younger strata in a downstepping geometry (Mitchum, 1977; Catuneanu, 2020).

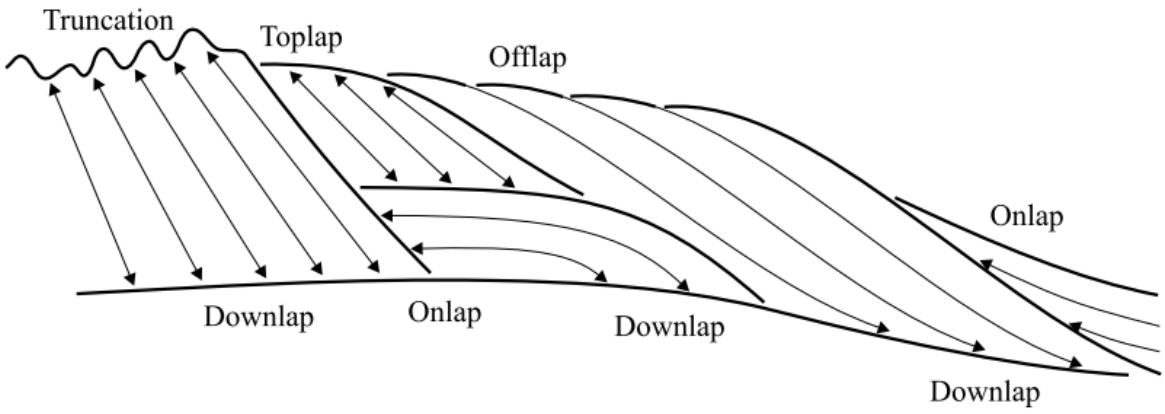

Figure 3.3: Stratal terminations in a system in sequence stratigraphy. They are helpful features to identify stratigraphic development, but their appearance may vary as a result of morphology (Catuneanu, 2002).

The lower boundary terminations onlap and downlap appear above a discontinuity. Onlap develops when a horizontal or lower angle strata terminate towards a surface with a steeper angle.

They often develop during transgression or normal regression due to sea-level rise (Fig. 3.3). Fluvial onlap develops during normal regression or transgression, coastal onlap develops during shoreline transgression, and marine onlap develops during normal regression or transgression on continental slopes. Downlap refers to steeper strata terminating down towards a horizontal or lower angle strata (Fig. 3.3). They usually develop in marine environments and set the base for prograding clinoforms. An example of a downlap surface is a maximum flooding surface (Mitchum, 1977; Catuneanu, 2002). The Seismic resolution and significant geological deformation limit the stratal terminations. Therefore, baselap could be used as a general term for onlap and downlap where they are indistinguishable.

3.2 Fault Theory

A fault develops when a slip surface occurs in a rock because it is subjected to high amounts of stress. Three-dimensional stress variations drive fault propagation, called Anderson's theory of faulting (Anderson, 1905). The theory explains three basic types of faults: normal, reverse, and strike-slip (Fig. 3.4). These faults are endmembers, and faults often form as a combination of them. The body is separated into a footwall and a hanging wall for normal and reverse faults. Relative to each other, the footwall is part of the stationary body, and the hanging wall is part of the body that moves.

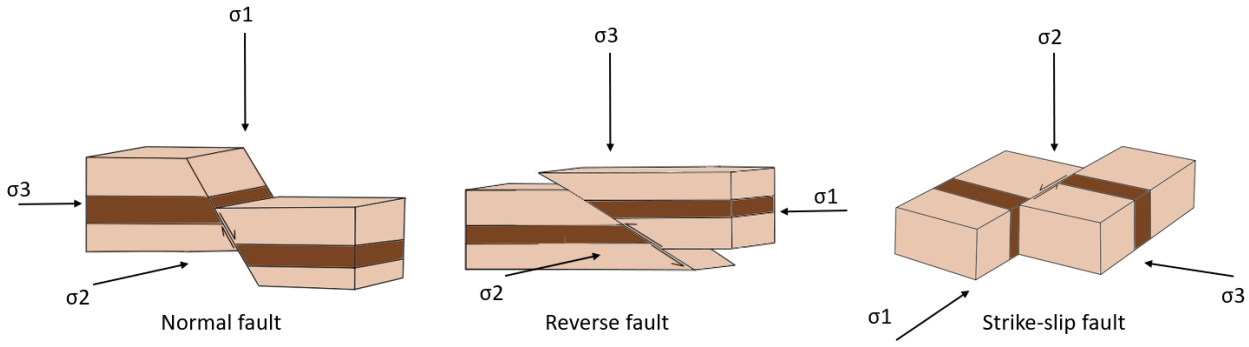

Figure 3.4: Anderson's theory of faulting. The stress vectors are in order σ1>σ2>σ3. The direction of the stress vectors defines what fault that will be created. Inspired by (Anderson, 1905).

A normal fault forms when the maximum stress is vertical. Normal faults have an angle of approximately 60^{o} and are common in an extensional regime. The fault identifies as the hanging wall drops down from the hanging wall. For a reverse fault, the maximum stress axis is

horizontal. Reverse faults form at an angle of approximately 30° and are identified by older strata moving over younger strata. Reverse faults are expected in a contractional regime. The third fault type is the strike-slip fault. A strike-slip fault only has horizontal movement and can be divided into sinistral (left lateral) and dextral (right lateral). For example, Fig. 3.4 shows a sinistral strike-slip fault because it has a left lateral offset of the marker bed. Even though faults have an approximately fixed angle when they form, the fault blocks can undergo rotation and other movements after their development, which can change the appearance and angle of the fault (Bhattacharya, 2022).

3.2.1 Fault development

The maximum throw (displacement) is towards the center when a fault develops, and the throw distribution will change when a fault propagates and potentially links up with other faults.

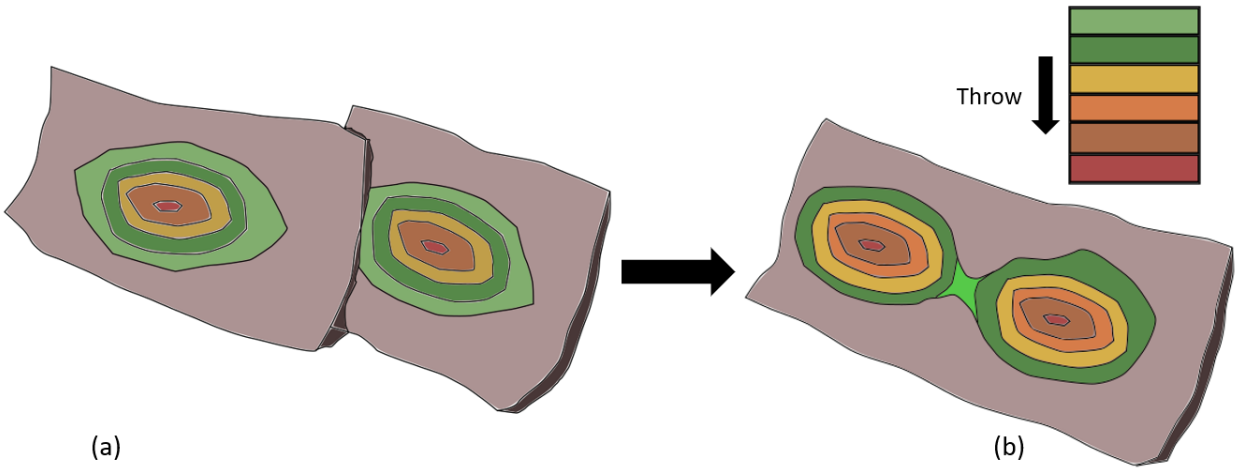

Figure 3.5: A fault has the most amount of throw in the center and has an ellipsoidal development. (a) Two soft-linked faults with the most amount of throw in their center. (b) The faults become hard-linked and the fault propagation merges. The maximum throw moves towards a new center.

Fault linkage separates into soft- and hard-linked faults. Soft linked faults (Fig. 3.5 (a)) do not accommodate throw from other faults and will develop relay ramps between each other before they potentially become hard linked. If the faults become hard linked, the throw accommodation will merge (Fig. 3.5 (b)) and the fault will continue to develop as a single fault (Duffy *et al.*, 2015). A relay ramp could be a potential pathway for CO_2 migration if permeable rocks juxta-pose.

Brittle and ductile rocks respond differently to applied pressure. Their difference in behavior is essential for sealing properties (Davatzes and Aydin, 2005). When brittle rocks deform, they develop brittle strain, such as fractures and faults. In contrast, a ductile rock will be folded and potentially smeared between harder rocks.

Sedimentation during faulting is key to determining when the fault was active. The sedimentation in an extensional regime separates into pre-, syn-, and post-rift. Pre-rift concerns all sedimentation happening before the fault was active. This succession is recognizable as it has an equal thickness throughout the hanging wall. Syn-rift defines the sedimentation occurring during rifting. It is distinguishable as the succession thickness increases towards the footwall. A more significant thickness variation towards the footwall indicates more throw of the fault. Post-rift sedimentation occurs after rifting. It could involve the reactivation of faults and post-rift subsidence, which could change the geometry of the basin (Whipp *et al.*, 2014).

The amount of syn-rift deposition can be measured by creating an expansion index (Fig. 3.6). The expansion index is the quotient of the hanging wall thickness and the footwall thickness of a stratigraphic layer. Much syn-rift deposition will lead to a high expansion index (Fossen, 2016).

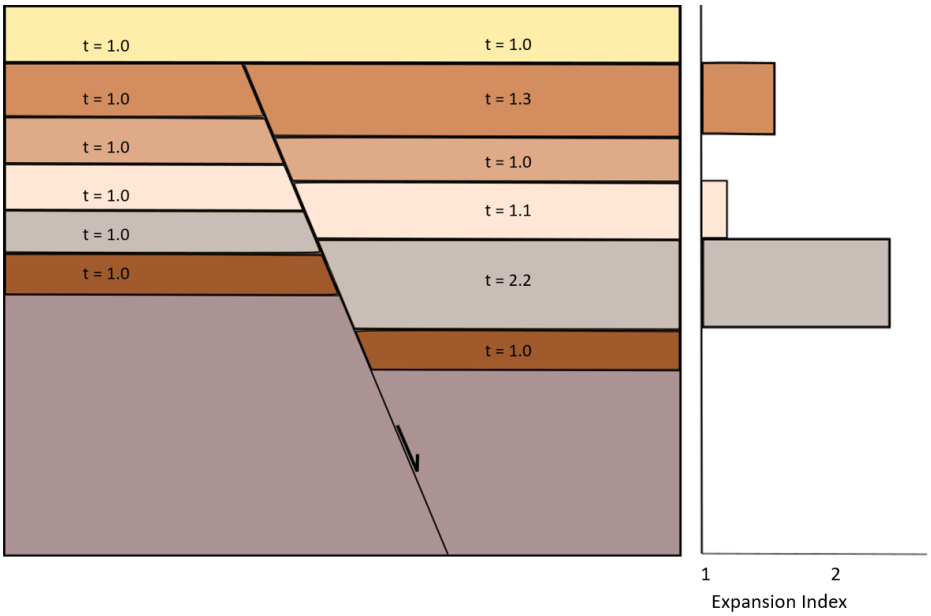

Figure 3.6: The expansion index gives a relative numerical value to stratigraphic layers in an extensional regime. The value depends on the thickness increase in the hanging wall, and it cannot be less than 1.0, because the sediments will always accommodate in the hanging wall. It is a great tool to identify when a fault/sedimentation was active. Modified from: (Fossen, 2016).

4 Data, Limitations, and Methods

4.1 Seismic data

This chapter will go through the various data used in this project. For the area south of ca. 61° N, I have used a subset of the CGG NVG 3D depth-migrated seismic cube, converted to two-way travel time (TWT). The data was collected in 2016 and processed in 2018. The cube covers an area of 5832.3 km^2 and goes down to a depth from 0 to -9000 ms TWT. The inline is oriented in the N-S direction, while the crossline is oriented in the E-W direction. They have an increment spacing of 12.5 m, respectively (Osmond *et al.*, 2022). Time migrated seismic generally has a better spatial resolution and is therefore preferred for detailed stratigraphy interpretation. Moreover, for the area north of ca. 61° N, I have used a subset of the CGG NVG 3D seismic cube in time versus depth (TVD). This subset covers an area of 7188 km^2 inside the coordinates:

ED50UTM1
X Y
501423.00,6689328.00
526983.00,6812361.00
574315.98,6812853.65
574315.98,6695797.86
539790.47,6695797.86
539790.47,6689130.01
501423.00,6689328.00

The TVD seismic cube covers a depth from 0 to 20 km below sea level. TVD is preferable to map faults, as these are migrated to correct position and geometry. The reflection pattern of the seismic waves gives the acoustic impedance (AI). The product of density and the seismic waves' velocity defines a medium's AI. Their increase in depth leads to an increase in AI (Eaton, Milkereit and Salisbury, 2003). The seafloor in these seismic cubes is a peak (positive amplitude), which means that going from a soft material (water) to a harder material (seafloor) gives a positive amplitude variation. Moving from hard to softer rock will reflect a trough (negative amplitude). At shallow depths, shales are usually not as compacted as sandstones and will therefore appear as a softer rock with a higher porosity compared to sandstone. As the depth increases, the porosity of a shale decreases more rapidly than for a sandstone, which means that the sandstone will appear as the softer rock (e.g. Magara, 1980).

The TWT cube requires 207 GB of storage, and the TVD cube requires 134 GB of storage. I used a cropped volume with a depth cutoff of 5000m for the TVD cube to prevent the computer from using too much RAM during interpretation.

4.2 Well data

Well data gives a significant advantage in subsurface research, and the area of interest contains 89 wells that should be utilized to get as much information about the area as possible. For interpreting The Top Sognfjord Fm., Draupne Fm., Cromer Knoll Gp. and Shetland Gp., the well data gave much information about the lithologies. Due to their location, I chose to focus on the wells 32/4-3S, 31/6-2, 31/6-6, 32/4-1 T2, and 32/2-1 because they are in the area with the best log data coverage of the uppermost Jurassic and Cretaceous successions (Fig. 4.1).

Well logs are helpful and can give much more detailed information about the lithologies than seismic data, and well logs used in this thesis are the gamma-ray, sonic, and density logs. The gamma-ray log is helpful because it measures the natural radioactivity of rocks. It is suitable for distinguishing between organic-rich and siliciclastic units because the organic content usually is much more radioactive. Natural radioactivity is also commonly found in K-feldspars and some clays/micas containing K. Shales are generally more prone to being radioactive than sands (as they often mainly consist of quartz). Therefore, this is an excellent well log to distinguish between shales and sandstones. Gamma-ray is measured in API units and is usually set between the values of 0 and 200 (Jr, Swift and Hartline, 1962). The sonic log measures the P- and S-wave velocities versus depth. The P-waves travel through the formations and back to the receiver. The sonic log is prominent for identifying fluids in rocks because the fluids such as oil/gas and CO_2 do not have a shear velocity. Therefore, a highly porous sandstone with gas will be a very slow formation, whereas a low porosity/high density carbonate will be a fast formation (Doh, 1959). The sonic log is often plotted with the density log, as they often give the opposite values. The density log measures a formation's bulk density, which is influenced by porosity and mineral composition.

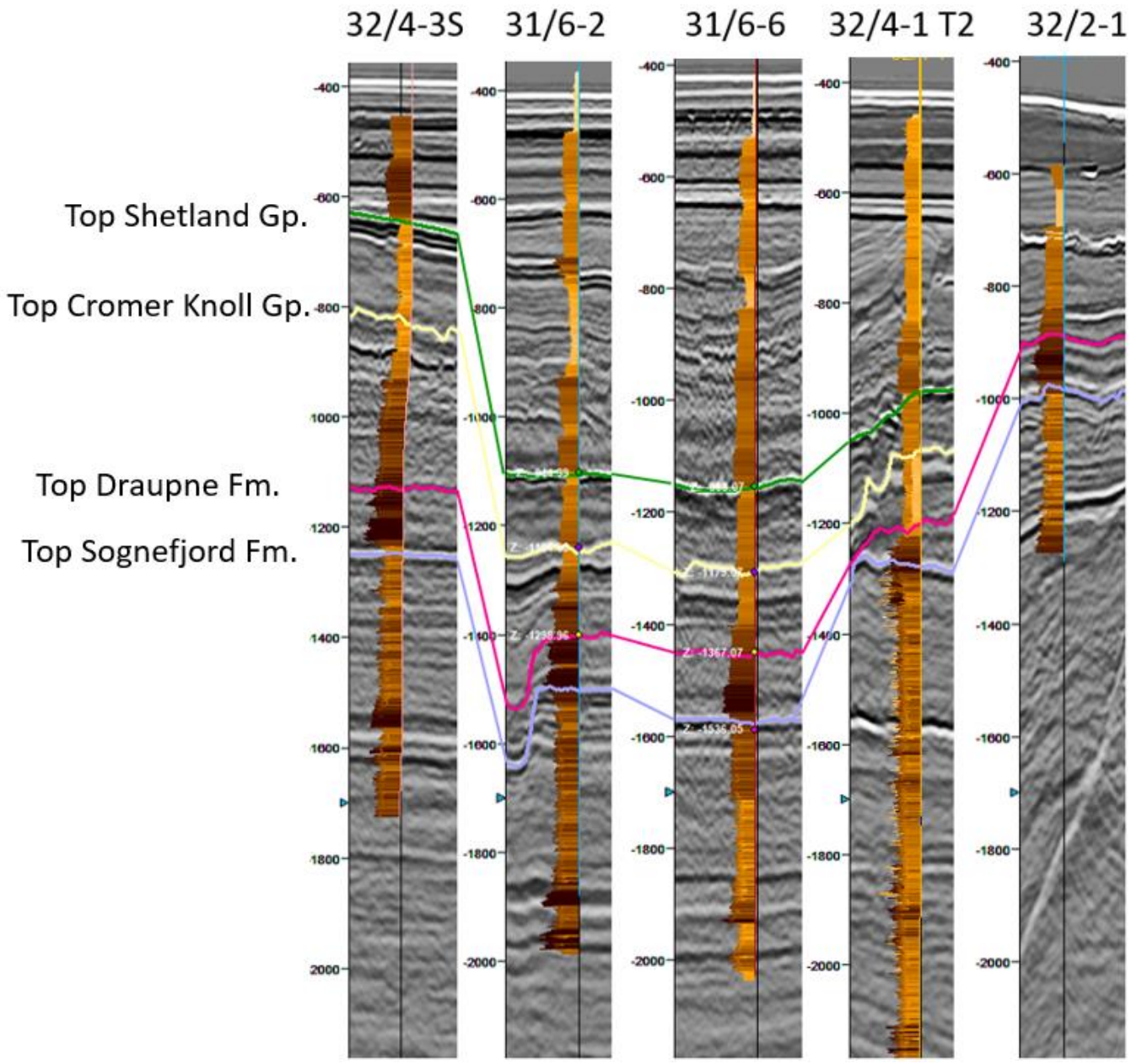

Figure 4.1: Selected wells with gamma-ray log plotted with the Top Shetland Gp., Top Cromer Knoll Gp., Top Draupne Fm. and Top Sognefjord Fm in TWT. Note that the Top Shetland Gp. and Top Cromer Knoll Gp. are not present in the well 32/2-1.

4.3 Seismic limitations

The seismic data can give access to much subsurface information, but it also has limitations. Understanding these limitations is essential when analyzing the subsurface because one needs to think critically. The subsurface can vary greatly, so getting to know the area is essential.

Restricting factors of the seismic data are the vertical and horizontal resolution. The vertical resolution in seismic is the minimum thickness of a medium for it to be visible on the seismic.

The layer can only be visible if it exceeds ¼ of the wavelength from the seismic wave (Sheriff, 1980). The wavelength usually increases with depth due to preferential absorption of the high-frequency part of the wave spectrum, which means the layers must be thicker to be visible at greater depths. The increase in wavelength means that thin layers might disappear on the seismic even though they exist.

The Fresnel zone governs the horizontal resolution (Fig. 4.2). The seismic wavefront requires a layer thickness above ¼ of the wavelength to be noticeable. If the distance of a horizontal layer is less than the Fresnel zone, the layer will not be visible on the seismic. One can improve horizontal resolution via migration, but this could also increase noise. Another limiting factor for horizontal resolution is spatial sampling. The geophones that receive the seismic signal needs a fixed spacing in relation to the subsurface. Therefore, an inaccurate geophone placement could decrease the seismic data quality (Sheriff, 1980). For this seismic dataset, the vertical resolution is from 5-10 meters, and the horizontal resolution is approximately 37.5 meters for the Jurassic up to the Paleogene successions (Osmond *et al.*, 2022)

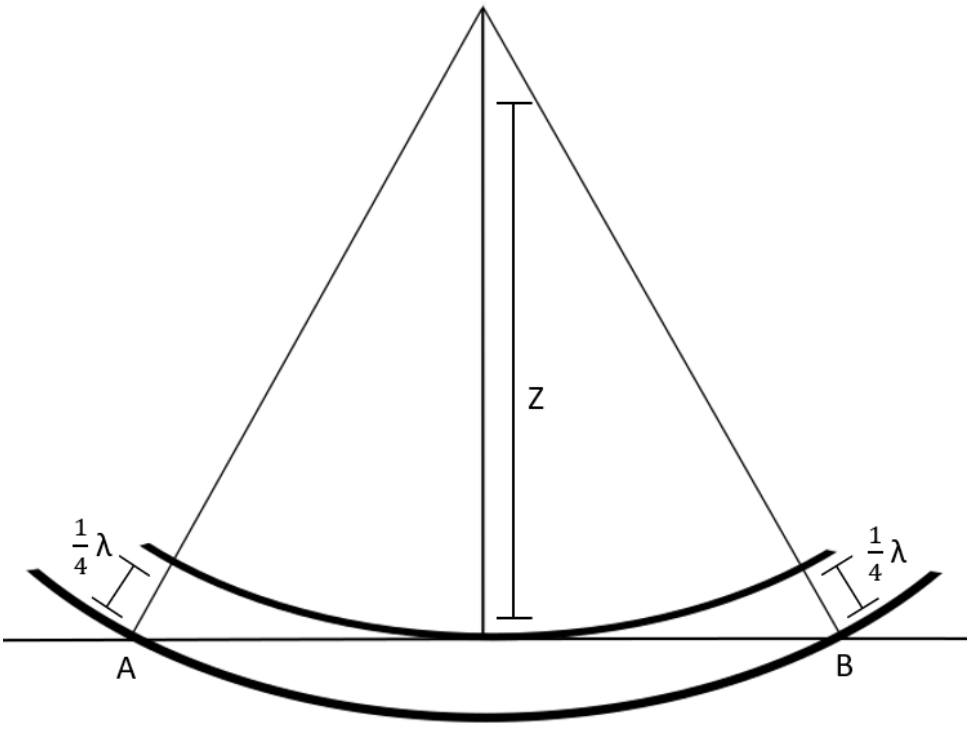

Figure 4.2: The Fresnel zone is the minimum width of a layer, for it to be caught by seismic waves. Z = Distance from geophone to layer, A-B = Width of the Fresnel zone. Modified from: (Sheriff, 1975).

4.4 Methods

My thesis focuses on the Upper Jurassic to Middle Cretaceous successions on the northern Horda Platform. This chapter will discuss the various methods I used to understand these successions and their influence on the top seal in the area of interest. There have been previous studies regarding the top seal of CO_2 storage sites on the Horda Platform (e.g., Osmond *et al.*, 2022; Rahman *et al.*, 2022; Wu *et al.*, 2021), but the Late Jurassic to Late Cretaceous successions in this part of the northern Horda Platform should be further investigated, as the quality of the seismic and knowledge of the area continuously improves. That is why the northern Horda Platform should be the next focus point. I will investigate this area using quantitative seismic data collected by CGG, reading previous studies, and creating figures to visualize them. This chapter divides into two segments: (1) a literature study and (2) seismic interpretation using Schlumberger's Petrel.

4.4.1 Literature study

Before doing a subsurface investigation, it is essential to know the area that is about to be investigated. Therefore, for the initial stages of my thesis, I sought key papers regarding the evolution of the Norwegian continental shelf. Once I understood the large-scale evolution, I focused more on the North Sea and the Horda Platform. Other studies regarding The Upper Jurassic to Lower Cretaceous succession around the area were also highly relevant to my thesis because they could directly influence my research.

4.4.2 Well-ties and horizon interpretation

I started with connecting wells in the 2D window in Petrel using the arbitrary composite line function. This area has received the most extension in the E-W direction, so I also focused on connecting most wells in the E-W direction. To get an overall image of the area, I connected some wells in the N-S direction across the seismic cube. The well-ties led to better vision of the structural elements on the seismic, as we are perpendicular to the faults. I visualized some of the wells on the seismic, which are the best lithology proxies, which made it easier to see the different lithologies of the seismic lines.

This thesis focuses on the successions of the Late Jurassic to middle Cretaceous deposited during syn- to post-rift. Therefore, the most relevant groups and formations were the Sognefjord Fm.,

Draupne Fm., Cromer Knoll Gp. (Fig. 4.3), and the Shetland Gp. I started by interpreting the top Shetland Gp. because it distinguishes easily from other seismic lines. It appeared as a strong peak in most instances, and since it's deposited after syn-rift 2 (Fig. 2.4) it has not experienced that much faulting. After that, I interpreted the Top Sognefjord Fm. (peak), Top Cromer Knoll Gp. (peak), and Top Draupne Fm. (through).

After making multiple Well-ties, I started mapping the area by creating a grid map. I initially interpreted intersections with an inline/crossline spacing of approximately 500 over the entire seismic cube. Depending on what formation I interpreted, I changed the increment. As some areas proved more challenging than others, I narrowed it down to a much closer spacing depending on the conditions. After I made a suitable grid map, I used the 3D auto-tracking function (Fig. 4.3) on the grid to track the seismic lines automatically. Even though the 3D auto tracker is a great tool, I had to manually go through the horizons to check if the automatic interpretations were correct. The auto tracker made errors along some faults that needed correction. Petrel's Parent/Child point function efficiently corrected errors in the 2D window because it easily connects the software's auto-tracked child and parent points.

Before generating the surfaces, I had to enclose the interpreted area within a polygon I created around each interpreted horizon. Once I generated the surfaces, I added the smooth surface attribute to erase minor irregularities within the formations and highlight this project's critical structures. The color table was adjusted to an automatic local color table for all surfaces to remove the outliers and highlight the local elevation change for each surface. To further examine the Cromer Knoll Gp., I divided it into multiple units to see how it was influenced by the Vette Fault.

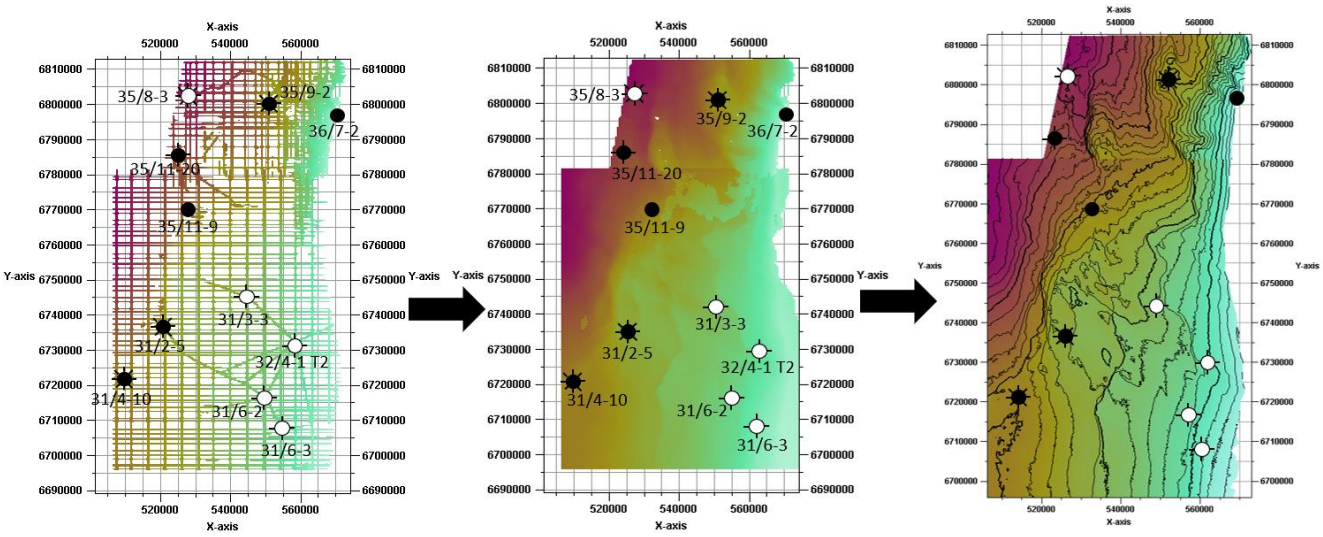

Figure 4.3: Example of the process in making a time structure map (Cromer Knoll Gp.). From left to right: 2D grid map of The Top Cromer Knoll Gp, 3D auto tracked interpretation, and The Top Cromer Knoll Gp. time structure map. Key wells used to identify the stratigraphy are added on the maps.

4.4.3 Fault interpretation

To visualize faults and fractures in Petrel, I used the volume attribute *Variance (Edge method)* to extract a variance cube from the original cube. The Variance attribute excludes amplitude variations between layers, which makes it easy to track discontinuities such as faults and fractures (Petrel E&P Software Platform, 2015). I made a time slice of the variance cube to get the Z – values for a more straightforward 3D mapping of the faults. As previously mentioned, the area has received an E-W extension, creating N-S-oriented normal faults. Therefore, it was essential to use the Xline or create composite lines orthogonal to the faults before interpreting them. I interpreted the faults with an increment of 25 -100 ms between each intersection, depending on their visibility on the seismic. It was also essential to consider the horizontal resolution of the seismic while interpreting. The seismic data used vertical exaggeration, causing the faults to appear sub-vertical in some instances. I started by interpreting the Øygarden-, Vette-, Tusse-, and Svartalv faults, as they were the most visible on the seismic. Following these master faults, I interpreted some synthetic and antithetic faults in the area.

4.4.4 Isopach maps

The units vary vastly in thickness across the northern Horda Platform. I created isopach maps of the interpreted units to visualize the thickness variations. I did this by subtracting the elevation of

the overlying units with the underlying, for example extracting the Top Cromer Knoll Gp. with the Draupne Fm.

4.4.5 Fault diagrams

As this thesis focuses on the Vette fault, structural mapping of the fault across the study area was a key objective. I first collected depth data of the units in the footwall and hanging wall of the Vette fault with in increment of 250 and added them to excel. I then subtracted the footwall depth with the hanging wall depth to get the throw of the units. The values were added together in a throw vs distance plot. Throw vs depth plots of the Vette fault were made from three key transects. The depth values were chosen as the midpoint between the footwall and hanging wall depths for each unit and plotted with the throw. Expansion indices were made by dividing the hanging wall thickness with the footwall thickness for all units.

5 Results

This chapter will involve the stratigraphic framework of the northern Horda Platform used to discuss the sealing capacities of the cap rock. I will describe key seismic cross-sections, surfaces, and surface attributes plotted with faults I interpreted. In the first part of the chapter, I describe the overall framework of the northern Horda Platform and how local and large-scale variations connect. In the second part I will focus on the local geological variations across the Vette Fault. I will primarily focus on the Cromer Knoll Gp. by dividing it into subdivisions of similar seismic and well log characteristics and describing how this changes spatially. I will solve this by creating surfaces, isopach maps, manual sequence stratigraphic interpretations, and fault diagrams.

5.1 Framework of the northern Horda Platform

The study area is located on the northern Horda Platform south of the Møre Basin and east of the Viking Graben (Fig. 5.1). The area contains several previously studied structural elements (e.g. Bell et al., 2014; Whipp et al., 2014; Wu et al., 2021), which influences the top seal in the area at multiple scales. Therefore, an establishment of the stratigraphic framework around the focus area should be done to contextualize it. I chose six transects that best visualize the variations across the TWT cube (Fig. 5.1).

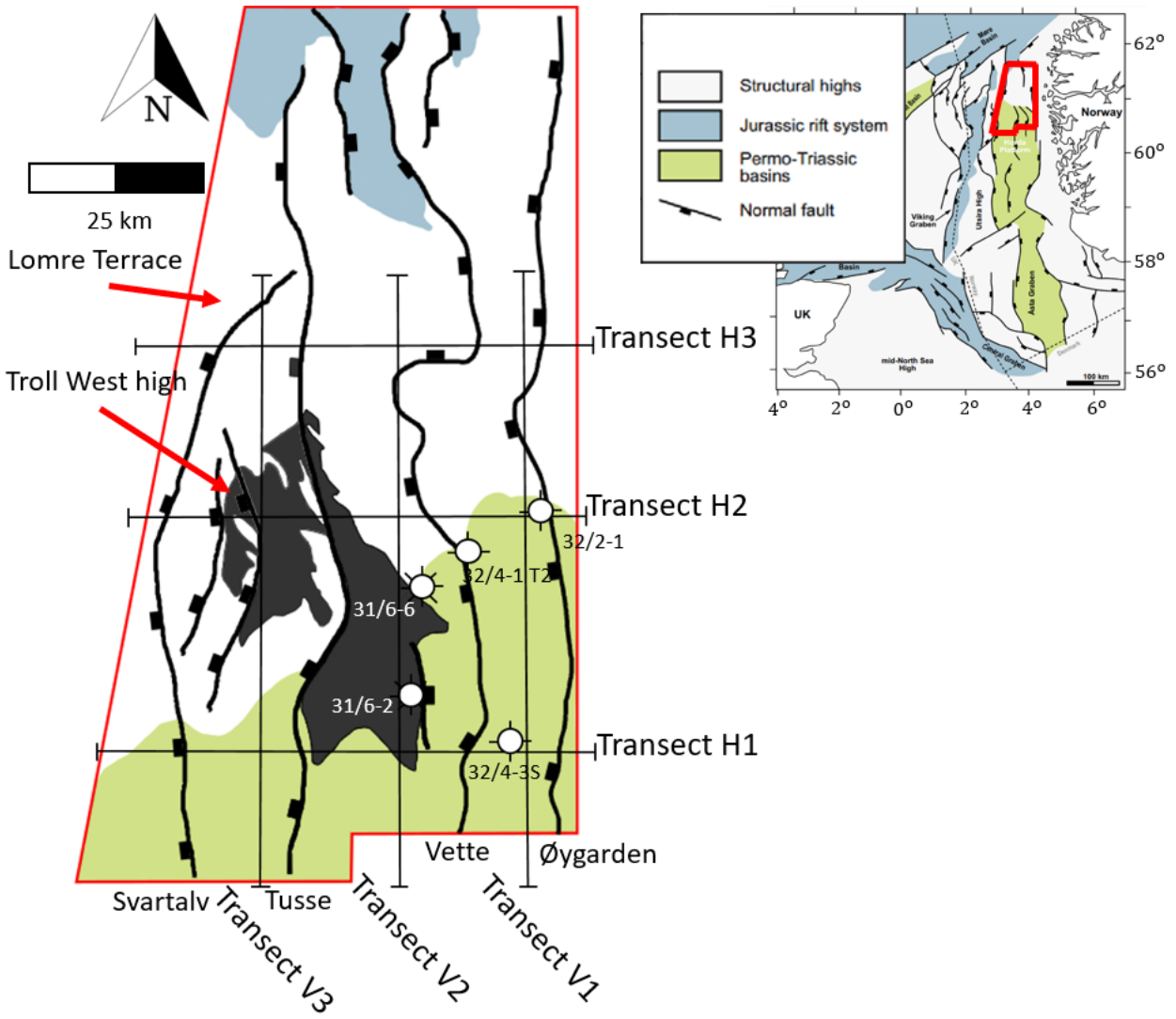

Figure 5.1: Zoomed in map of the study area with added major normal faults. The map includes the master faults, The Troll Field, and key wells around The Vette Fault used in this thesis. Transects V1-V3 and H1-H3 are key transects to describe the stratigraphic framework of the area, which will be discussed in the next chapter. The index map is modified from: (Whipp et al. 2014).

The lowermost formations vary the most in elevation and have more faults/fractures than the overlying successions (Fig. 5.2). The relief at Top Sognefjord Fm. changes from ca. -3450 ms depth in the NW to ca. -700 ms in the SE. The Top Draupne Fm. varies in depth from ca. -3400 ms in the NW to ca. -700 ms in the SE. The Top Cromer Knoll Gp. changes in depth from ca. -3000 ms in the NW to ca. -600 ms in the SE. The Top Shetland Gp. varies less in elevation than the underlying units and changes in depth from ca. -2300 ms in the NW to -600 ms in the SE (Fig. 5.2).

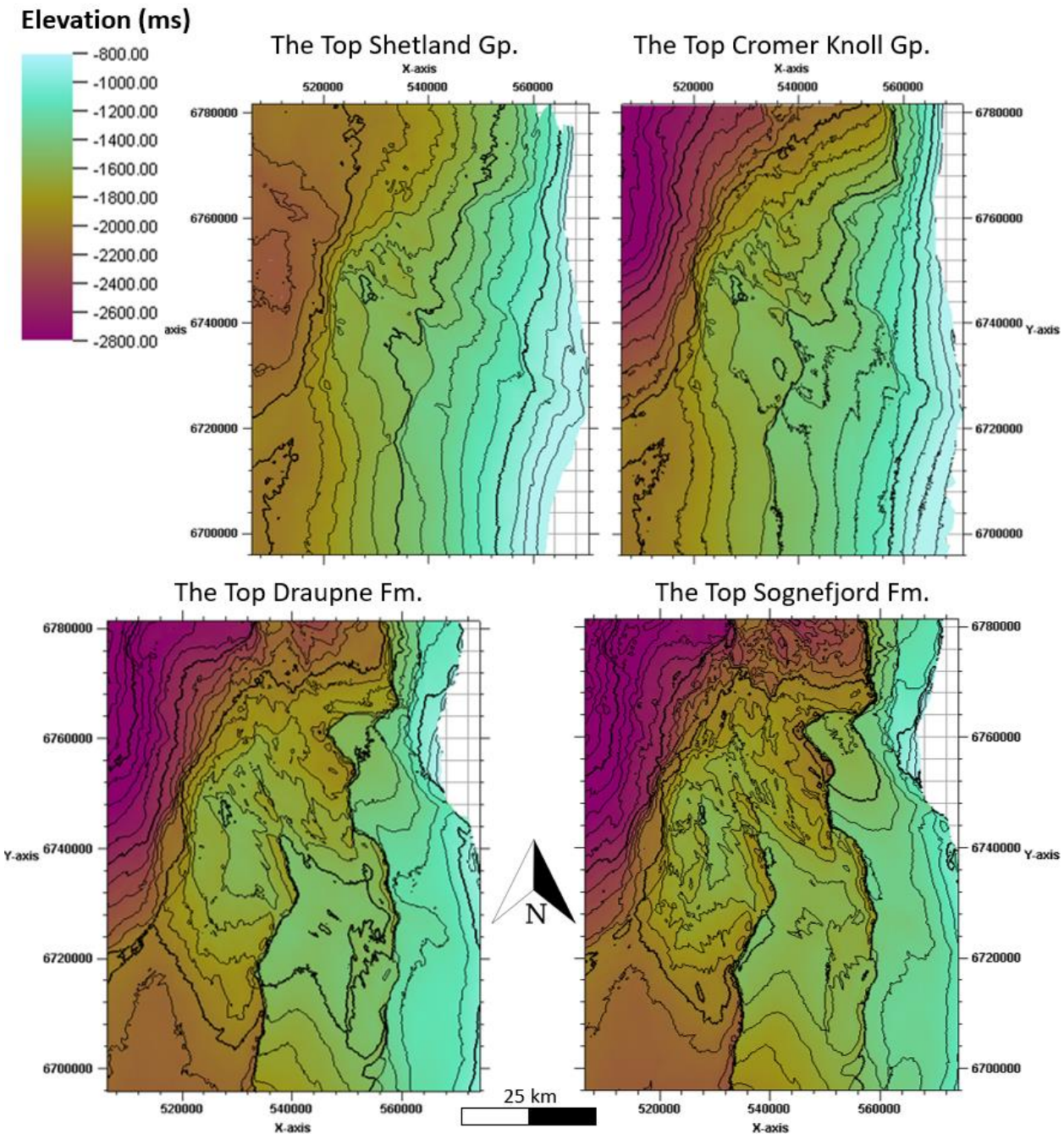

Figure 5.2: Time structural maps in TWT plotted with a global color table. The surfaces have a contour line spacing of 100 ms and are plotted with the "Hawaii" color table (Crameri, 2018), meaning they are plotted without visual distortion.

The Shetland Gp. and The Cromer Knoll Gp. are truncated at Base Quaternary Unconformity (BQU) in the eastern parts of the study area and the BQU was therefore interpreted above the Tusse and Vette Fault blocks (Fig. 5.5, Fig. 5.6). The BQU is sub-horizontal and ranges in depths from approximately -600 to -800 ms (Fig. 5.3).

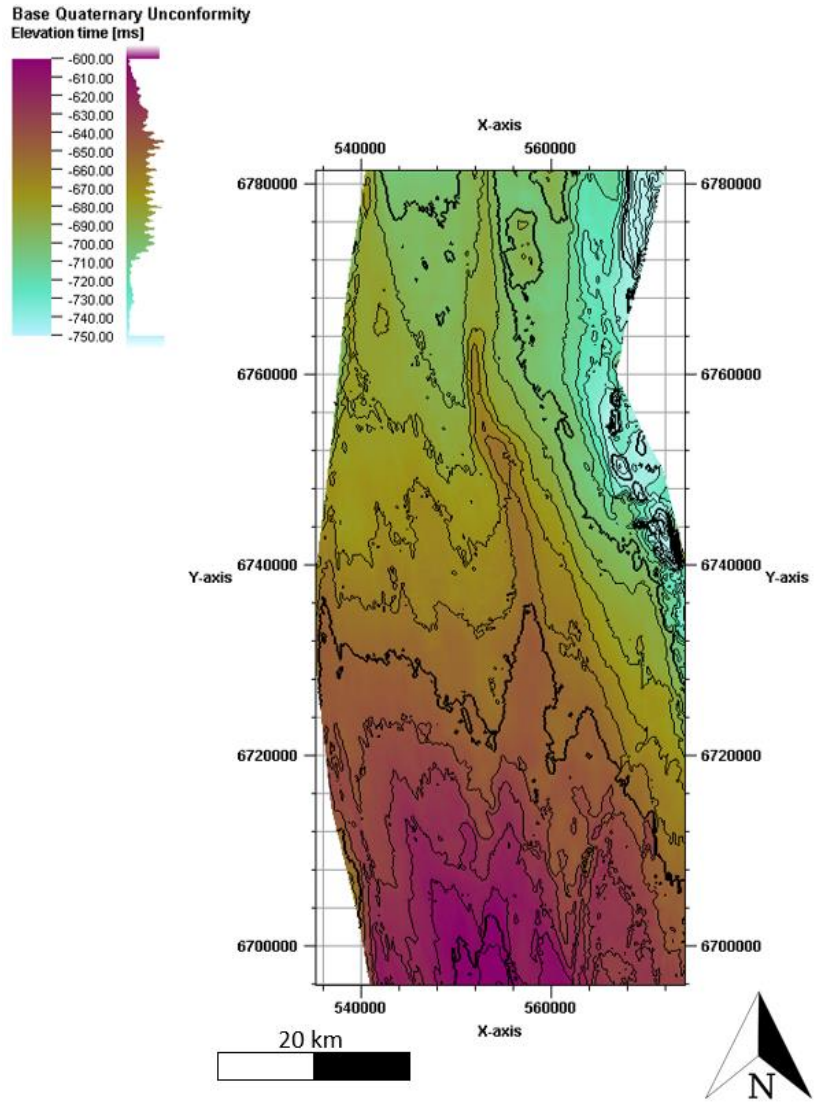

Figure 5.3: Base Quaternary Unconformity in the area of the Tusse and Vette fault blocks.

5.1.1 The Draupne Fm.

The Draupne Fm. is the oldest part of the studied stratigraphy (Fig. 2.4) and consists of shales with high organic content deposited in anoxic conditions. This section will cover my interpretations of The Draupne Fm. in the area of interest.

The Draupne Fm. has a uniform thickness of around 130 ms across the southeastern parts of the study area but thins out towards the Troll West high (Fig. 5.4, Fig. 5.7 (a)). The formation also thins out along the fault scarps of the footwalls, with a decrease in thickness towards the north.

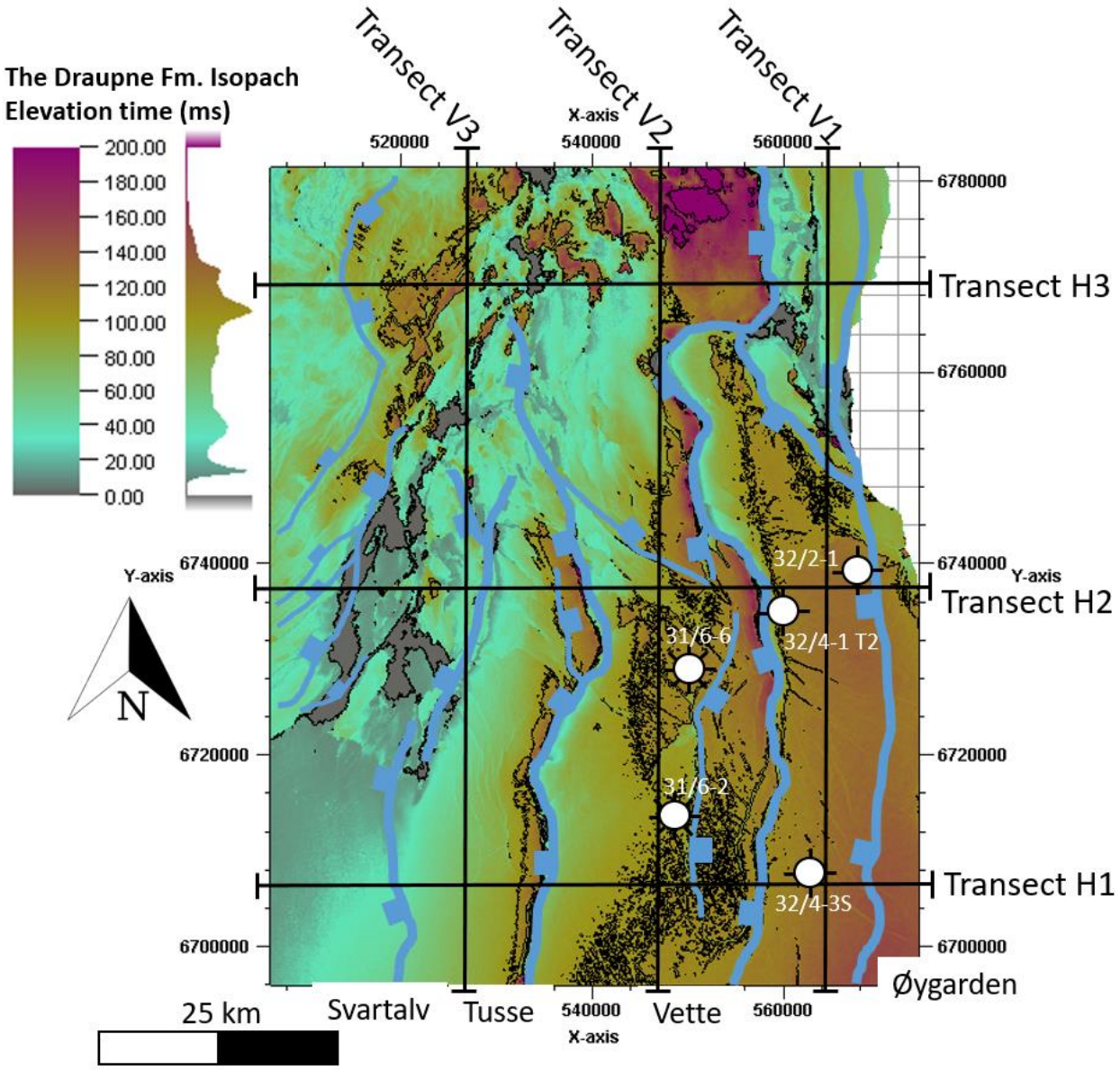

Figure 5.4: The Draupne Fm. isopach map is plotted with a thickness of 0 – 200 ms. Areas with 5 ms thickness or less are marked as grey areas. The map has a contour line spacing of 100 ms. The transects H1-H3 and V1-V3 and key wells from the focus area are added to the map.

In the southern areas, the formation has a uniform thickness of around 130 ms, with an anticline in the hanging wall of the Vette fault, seen in Transects H1 and H2 (Fig. 5.7 (a, b)). The formation decreases gradually in thickness towards the west, where the thickness decreases to about 12 ms (Fig. 5.4, Fig. 5.7 (a)).

Further north, the thickness constantly remains at around 130 ms in the Vette fault block (Fig. 5.4, Fig. 5.7 (b), Fig. 5.8 (a)). Synclines are observed in the formation in the hanging wall of the master faults as the formation is dragged up the fault planes (Fig. 5.7 (b)). Anticlines accompany

the synclines in the Øygarden and Tusse faults hanging walls. On the Tusse faults block, the thickness decreases towards the west on the higher elevations of ca. -1600 ms, as the formation becomes absent on the Troll West high (Fig. 5.4, Fig. 5.7 (b), Fig. 5.8 (c)). West of the high, the formation is downfaulted to a depth of around -2600 ms with a thickness of up to around 60 ms (Fig. 5.7 (b)).

In the northern parts of the study area, the Draupne Fm. continues to have a thickness of around 100 ms along the Vette fault block at a depth of -1100 to -1300 ms (Fig. 5.7 (c), Fig. 5.8 (a)). The formation increases in depth towards the west, and it becomes absent at the Troll West high. Just west of the high, it has a section where the formation's thickness becomes ca. 100 ms, but the thickness decreases to around 30 west in the study area (Fig. 5.7 (c), Fig. 5.8 (c)).

5.1.2 The Cromer Knoll Gp.

The Lower Cretaceous Cromer Knoll Gp. (Fig. 2.4) is described in chapter 2.2 as a fine-grained deep-marine clastics and carbonates with interbedded sandstones. This section will include my interpretations of the Cromer Knoll Gp.

In the eastern area along the Øygarden fault, the Cromer Knoll Gp. is truncated below the BQU at ca. -700 ms depth (Fig. 5.7). In the southern areas, represented by transect H1 (Fig. 5.7 (a)) the group reaches its maximum thickness (ca. 450 ms) in the hanging walls of the Vette and Tusse faults and generally thins westward toward the crests of the major footwall blocks (Fig. 5.5, Fig. 5.7 (a)).

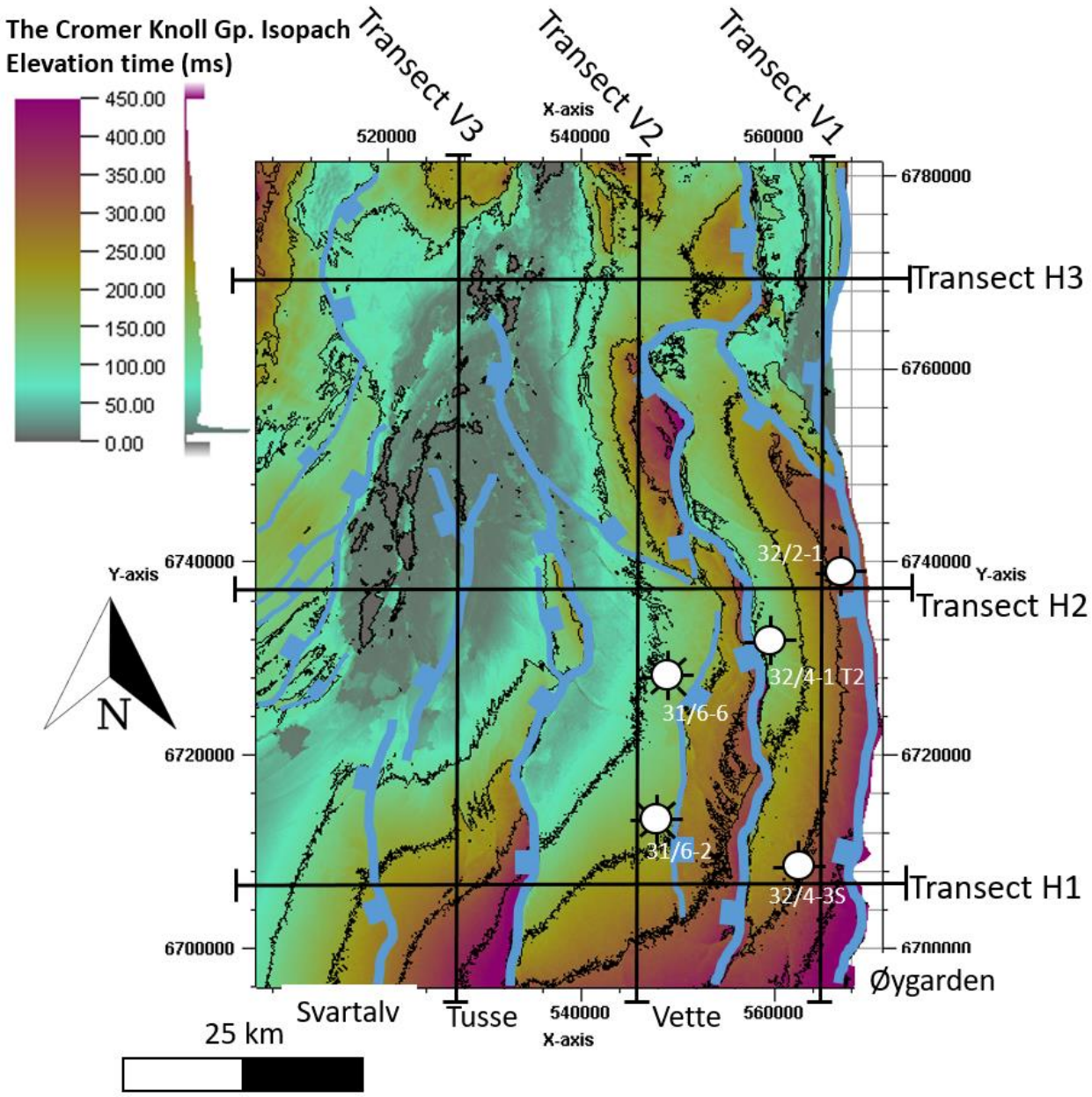

Figure 5.5: The Cromer Knoll Gp. isopach map. Plotted with a thickness from 0 to 450 ms. Thicknesses below 5 ms are marked as grey area. The Isopach map has a contour line spacing of 100 ms. The map includes the Transects H1-H3 and V1-V3 and key wells in the focus area.

The Cromer Knoll Gp. has the same trends further north in transects H2 and H3 (Fig 5.7 (b, c)), where the thickness decreases westwards toward the crests of the fault blocks. The group is eroded on the Troll West high. In transects H2 and H3, the group re-appears down flank of the Troll West block at approximately -2200 ms depth with thicknesses up to 150 ms (Fig. 5.5, Fig. 5.7 (b, c), Fig. 5.8 (c)).

North in the study area, represented by section H3, the group becomes thinner, with thicknesses up to ca. 300 ms in the hanging walls and down from the Troll West high, and has an increase in thickness towards the Lomre Terrace in the north-west direction (Fig. 5.2, Fig. 5.5, and Fig. 5.8).

5.1.3 The Shetland Gp.

The Upper Cretaceous Shetland Gp. (Fig. 2.4) consists of open marine limestones, mudstones, marls, and shales, as described in section 2.2. This section will include my interpretations of the Shetland Gp.

In the southern area, the Shetland Gp. is truncated by the BQU in the east at -600 to -700 ms depth, reaching a maximum thickness of approximately 180 ms (Fig. 5.6, Fig. 5.7 (a), Fig. 5.8 (a)). The group gradually thins out towards the west and is absent on the crest of the Svartalv fault block at around -1833 ms depth, as seen in transect V3 (Fig. 5.6, Fig. 5.7 (a), Fig. 5.8 (c)).

Further north, the group is truncated at around -800 to -1000 ms depth on the Vette fault block (Fig. 5.7 (b, c)). The group thins towards the west and is absent above the Troll West high. North of the Horda Platform the Shetland Gp. thickens onto the Lomre Terrace and exceed 900 ms at the northwestern edge of the cube (Fig. 5.6, Fig. 5.7 (b, c), Fig. 5.8 (b, c)).

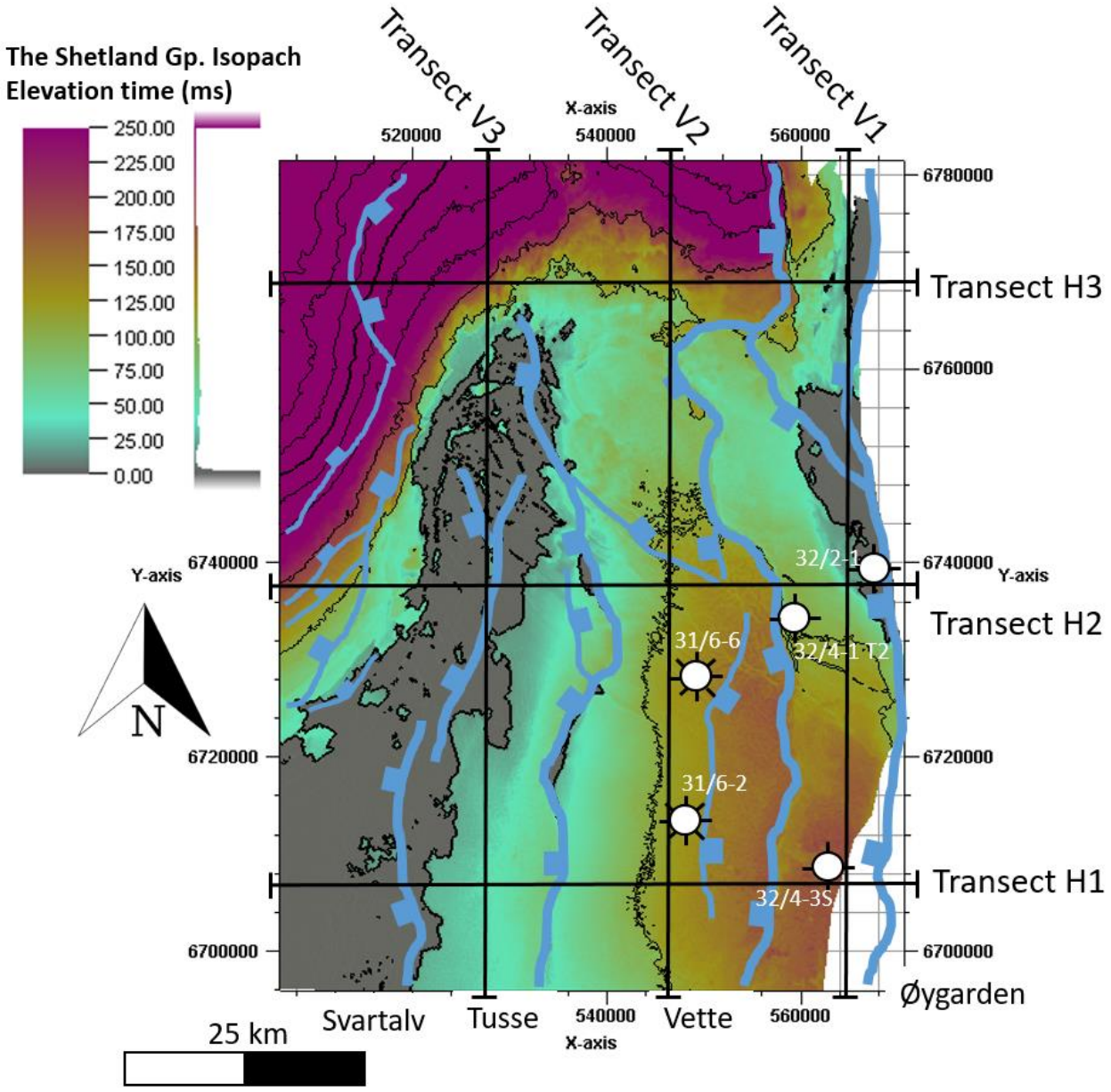

Figure 5.6: The Shetland Gp. Isopach map plotted with a thickness from 0 to 250 ms. Thicknesses less than 5 ms are marked as a grey area. The Isopach map have a contour line spacing of 100 ms. The map is plotted with transects H1-H3 and V1-V3 with the selected wells from the focus area.

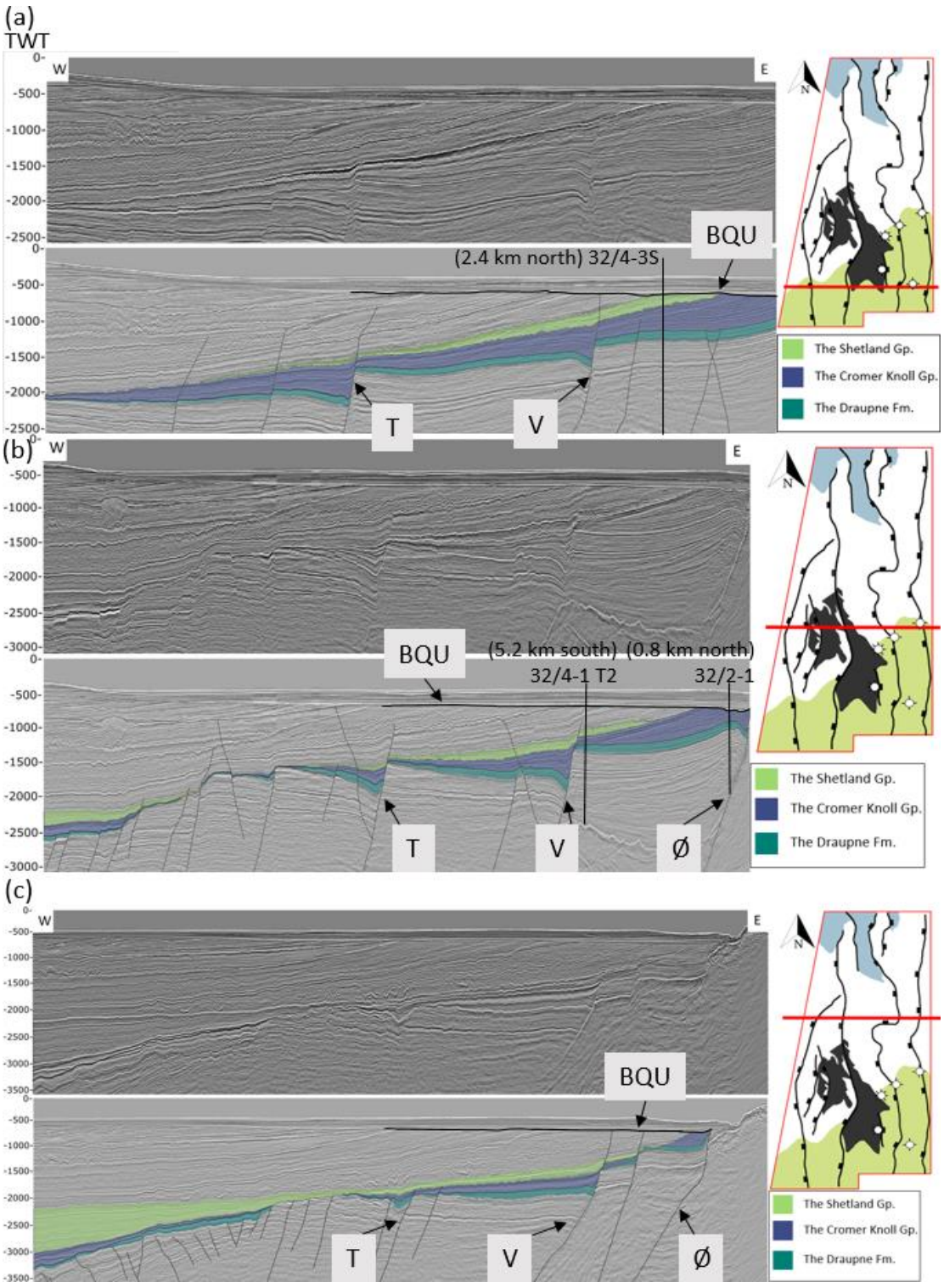

Figure 5.7: The E-W cross sections from the study area from south to north in TWT. Each transect has clean cross sections in "black grey white" with an interpreted version below. (a) Southern transect H1 from Xline 22075. (b) Transect H2 from Xline 24575. (c) Transect H3 from Xline 27075. BQU = Base Quaternary Unconformity, T = the Tusse fault, V = the Vette fault, and Ø = the Øygarden fault.

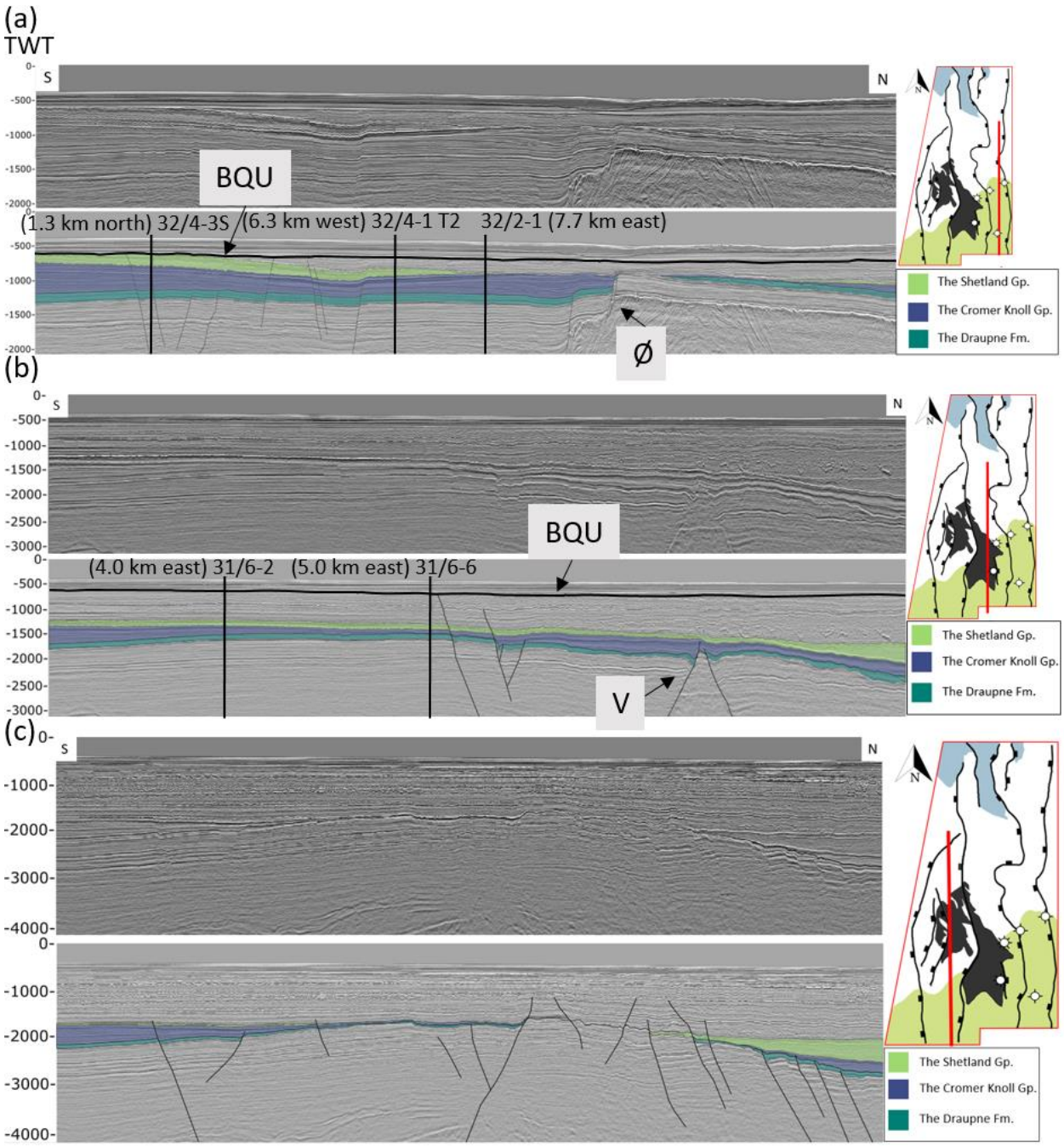

Figure 5.8: The N-S cross section from the study area from east to west in TWT. Each transect has a clean cross section in "black grey white" above it. The red marker on the map indicates where the cross section is from in the seismic cube. (a) Easternmost transect V1 from Xline 9750. (b) Middle transect V2 Xline 8750. (c) Westernmost transect V3 from Xline 7750. BQU = Base Quaternary Unconformity, V = the Vette fault, and Ø = the Øygarden fault.

5.1.4 Master Faults

The faults in the area have an N-S striking trend and are western dipping listric normal faults (Fig. 5.9). They are thick skinned, identified as the fault planes accommodate throw into the

basement (Fig. 5.9 (b)). Some N-S trending easterly dipping antithetic faults (blue) are present in the hanging wall slopes. The fault density increases towards the north.

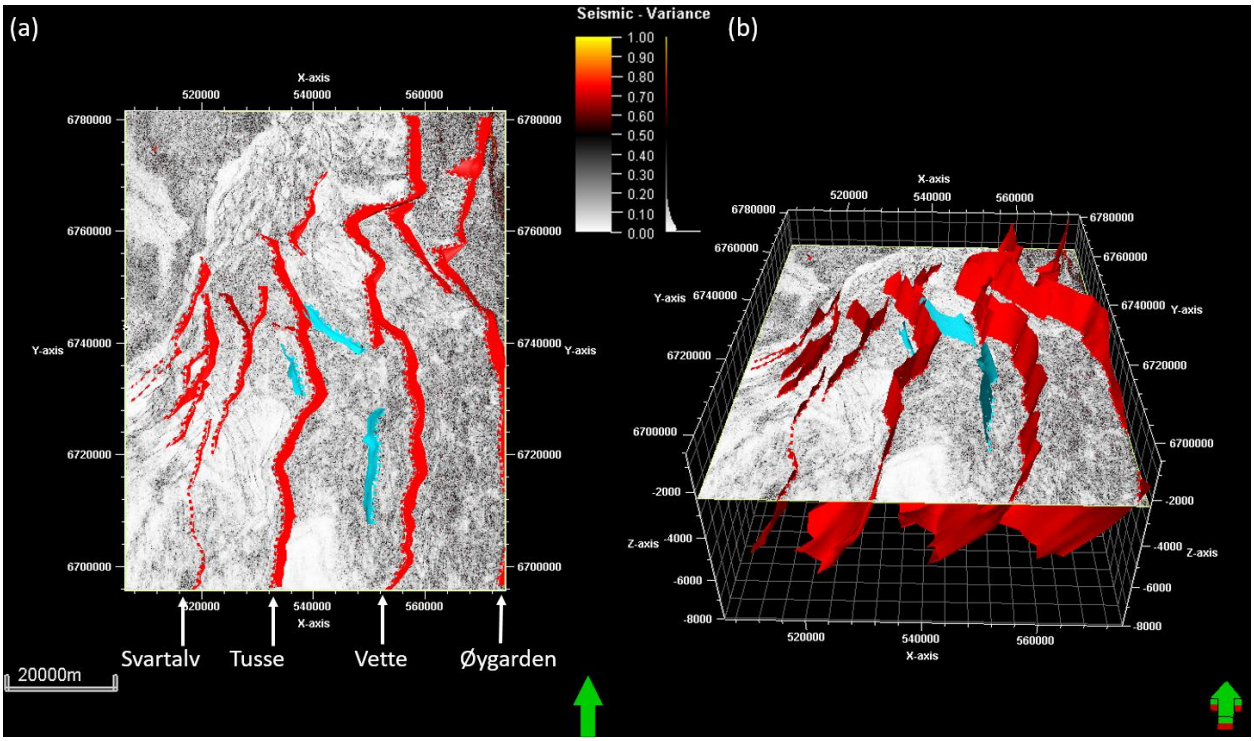

Figure 5.9: Interpreted faults plotted with the variance cube at -2300 ms depth TWT. Most faults are N-S trending, and red faults dip towards the west and blue faults dip towards the east. (a) visualizes the faults in a 2D window in petrel, while (b) showcases them in a 3D window.

The Øygarden fault complex is a series of faults comprising the easternmost master faults in the study area (Fig. 5.9). The fault complex accommodates throw from the BQU at the top down into the basement. The fault complex protrudes towards the west, located south of the 6760000 mark in the seismic survey (Fig. 5.9 (a)). The Vette fault zone locates west of the Øygarden fault complex (Fig. 5.9). The throw of the fault zone varies vastly across the area (Fig. 5.20), the cause for which will be covered in further detail in section 5.2. The fault has some antithetic faults in the hanging wall and a protrusion towards the west at the 6760000 mark. The fault has a section that dips towards the NW and SW north and south of the protrusion. The faults located west of the Vette fault zone are the Tusse and Svartalv fault zones (Fig. 5.9). These faults offset all the interpreted successions, including the basement. They accommodate the maximum amount of throw in the central to southern parts of the area. The faults included in the Svartalv fault zone become more NNE-SSW oriented on the Troll West High (Fig. 5.9).

5.2 Focus area

The Cromer Knoll Gp. can be subdivided into seismically defined units A, B, and C, labelled from base upwards (Fig. 5.11, Fig. 5.12, and Fig. 5.13). The units were chosen based on their reflection strength and how they changed spatially.

5.2.1 Cromer Knoll unit A

The Cromer Knoll Unit A is the lowermost unit and locates at about -730 ms depth in the southeastern area. The top of the unit has a general increase in depth towards the north and west, reaching a maximum depth of approximately -2100 ms (Fig. 5.10).

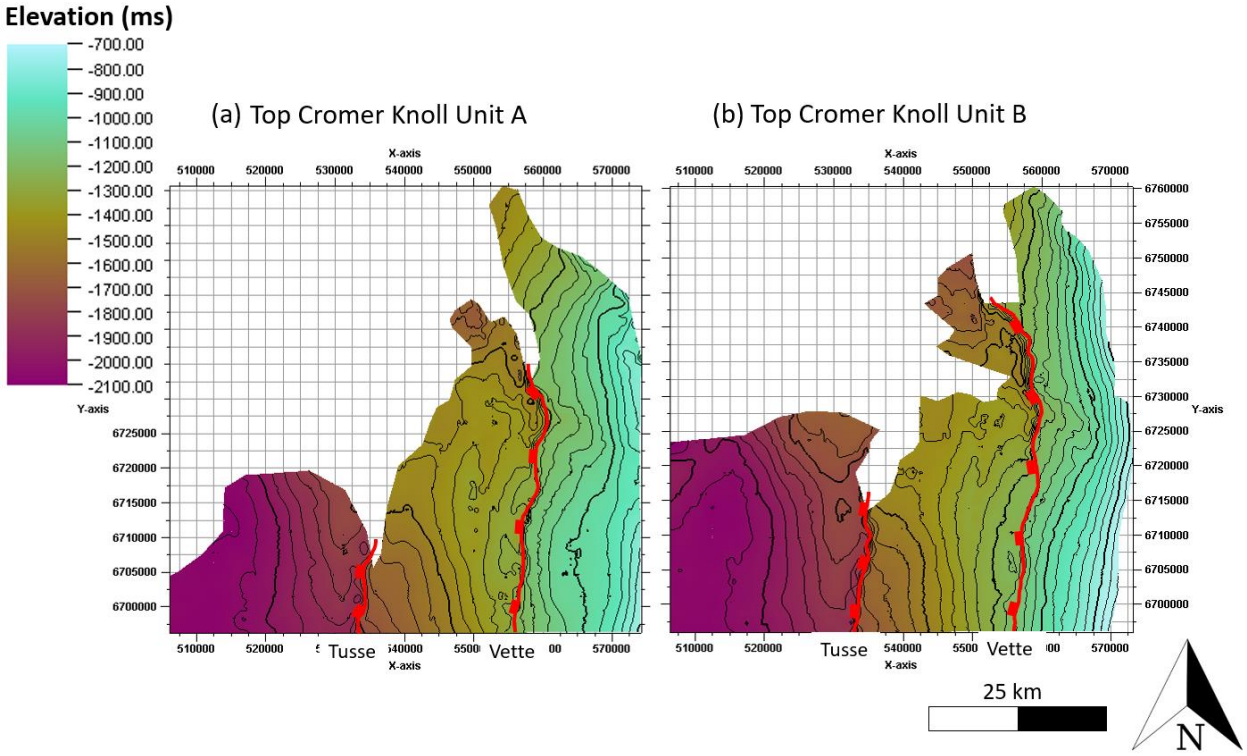

Figure 5.10: Time structure maps of the Top Cromer Knoll Unit A and B with a global color table. The Tusse and Vette faults are added as a red line. Top units A and B have their highest structural elevation in the east towards the Øygarden fault, and generally decreases in elevation towards the west and north.

The unit reaches a thickness of up to 320 ms in the hanging walls of the master faults south in the study area. It gradually thins out towards the fault scarps and extends towards the west until it pinches out on the Svartalv fault block (Fig. 5.11 (a)).

As the unit thins out further north, a syncline and an anticline are present in the hanging wall of the Øygarden fault, and Cromer Knoll unit A becomes lens shaped along the Vette fault block

(Fig. 5.12 (b)). The unit increasingly thins out further west on the Vette fault scarp. In the hanging wall of the Vette fault, the unit extends westward on the Tusse fault block until it is truncated below Cromer Knoll unit B (Fig. 5.11 (a), Fig. 5.12 (b)).

Cromer Knoll unit A has a lower gamma-ray than the Draupne Fm. but has a relatively high gamma-ray compared to the overlying units. The unit has a high gamma-ray throughout all wells except 32/4-1 T2, which is located at the crest of the Vette fault (Fig. 5.14).

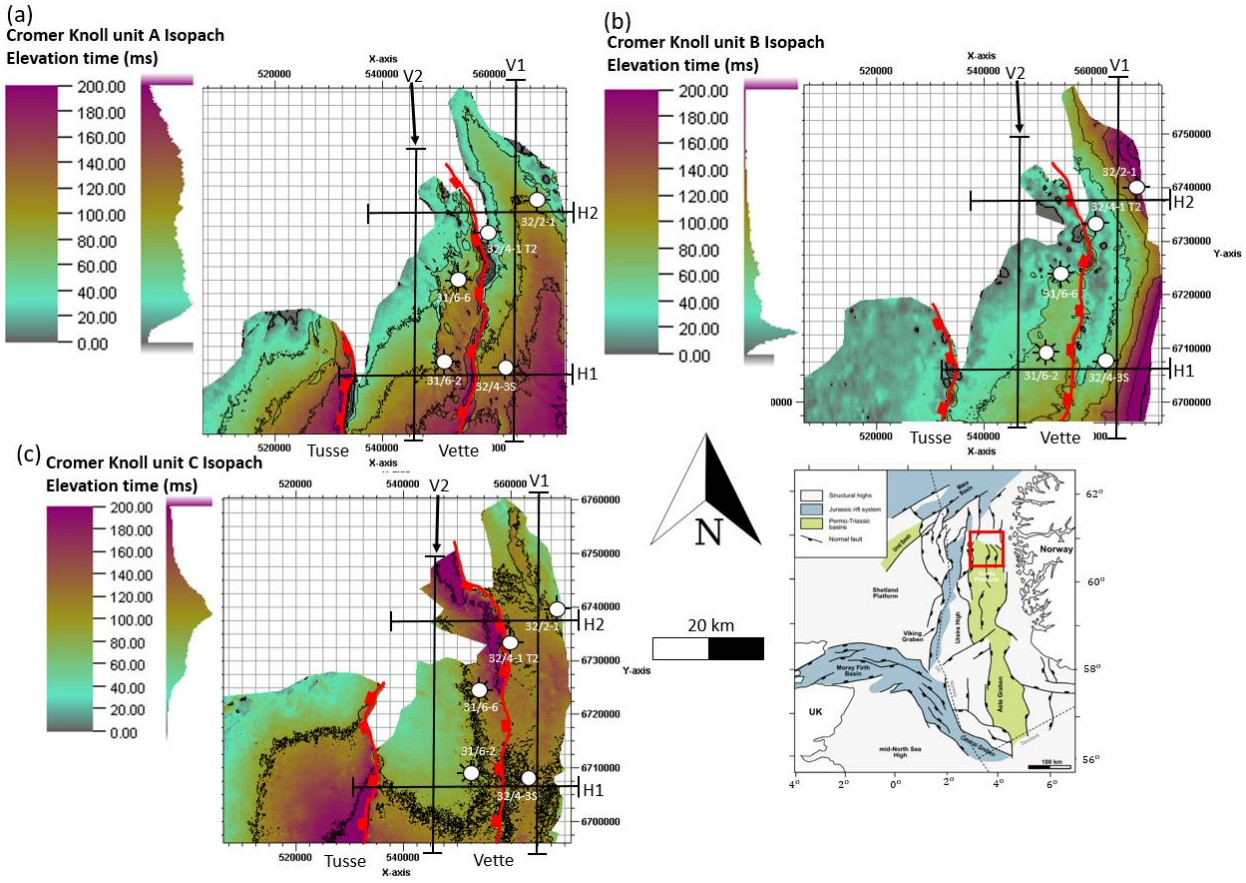

Figure 5.11*: Cromer Knoll units A, B, and C* isopach *maps plotted with a thickness from 0 to 200 ms. Thicknesses less than 5 ms area marked as a grey are. Unit A and B are plotted with a contour line spacing of 50 ms, while unit C is plotted with 100 ms. The maps are plotted with the zoomed in transects H1-H2, and V1-V2 with key wells added.*

5.2.2 Cromer Knoll unit B

Cromer Knoll unit B is located directly above unit A in the stratigraphy. The unit reaches its maximum thickness of approximately 260 ms in the eastern parts of the study area, where the BQU caps it at around -650 ms depth. It extends further towards the NW than unit A and has its lowest point at -2100 ms depth (Fig. 5.10 (b), Fig. 5.11 (b)).

The unit vastly decreases in thickness towards the crest of the Vette fault block, where it becomes ca. 80 ms in the south. The thickness then increases in the Vette and Tusse faults hanging walls until it gradually thins out and becomes absent in the west (Fig. 5.11 (b), Fig. 5.12 (a)).

The unit becomes absent along the Vette fault scarp northwards (Fig. 5.12 (b), Fig. 5.16). The thickness increases in the Vette fault hanging wall as the unit continuously extends toward the west until it is truncated above the Draupne Fm. (Fig. 5.12 (b)). The unit thins out towards the north until the 673000 mark in the seismic survey, and then it becomes thicker towards the Øygarden fault hanging wall, where it is approximately 190 ms thick (Fig. 5.13 (a)).

Cromer Knoll unit B has a lower gamma-ray than unit A. The unit has the highest values in its lower and upper parts, with a decrease towards the middle. The unit has its lowest gamma-ray value across the 32/4-1 T2, where it becomes inseparable to the unit A due to seismic resolution (Fig. 5.14).

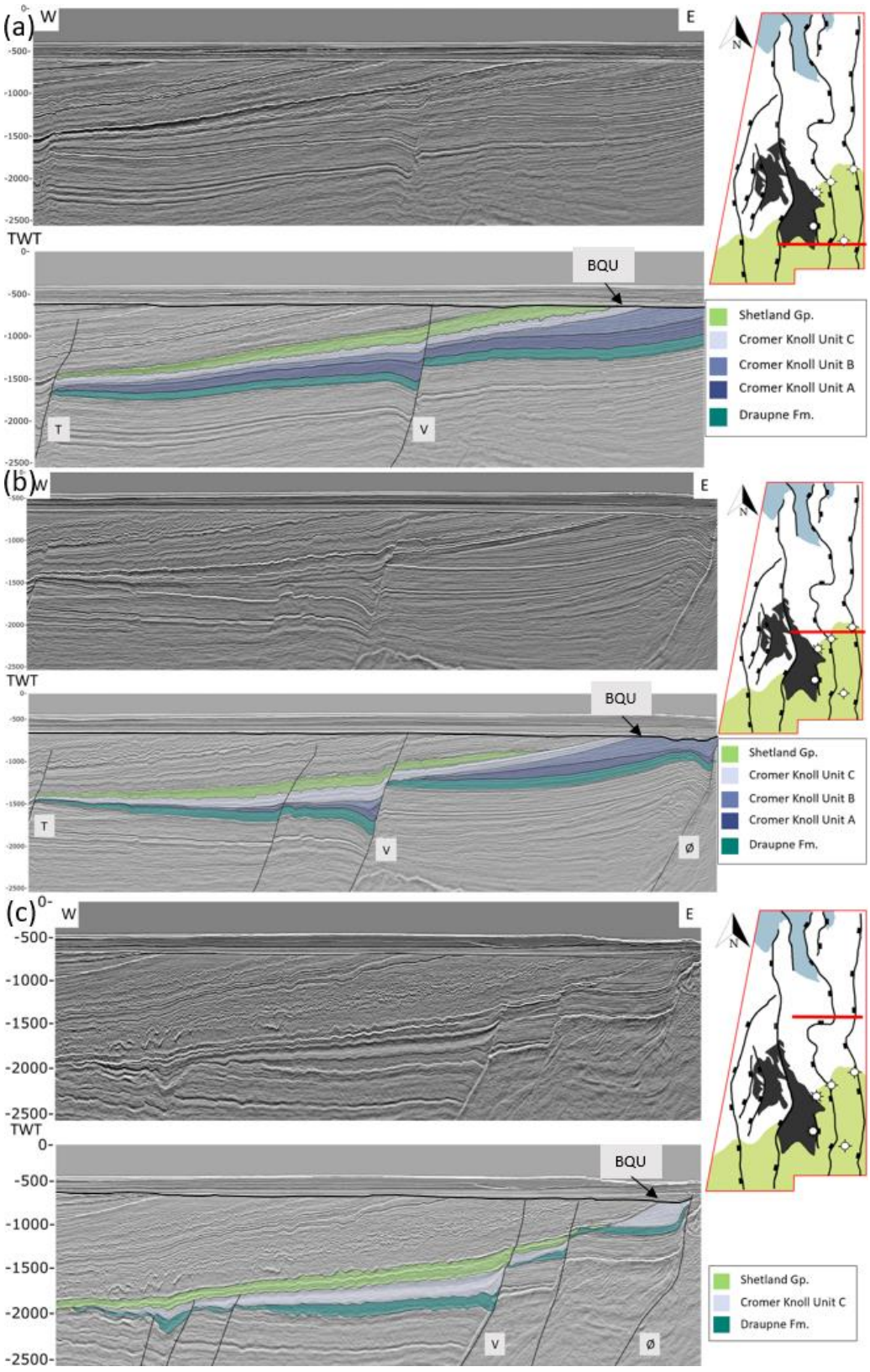

Figure 5.12: Zoomed in transects H1-H3 in the E-W direction with the division of the Cromer Knoll Gp. Ø = the Øygarden fault, V = the Vette fault, T = the Tusse fault, and BQU = Base Quaternary Unconformity.

5.2.3 Cromer Knoll unit C

The uppermost unit C is bound by the Shetland Fm. in the west or by the BQU in the east at ca. -650 ms depth. This unit is approximately 120 ms thick with little variations in the southeastern areas. The thickness increases to around 250 ms in the southern parts of the Tusse fault hanging wall but thins out towards the west of the seismic cube (Fig. 5.11 (c), Fig. 5.12 (a)).

Further north, the unit extends westwards with a uniform thickness of approximately 100 ms along the Vette fault block. It increases in thickness to ca. 210 ms in the Vette fault hanging wall, becoming around 45 ms thick at the Tusse fault scarp (Fig. 5.11 (c), Fig. 5.12 (b)).

Cromer Knoll unit C extends further northward that the underlying units A and B (Fig. 5.11 (c), Fig. 5.12). Cromer Knoll unit C has a lower gamma-ray than unit B. The gamma-ray within the unit decreases upwards in stratigraphy and appears similarly across all target wells. Unit C is absent in well 32/2-1 (Fig. 5.14).

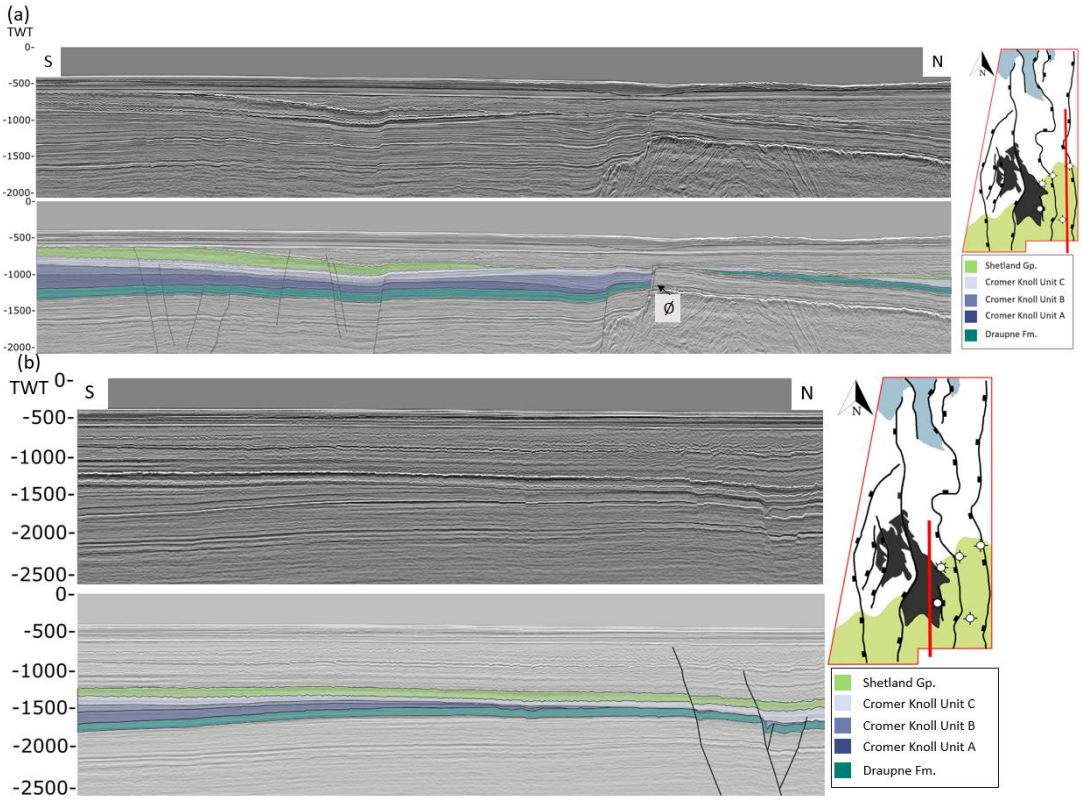

Figure 5.13: N-S transects V1 and V2 with the division of the Cromer Knoll Gp. (a) Transect V1 along the Vette fault block: Both units A and B are absent north of where the Øygarden fault cuts through the cross section, as only unit C extends further

overlying the Draupne Fm. (b) Transect V2 along the Tusse fault block: Unit A and B are absent north in the transect and The Cromer Knoll Gp. extends as unit C northwards. Ø = The Øygarden fault

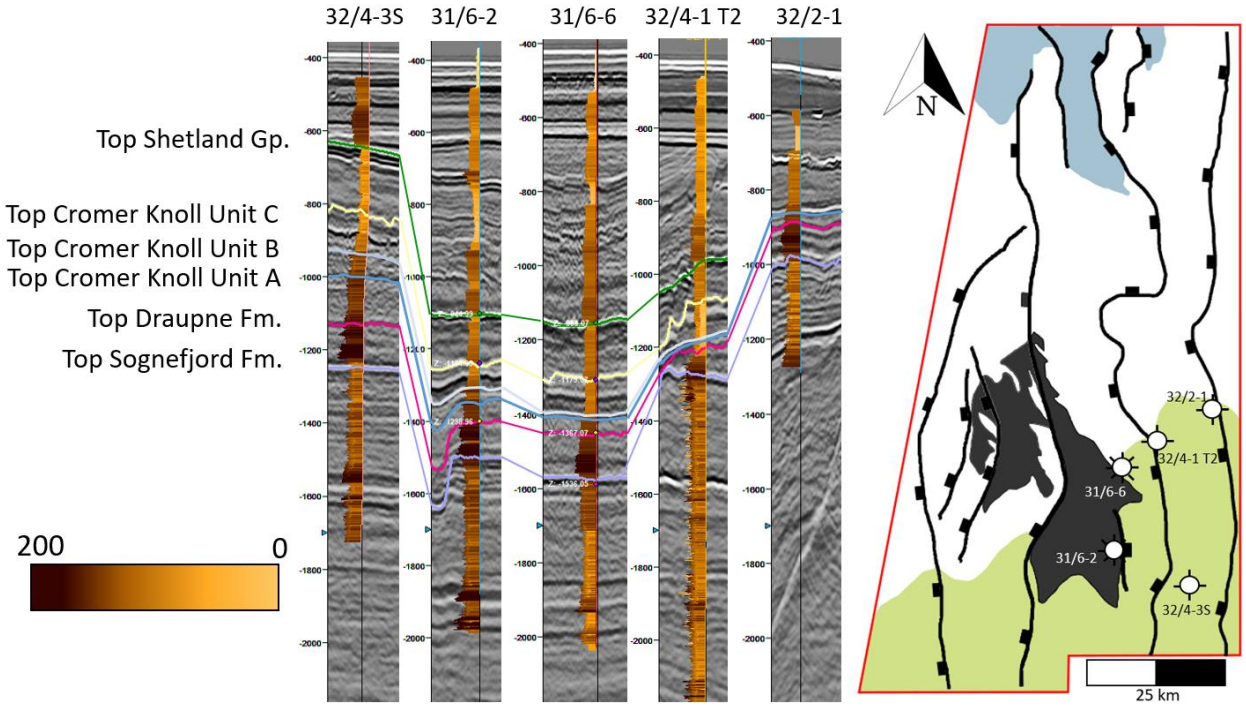

Figure 5.14: The interpreted horizons across key wells in the study area with the gamma-ray log. The map shows the wells' locations in the area. The gamma-ray log ranges from 0 to 200 API with an increasing value towards the left on the well log.

5.2.4 Stratal Terminations

To better understand the sequence stratigraphy of the study area, I focused on identifying the stratal terminations within the Cromer Knoll units. To identify the stratal terminations of the seismic horizons more easily, I flattened Top Cromer Knoll unit A across the Vette fault block on the transects H1-H2 and V1 (Fig. 5.15, Fig. 5.16, and Fig. 5.17) and added stratal terminations to transect H3 (Fig. 5.19).

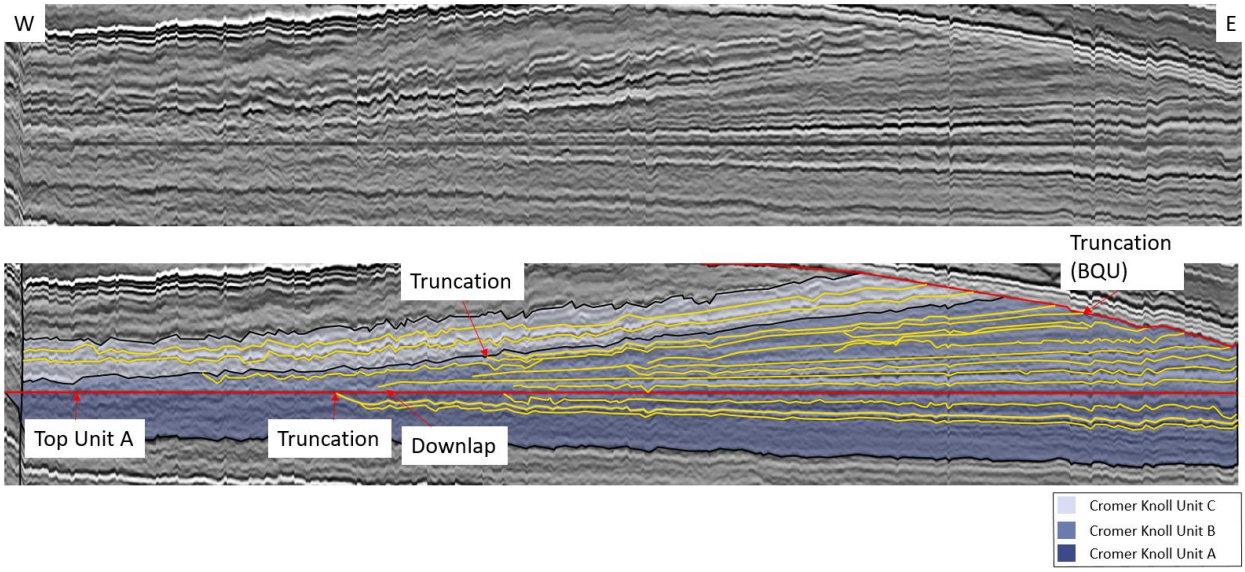

Figure 5.15: Transect H1 flattened on Top unit A (red) with some of the stratal terminations added. Cromer Knoll units A, B, and C are added with 50% opacity.

Cromer Knoll unit A

In the southern part of the study area, Cromer Knoll unit A is seismically transparent in the lower parts, making it difficult to track continuous reflectors in the east-to-west direction. The reflectors become more apparent in the upper part of the unit, and most of these are truncated at the base of Cromer Knoll unit B (Fig. 5.15). Furth north, the reflectors become clearer, and the horizons of Cromer Knoll unit A are truncated at the base of Cromer Knoll unit B in the west and eastern parts of the Vette fault block, creating a convex shape (Fig. 5.16). Unit A is truncated below unit B in the N-S direction and becomes absent north towards the Øygarden fault in transect V1 (Fig. 5.17).

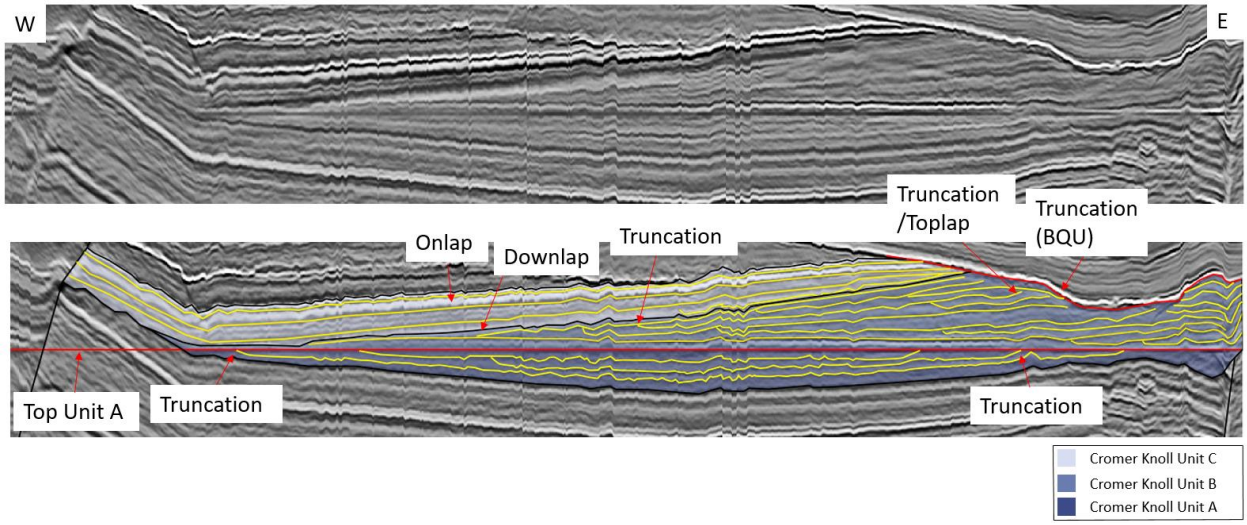

Figure 5.16*: Transect H2 flattened on Top unit A (red) with some of the stratal terminations added. Cromer Knoll units A, B, and C are added with 50% opacity.*

Cromer Knoll unit B

Cromer Knoll unit B thins vastly towards the west on the Vette fault block (Fig. 5.11 (b), Fig. 5.12 (b, c)). Geometrical relations of the lowermost part of the unit close to the Øygarden fault is not possible due to limited seismic coverage. However, it becomes possible upwards in the unit as the reflectors are truncated at the BQU (Fig. 5.15). The lowermost reflectors are interpreted to downlap onto unit A in a westward direction. Upwards in the unit, I identified sequences of internal truncation and downlap, and the unit's uppermost part was interpreted to be truncated at the base of Cromer Knoll unit C. Further north, more terminations of truncation/toplap are identified but are difficult to distinguish due the reflectors having a low angle discontinuity. Towards the west, the reflectors are internally truncated below their overlying successions, until top unit B is truncated below Cromer Knoll unit C (Fig. 5.16). In the N-S direction, the lowermost unit B observation identifies an internal backstepping geometry/erosional scar followed by a series of onlap northwards. To look further into this geometry, I flattened the erosional scar (Fig. 5.17) in the E-W direction. The erosional scar's extension is rather local and I observed horizons truncated below it (Fig. 5.18).

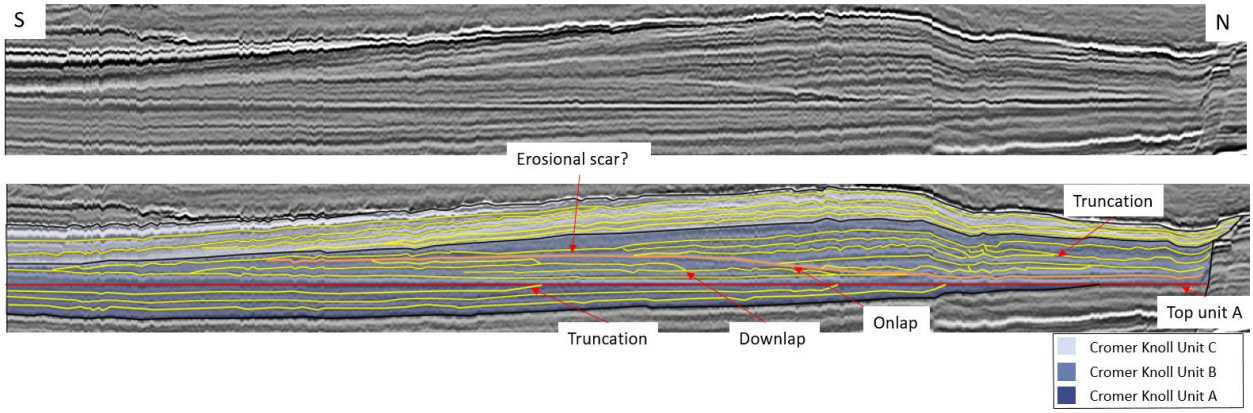

Figure 5.17: Transect V1 zoomed in and flattened on Top unit A (red) with some of the stratal terminations added. Cromer Knoll units A, B, and C are added with 50% opacity. The horizon marked as an erosional scar is colored orange.

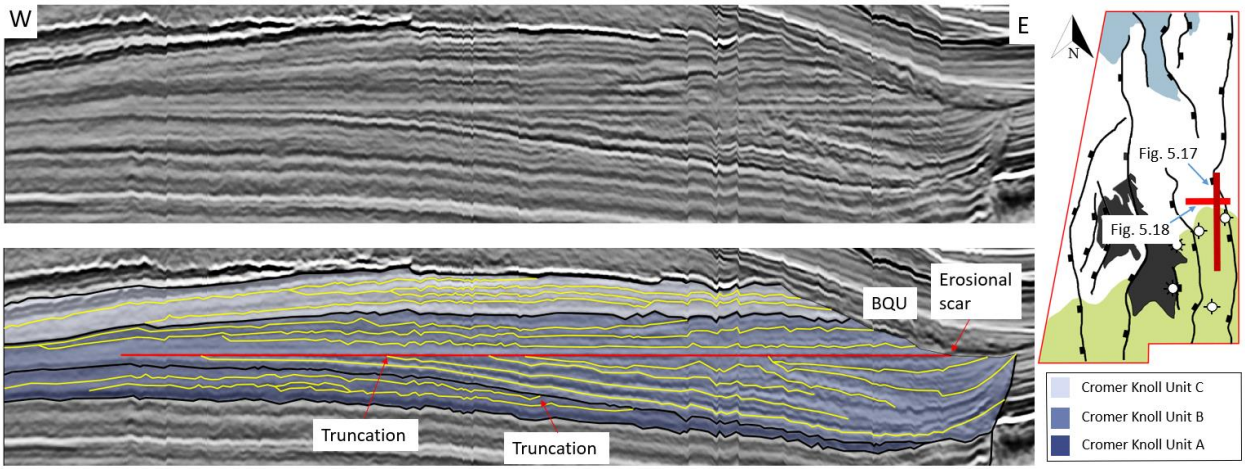

Figure 5.18: Flattened erosional scar in the E-W direction. The map shows where the cross section is taken from Fig. 5.17.

Cromer Knoll unit C

The uppermost Cromer Knoll unit C is observed as relatively conform compared to the lower units. The unit is truncated at the BQU in the east and extends westwards to the Vette fault with little signs of terminations (Fig. 5.15). The uniformity continues northwards as the unit is truncated at the BQU in the east. There are signs of downlap down to Top unit B, but the reflectors are poor. Upwards in stratigraphy, the unit is conform with highly visible reflectors (Fig. 5.16). The amplitude variations decrease on transect H3, making it more challenging to trace individual continuous reflectors. The lowermost reflectors onlap the Øygarden fault footwall in the east, while reflectors further up in the unit are truncated at the BQU in the east. On the easternmost fault block in H3, the termination within unit C is interpreted as baselap because it is difficult to distinguish between downlap and onlap. Further up in the stratigraphy,

the reflectors are truncated below the overlying horizons. Offlap is observed on the fault block adjacent to the left, and the unit extends uniformly towards the west until it downlaps onto the Draupne Fm. (Fig. 5.19). The trends are similar in the N-S direction. The unit is uniform, with some downlap above unit B in the southern part of V1 (Fig. 5.17).

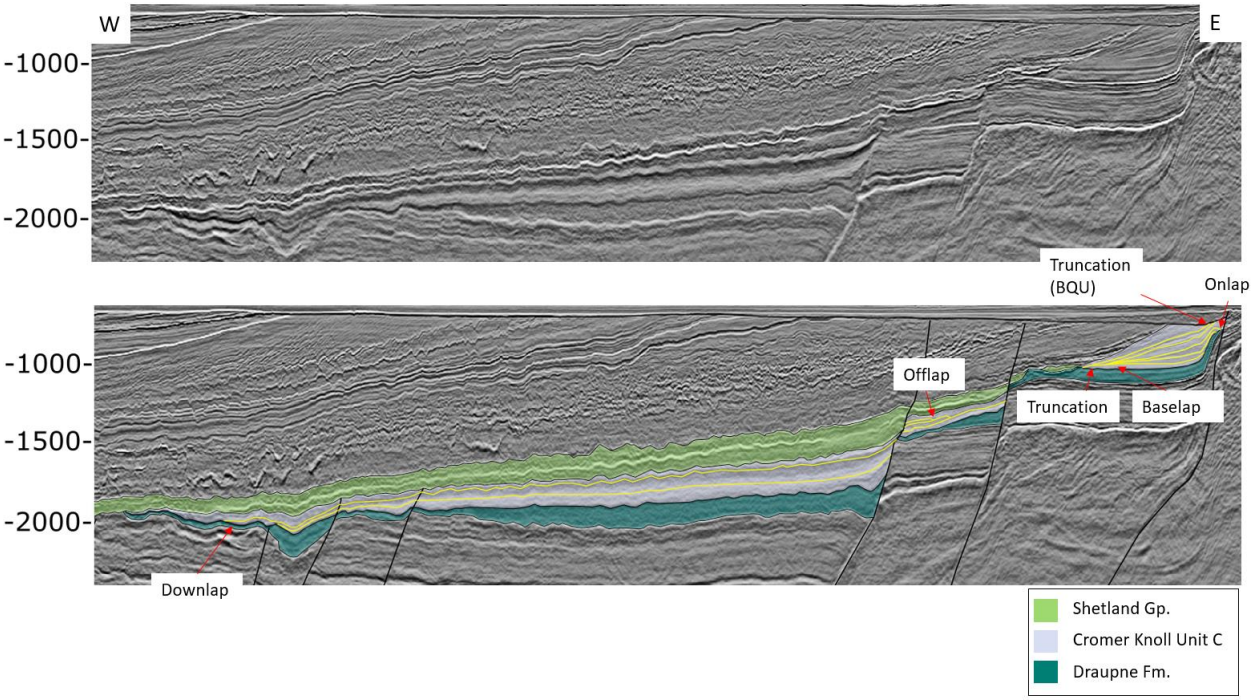

Figure 5.19*: Transect H3 with some of the stratal terminations added. Cromer Knoll units A and B are absent, and unit C is added with 50% opacity.*

5.2.5 The Vette Fault

The throw of the Vette fault varies in the N-S direction along strike, and I have plotted the offset of my interpreted horizons at every 250 lines (3.125 km) for the approximately 81 km covered by the TWT cube (Fig. 5.20). The Top Sognefjord Fm. has the greatest throw with a minimum of 85 ms in the south. Towards the north, it increases to a maximum of 635 ms at 56.25 km and reaches a local bottom value of approximately 300 ms at 65.625 km (Fig. 5.20). The Draupne Fm. has similar trends to the Top Sognefjord Fm. with a minimum throw of 80 ms in the south, increasing northwards to a maximum throw of 533 ms at 56.25 km. Cromer Knoll unit A has a minimum throw of 37 ms. The throw increases northwards until it reaches a peak of 298 ms at 46.875 km (Fig. 5.20). This unit is also absent north of this point. Cromer Knoll unit B has less offset than unit A, with no throw in the south, which increases northwards and has a maximum throw at 271 ms at 37.5 km. This unit is absent north of 46.875 km. Cromer Knoll unit C has no

throw in the south. Towards the north, it has a peak of 123 ms throw at 37.5 km north and a maximum throw of 186 ms at 81.25 km (Fig. 5.20). The Shetland Gp. has received the least faulting, with a minimum throw of 0 in the south and a maximum value of 83 ms 75 km towards the north (Fig. 5.20).

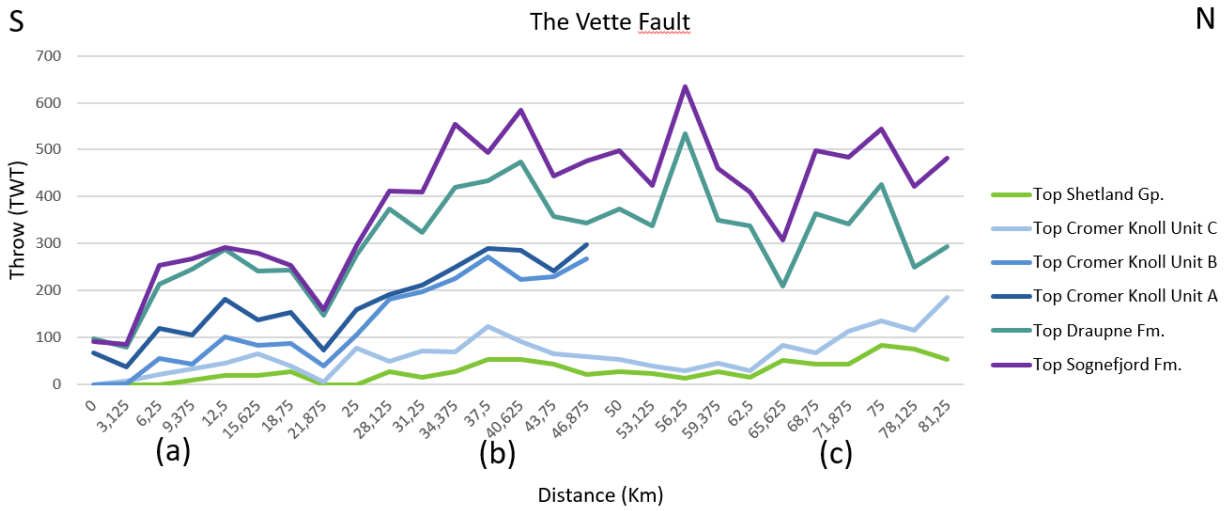

Figure 5.20: Throw vs distance profile of the Vette Fault covering approximately 81 km. The throw vs distance profile covers the studied units from south to north. Note that the Cromer Knoll Units A and B are absent north of 47 km. (a) is from transect H1, (b) from transect H2, and (c) from transect H3. They will be covered in figure 5.17.

The Vette fault reaches its maximum throw at the greatest depths, and the Top Sognefjord Fm. has a throw of 267 ms in the southern parts of the study area at around -1500 ms depth (Fig. 5.21 (a)). Moving northwards, the throw of the formation generally increases with some local top- and bottom points (Fig. 5.21 (b, c)).

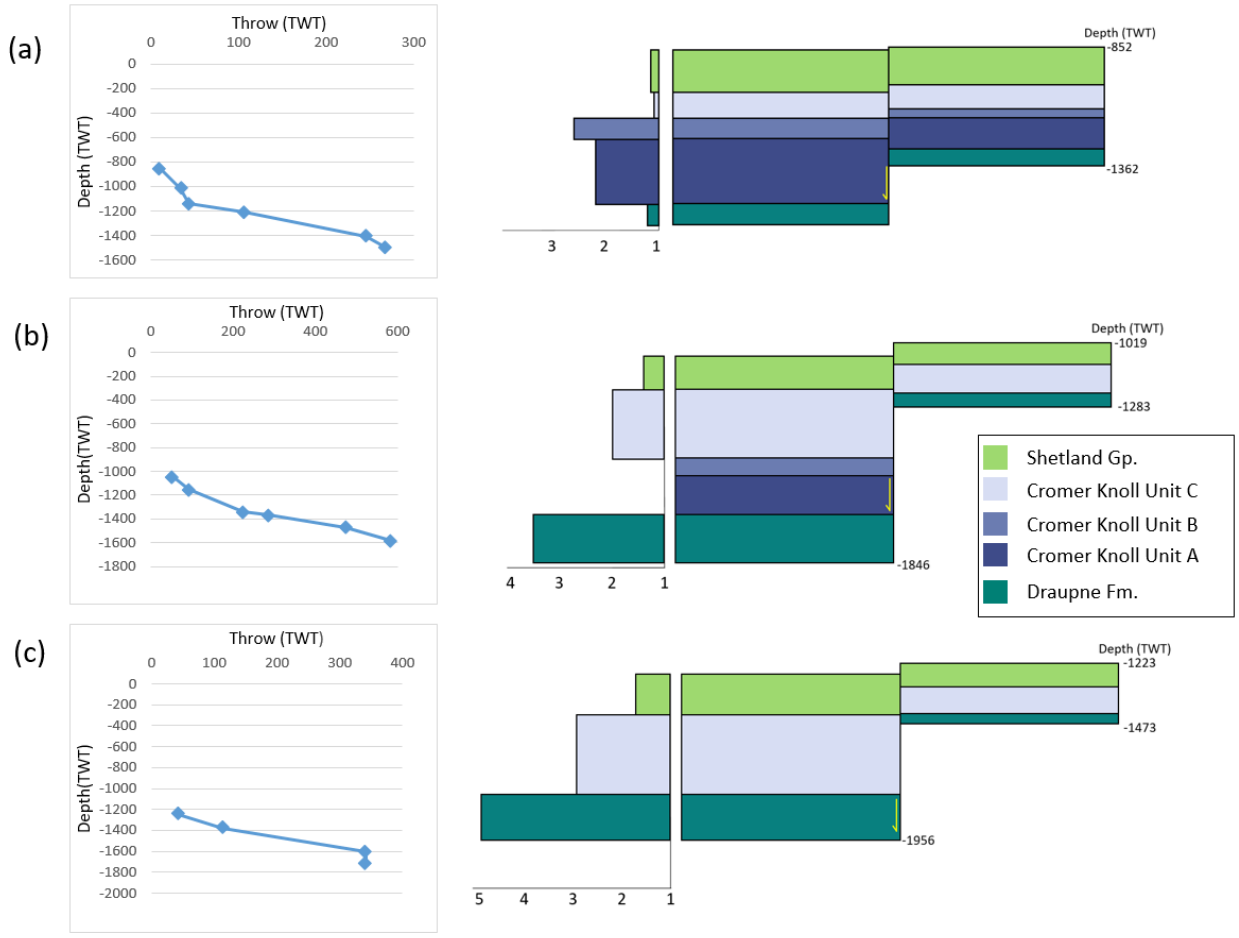

Figure 5.21*: Corresponding Throw vs Depth profiles and expansion indices (E.I.) from three target locations H1-H3 along the Vette fault. (a) Locates at H1 9.375 km along the fault, (b) locates at H2 on the 40.625 km, and (c) locates at H3 on the 71,875 km mark. The depth measurements in the throw vs depth profile are taken from the middle points between the top units in the footwall and the hanging wall.*

Upwards in stratigraphy, the Top Draupne Fm. has received less displacement, but it has much of the similar trends as the Top Sognefjord Fm (Fig. 5.21 (a, b, c)). The thickness of The Draupne Fm. increases from the footwall to the hanging wall and has an E.I. of 1.3 in the south (Fig. 5.21 (a)). The E.I. increases rapidly northwards and becomes 3.5 at the 41 km mark (Fig. 5.21 (b)). In the north of the study area, the formation reaches its maximum with an E.I. of 5.9 km (Fig. 5.21 (c)).

Cromer Knoll units A and B have a general increase in throw towards the north until they become absent. They become absent at around 41 km north in the footwall, and km in the hanging wall (Fig. 5.22, Fig. 5.23). They are therefore not included in the northernmost E.I. (Fig. 5.21 (c)). In the southern transect, unit A has an E.I. of 2.1 and unit B has an E.I. of 2.5 (Fig. 5.21)

The top Cromer Knoll unit C has received less displacement than the underlying Cromer Knoll units, with a throw of 34 ms in the south at -1019 depth (Fig. 5.21 (a)). The throw does not increase significantly further north (Fig. 5.20, Fig. 5.21 (b)), but contrary to the lower units, unit C increases in the throw furthest north in the study area, where it becomes 114 ms (Fig. 5.21 (c)). Based on my wheeler diagrams (Fig. 5.22, Fig. 5.23), this unit is more uniform than the underlying units and has an E.I. of 1.1 in the south, which increases to 2.0 and 3.0 north along the Vette fault (5.21).

The Top Shetland Gp. has no displacement in the south but has some increase northwards along the Vette fault (Fig. 5.20, 5.21 (a)). The E.I. increases northwards, as it is ca. 1.2 at 9.4 km, 1.4 at 41 km, and 1.7 at 72 km north (Fig. 5.21).

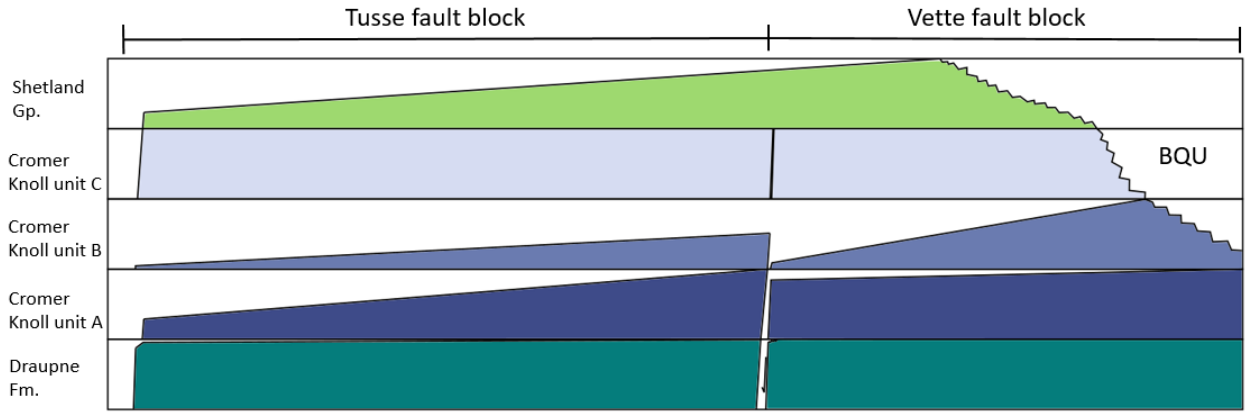

Figure 5.22: Wheeler diagram of the studied units from the zoomed-in intrasect H1. The BQU is marked as an erosional surface on Cromer Knoll unit B, C, and the Shetland Gp. The white spots between the units are hiatuses in the deposition.

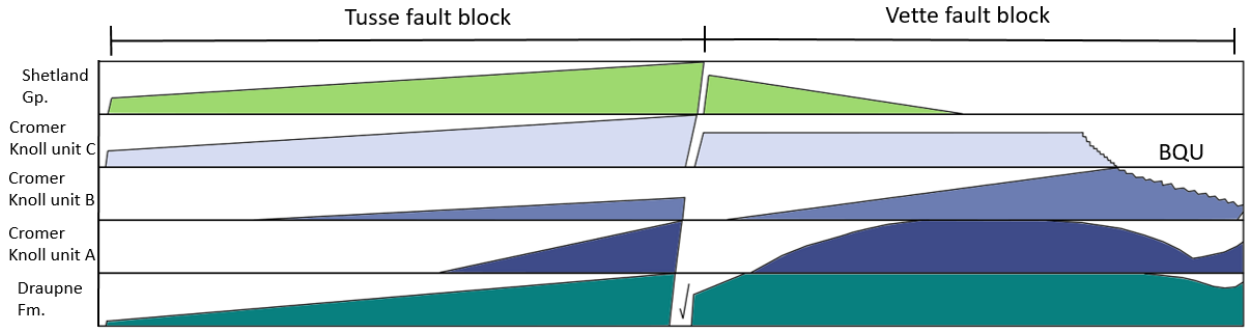

Figure 5.23: Wheeler diagram of the studied units from the zoomed-in intrasect H2. The BQU is marked as an erosional surface on Cromer Knoll unit B and C. The white spots between the units are hiatuses in the deposition.

6 Discussion

This chapter will discuss possible implications for CO_2 storage in the area of interest on the northern Horda Platform. In the previous chapter, I described the framework of the northern Horda Platform, where I covered the Draupne Fm., Cromer Knoll Gp., Shetland Gp., and the master faults in the area. I also described a focus area along the Vette fault with a focus on the Cromer Knoll Gp., which I will use to discuss the sealing capacities in the area. Furthermore, I will discuss the limitations and uncertainties of my studies and make suggestions for further research.

6.1 Evolution

In this section, I will discuss the structural and depositional evolution of the regional and the focus area. I will first discuss the regional evolution and then focus on the local evolution along the Vette fault from Middle Jurassic to Late Cretaceous.

6.1.1 Middle Jurassic – Lower Cretaceous

As described in section 2.2.4, the initiation of rifting phase 2 occurred during the Middle Jurassic (Duffy et al., 2015). Subsidence during this time led to the deposition of marine shales, and the North Sea was flooded during the Late Kimmeridgian to Late Berriasian. Anoxic conditions became the result, which led to the deposition of the organic-rich shale known as the Draupne Fm. (Whipp et al., 2014). This formation is a primary seal for potential CO_2 storage sites on the Horda Platform (Fawad, Rahman and Mondol, 2021).

A key sign of syn-rift deposition is a thickening of the formation in the hanging wall in relation to the footwall (Whipp *et al.*, 2014). My interpretation is that there were more tectonic activity northwards in the study area during the deposition of the Draupne Fm. This is shown in my results, as the formation's E.I. increases from 1 to 5 northwards (Fig. 5.21). My interpretation shows an eastern rotation of the Vette fault block from transect H1 to H2 (Fig. 5.7 (a, b)). The eastern rotation is accompanied by an increase in throw from transect H1 to H2 (Fig. 5.21 (a, b)). Eastern rotation and an increase in throw indicates that an increase in faulting led to flexural uplift of the footwall (Weissel and Karner, 1989). Based on my wheeler diagrams (Fig. 5.22, 5.23), the Draupne Fm. has not undergone much erosion on the Vette fault footwall. The

formation has likely been subjected to more erosion towards the Troll West high, as there more stratigraphic hiatuses located towards that direction (Fig. 5.22, 5.23)

Shales are very ductile, and some of the shales could be smeared along the fault plane during faulting due to friction. I interpreted shale smear along the fault plane of the Vette fault, this is seen as the Draupne Fm. is dragged up the fault plane of the Vette fault (Fig. 5.12). The shale smear increased the hanging wall thickness of the Draupne Fm. towards the fault plane.

6.1.2 Lower - Middle Cretaceous

The Cromer Knoll Gp. was deposited after the Draupne Fm. from the Lower Beriasian to Upper Albian. The group comprises the Åsgard, Tuxen, Mime, Sola, and Rødby formations and the Ran sandstone units (Isaksen, and Tonstad, 1989). It comprises fine-grained deep-marine clastics and carbonates with interbedded sandstones (Gabrielsen et al., 2001). This group acts as a secondary seal for potential CO_2 storage sites on the Horda Platform (Osmond et al., 2022).

As the group was deposited during the later stages of syn-rift 2 (Kyrkjebø, Gabrielsen and Faleide, 2004), one could expect a greater thickness in the hanging wall compared to the footwall of the master faults. My regional description of the Cromer Knoll Gp. shows a thinning from the south towards the north. Like the Draupne Fm., moving northwards, the relative thickness of the Cromer Knoll Gp. thins in the footwall and thickens in the hanging wall (Fig. 5.5 (a, b)). Based on these observations, I would interpret that there was increased tectonic activity northwards during the deposition of the Cromer Knoll Gp. More fault activity led to increased accommodation in the hanging wall of the master faults (Fig. 5.5). The Cromer Knoll Gp. in the north were therefore placed at a higher elevation than in the south, which led to the Cromer Knoll Gp. being subjected to more erosional processes northwards (Fig. 5.22, 5.23).

The lowermost unit A had a significant amount of thickness increase in the hanging wall compared to the footwall (Fig. 5.11, Fig. 5.13). A thickness increase is to be expected, as the lower Cromer Knoll Gp. was deposited during the later part of rift phase 2 (Kyrkjebø, Gabrielsen and Faleide, 2004). My interpretation of Cromer Knoll unit A, is that the Vette fault block was likely subjected to erosion after it was deposited. The erosion is observed as the unit A is truncated below Cromer Knoll unit B at the crest of the fault block. Moving northwards, unit A becomes lens-shaped, and the stratal terminations become more evident than in the south (Fig.

5.15, Fig. 5.16, Fig. 5.17). Truncations and a lens-shaped succession are indicators that unit A received more erosion further north than in the south (Catuneanu, 2020). Fault data indicates that Comer Knoll unit A received the most throw to the north (Fig. 5.20, Fig. 5.21). An increase in throw could mean more flexural uplift and more areas prone to erosion (Weissel and Karner, 1989).

Based on my results I interpret that erosional events occurred during the deposition of Cromer Knoll unit B. This is because internal strata within the unit continuously gets truncated by its overlying horizons. The erosion becomes more visible in the reflectors northwards, indicating a higher angel unconformity (Fig. 5.15, Fig. 5.16). An erosional scar is observed north in the focus area (Fig. 5.17, Fig. 5.18). The erosion is observed as internal strata is truncated below it in the E-W direction. This is a clear indication that Cromer Knoll unit B was eroded during deposition, followed by onlap of younger stratigraphy (Fig. 5.17). The Top Cromer Knoll unit B was also eroded after its deposition, as the horizons of the unit are truncated by base Cromer Knoll unit C (Fig. 5.16, Fig. 5.17).

The fault data indicates more throw of the Vette fault to the north (Fig. 5.20, Fig. 5.21 (a, b)). The unit is absent along the Vette fault scarp in the E.I. of Fig. 5.21 (b), which is also visualized by the wheeler diagrams (Fig. 5.22, 5.23). Together with an increased thinning in the NW direction (Fig. 5.11 (b)) and stratal terminations (Fig. 5.17, Fig. 5.18), this indicates that the erosion was more prominent in the north. I interpret based on these results that the Vette fault footwall received a flexural uplift during faulting. The footwall, which was placed at a higher elevation than the hanging wall was prone to erosion. The erosion of unit B is shown by figures 5.15 and 5.16.

The uppermost Cromer Knoll unit C was deposited after unit B during the later stages of rift phase 2. Based on my interpretation I would suggest that Cromer Knoll unit C was deposited while there still was an increase in tectonic activity northwards along the Vette fault. The unit was likely deposited in a period with lower tectonic activity compared to unit A and B. This is because the unit has a lower throw, and the E.I. is comparably lower than for the underlying units (Fig. 5.20, Fig. 5.21). The unit is conform, and based on my wheeler diagram it shows minor thickness variation along the Vette fault block (Fig 5.22, Fig. 5.23). I would therefore suggest that the footwall of Vette fault was located in a deeper environment less prone to erosion during

deposition. In addition, the unit contains a low number of stratal terminations across the Vette fault block (e.g. Fig. 5.15).

6.1.3 Middle – Upper Cretaceous

The Shetland Gp. was deposited during the Late Jurassic (section 2.2.5). The four lower Hidra, Hod, Tor, and Ekofisk formations result from open marine conditions with debris infill during a rise in sea level and consist of limestones, marls, mudstones, and shales (Deegan and Scull, 1977). The depositional environment became more open marine, which led to the deposition of the six upper Svarte, Blodøks, Tryggvason, Kyrre, Jorsalfare, and Hardråde formations consisting of siliciclastic shales and mudstone with some limestone interbedding (Isaksen and Tonstad, 1989). This group works as a tertiary seal for the Troll Field and potential future CO_2 storage sites (Osmond et al., 2022). My interpretation of the general thickness increase northwestwards is that the sink was based at the Lomre Terrace (Fig. 5.6). The Lomre Terrace was the deepest part of the area, which had the most sediment accommodation. The gamma-ray value of the Shetland Gp. increases from east to west, indicating more distal deposition at the Lomre Terrace, in relation to the Vette fault block (Fig. 6.1). The marine conditions at the Lomre Terrace led to the deposition of clay-rich units.

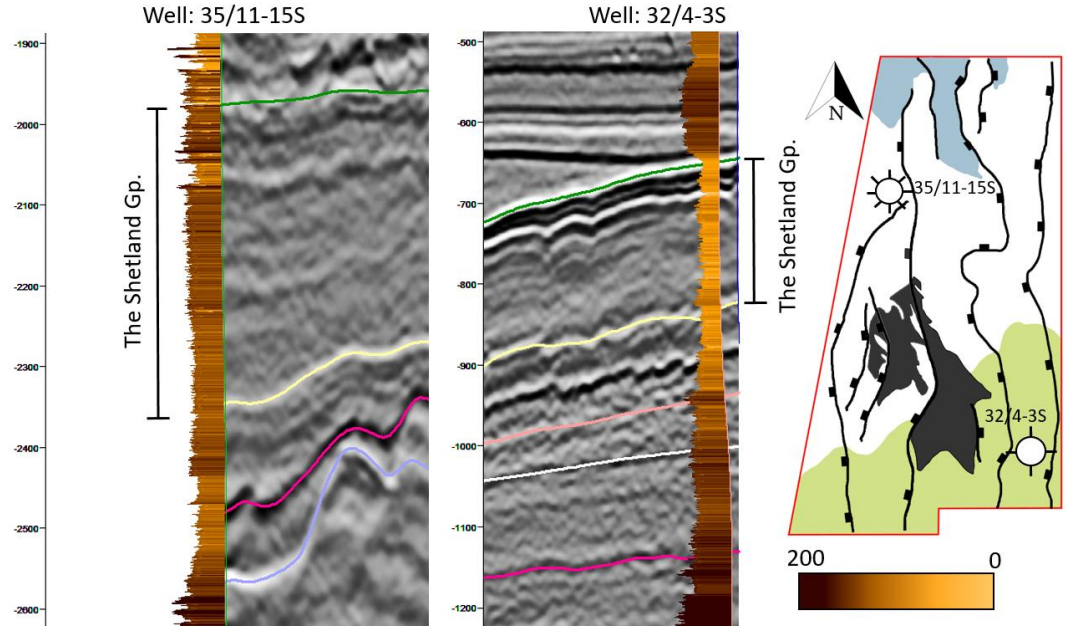

Figure 6.1: Well 35/11-15S located at the Lomre Terrace and well 32/4-3S located at the Vette fault block. The gamma-ray log is measured from 0 to 200 API.

Reactivation of the Master faults occurred after the deposition of the Shetland Gp., as the throw of the Top Shetland Gp. increases northward along the Vette fault. According to previous studies, The Troll West high was likely eroded during the Jurassic – Cretaceous (Known as the BCU). The high being located at high elevation during this time at a place where there were little accommodation, which led low amounts of deposition of The Cromer Knoll and Shetland groups (Kyrkjebø, Gabrielsen and Faleide, 2004).

Uplift during the Neogene led to an erosional event before the deposition of the Nordland Gp. (Wu et al., 2021), often labeled as the BQU. The BQU is seen as an angular unconformity that Cromer Knoll units B, C, and the Shetland Gp. is truncated below in my study area (Fig. 5.12).

6.1.4 The Vette fault

The throw vs distance diagram shows a general increase in throw northwards, but the throw of the Vette fault varies much locally (Fig. 5.20). Based on my results, I interpret that the Vette fault is hard-linked, as the fault accommodates throw across all my study area. I would suggest that the fault started out as smaller fault segments, but has linked up at later stages. These link-up points are located at the bottom-points in my throw vs distance plot (Fig. 5.20). The peaks are likely located where the fault segments initially started to breach. The fault interpretation in figure 5.9 shows that the Vette and Øygarden faults are close to linking up. My throw vs depth diagram indicates that fault activity was close to dying out during the deposition of the Shetland Gp., and further studies have concluded that there has been no reactivation of the Vette fault after the Early Cretaceous (Whipp *et al.*, 2014).

6.2 Sealing properties across the focus area

Factors controlling if a storage site is suitable for CO_2 storage are that the seal of the storage is impermeable, meaning no CO_2 can migrate through it. The storage site also needs to be located below -800 m depth, and if converted with a seismic wave velocity of 2 km/s to TWT, will be approximately:

$$TWT(ms) = \frac{Depth(m) * 2}{Vel\ (m/s)} = \frac{-800\ m * 2}{2\ km/s} = -800\ ms$$

Estimation with an average seismic velocity of typically 2 km/s leads to a depth of -800 ms.

The primary seal for potential CO_2 storage sites is the Draupne Fm. Therefore, a storage site where this formation is present would be preferable. Moving northwards along the Vette fault, the Drapune Fm. becomes eroded (Fig. 6.2). Injecting CO_2 at a lower elevation and letting it migrate upwards below the cap rock to the main structural trap would be preferable because the extended migration pathways would lead to more residual, solubility, and mineral trapping. The CO_2 will contact more grains over a larger area, immobilizing more CO_2 in the pore spaces. The CO_2 will then have more brine to react with, leading to solubility trapping. In addition, the CO_2 will later be mineralized (Fig. 1.3).

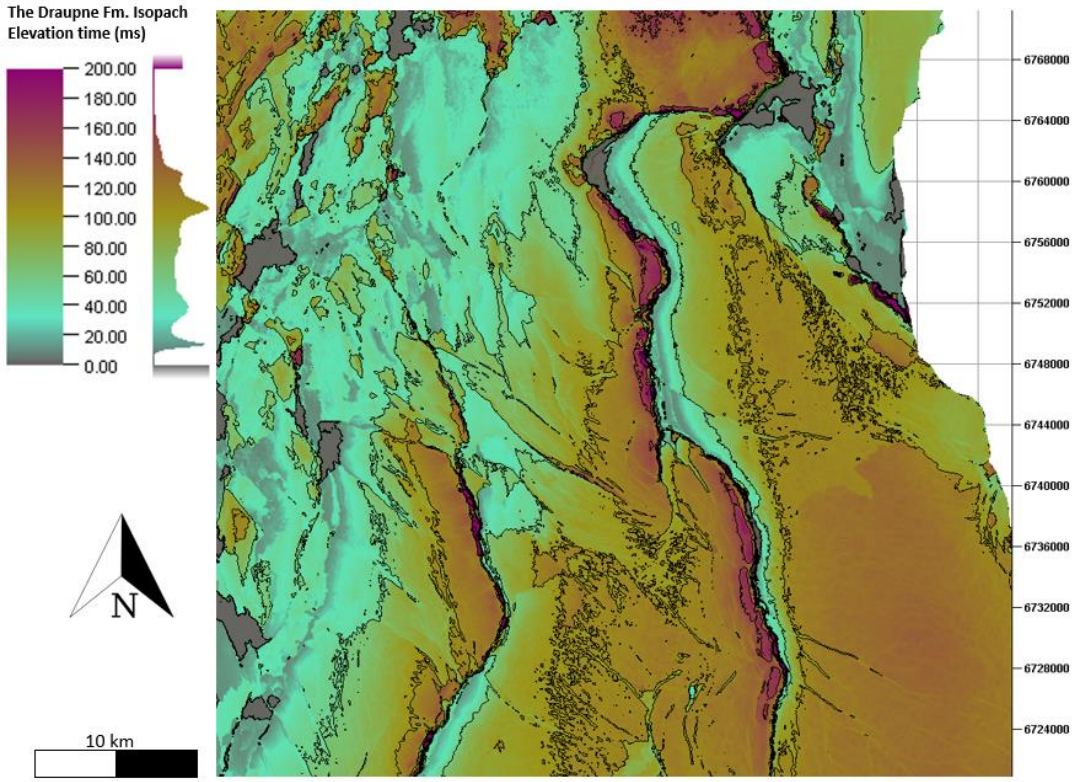

Figure 6.2: Zoomed in Isopach of the Draupne Fm. with a contour line spacing of 50 ms. Areas less than 5 ms thick are marked as grey areas.

Since the Draupne Fm. is eroded along the Vette fault Scarp (Fig. 6.2) and it is preferable to inject the CO2 at an elevation below the structural trap (Fig. 5.2), the overlying secondary/tertiary seals should be considered in areas where the Draupne Fm. is absent/thin.

I separated the Cromer Knoll Gp. into units A, B, and C as the lithology of the group change upwards in section (Fig. 6.3). Cromer Knoll unit A has a high gamma-ray value, which is often associated with shales. I suggest this unit has the best sealing properties of all the Cromer Knoll

units. Cromer Knoll unit B has the second-highest gamma-ray value of the Cromer Knoll units, so this unit should have the second-best sealing property. The uppermost Cromer Knoll unit C has a significantly lower gamma-ray than the other Cromer Knoll units, so this unit has poorer sealing properties.

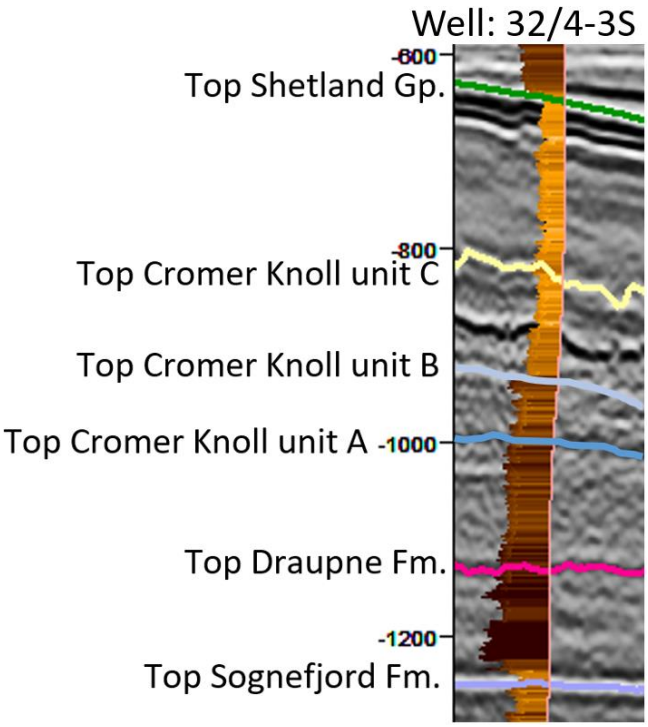

Figure 6.3: Gamma-ray log from well 32/4-3S from the Top Sognefjord Fm. to the Top Shetland Gp. The well log shows how the gamma-ray changes within the Cromer Knoll Gp.

Knowing the relative sealing properties of the Cromer Knoll units, the next step is to map their extension. After mapping units A and B, I can see that they truncate above the Draupne Fm. and have a shorter extension across the study area. Therefore, these units will not be sufficient direct seals where the Draupne Fm. is absent but as a secondary seal where thin successions of the Draupne Fm. could be a weak point. Based on my interpretation, the CO_2 traps are located in areas where the Draupne Fm. and Cromer Knoll units A and B are thin. The traps along the Vette fault footwall are created by uplift of the footwall, and the effect of the footwall uplift is that the sealing units became prone to erosional processes. It is therefore expected that the seal is eroded at potential storage sites.

As Top Cromer Knoll unit A likely has been eroded (Fig. 5.16), this could impact its sealing properties because the erosion could make the unit more heterogeneous (Holland and Elmore,

2008). According to wells in the focus area (Fig. 5.14), the gamma-ray is consistent upwards in the stratigraphy, indicating that the shale ratio remains the same across the unit.

As the erosion increases northwards, the sealing properties will likely decrease. Cromer Knoll unit B has been through a series of transgression, regression, and erosion (Fig. 5.15, Fig. 5.16, Fig. 5.17), events that could increase the heterogeneity. The Vette fault block has also undergone eastward rotation from transect H1 to H2. Therefore, the units have likely been more eroded towards the Vette fault scarp than towards the Øygarden fault (Fig. 5.12 (a, b)).

Cromer Knoll unit C is present across the whole focus area with no apparent signs of erosion except for the BQU, meaning there are no erosional events during the deposition of the unit to influence its heterogeneity. However, this unit has some significant amplitude variations, which is a sign of heterogeneities within the unit (Fig. 5.15, Fig. 5.16, Fig. 5.17). The large amplitude variations within this unit shows that the heterogeneities are not necessarily related to erosion, but rather a change in depositional system.

6.2.1 Potential Storage sites

My interpretation for a suitable potential CO2 storage site depending on the sealing properties, is based on the permeability and that the cap rock creates a secure trap to store it. Based on my results, this section will suggest preferred storage locations. I will then compare it to previous studies done for CO2 storage in this area. These factors indicate that storage sites 1 and 2 (Fig. 6.4) are the most secure CO2 sites.

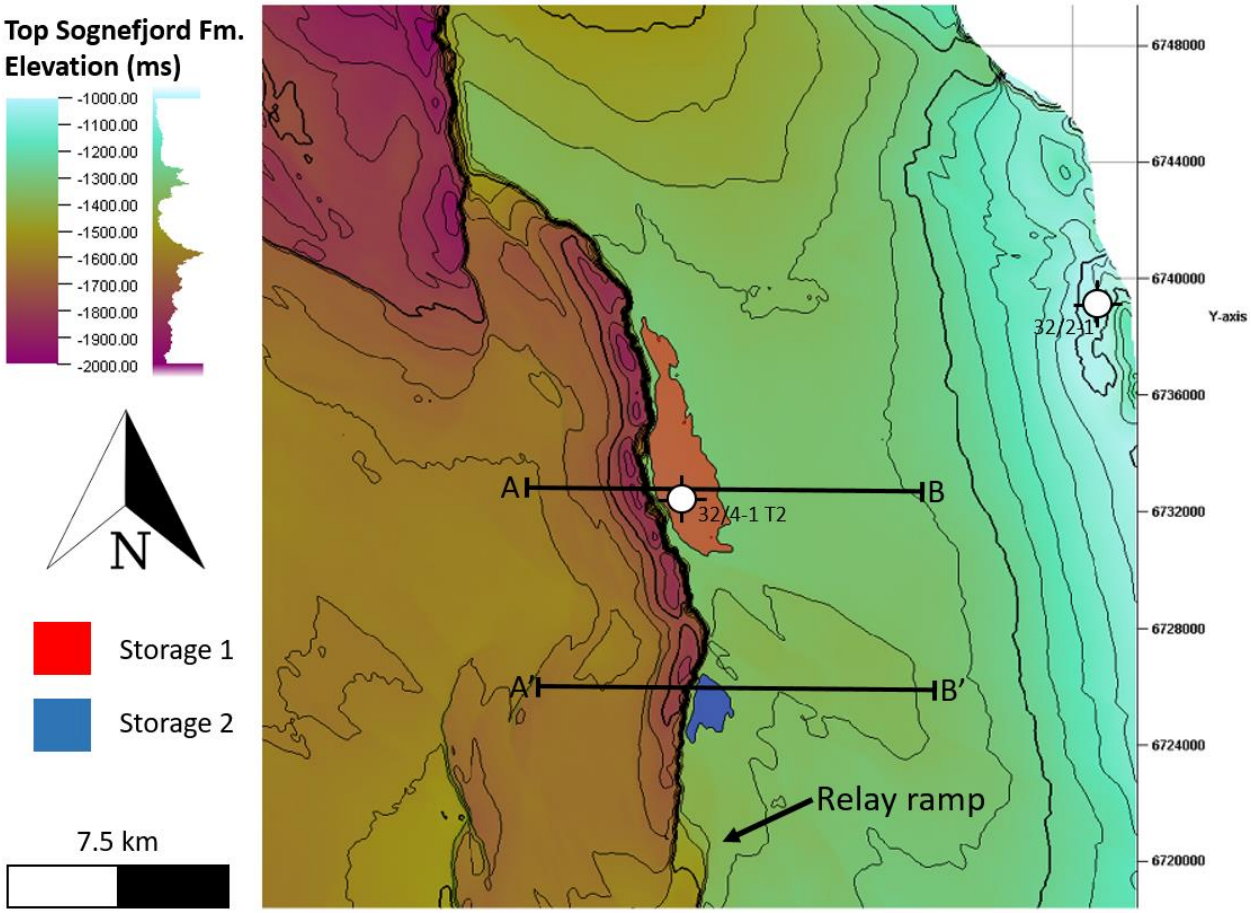

Figure 6.4: Zoomed-in time structure map of the Top Sognefjord Fm. with my interpreted storage sites. A-B covers an E-W transect of storage site 1, and A'-B' covers a transect of storage site 2.

Storage site 1

Storage site 1 locates at a footwall transverse anticline on the Vette fault (Fig. 6.4), which is bounded by flexural uplift of the Draupne Fm. and juxtaposition of Cromer Knoll unit C (Fig. 6.5 (a)). This storage site is located further north in an area with more erosion and where the Vette fault's throw is higher than the second storage site. This site is also sealed off in the hanging wall by Cromer Knoll unit C, which has a relatively low gamma-ray value with signs of heterogeneities. This storage site covers a larger volume than storage site 2, but the sealing properties are more uncertain.

Storage site 1 has previously been studied as a potential CO2 storage site, where this storage site was proposed as the Alpha storage site (Mulrooney et al., 2020; Wu et al., 2021). The studies proposed that injection beyond the spill point will accumulate in a Beta storage site in Øygarden fault hanging wall near well 32/2-1 (Fig. 6.4). Well 32/4-1 T2 is drilled through the seal and aquifer of potential Storage site 1 (Fig. 6.4). In this well, a 107 m thick succession of the

Draupne Fm., 3 m thick succession of the Åsgard, 25 m thick succession of the Rødby formation and a 235 m thick succession of the Shetland Gp. (Where the lower 125 m are the Svarte Fm.) are present in well 32/4-1 T2 (NPD, 2002). The Svarte Fm. is included as a part of the Upper Cromer Knoll Gp. in this study (Chapter 2.2). This implies a thick seal of low permeable rocks above the aquifer, and indicates that the highest risk is related to the juxtaposition seal of Cromer Knoll unit C.

Wu et al. covers the sealing capacities of the southern parts of the storage site at well 32/4-1 T2, but as this study area has a northward thinning of the top seal, more detailed studies should be done on the northern parts of this storage site, as the well data is more limited.

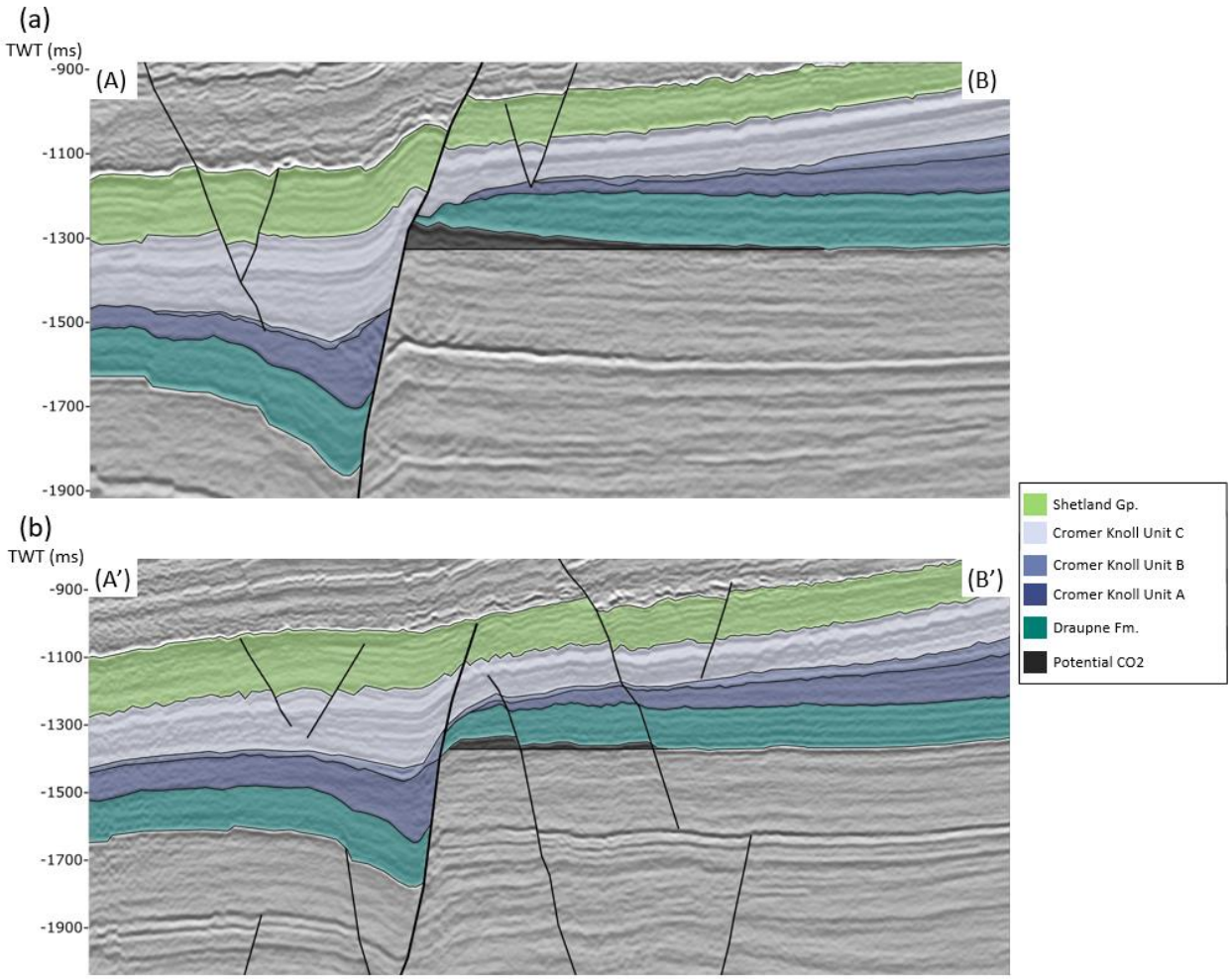

Figure 6.5: Potential aquifers for CO_2 storage with CO_2 added. (a) E-W transect of storage site 1, and (b) storage site 2 marked on Fig. 6.4.

Storage site 2

Storage site 2 is located south of storage site 1 and is located on the Vette fault footwall (Fig. 6.4). This storage site covers a smaller volume than storage site 1 but is placed in an area where the throw of the Vette fault is lower than for storage site 1 and there are also fewer signs of erosional events. However, antithetic faults are present through the potential storage site, which could influence the seal (Fig. 6.5 (b)). This storage site is likely capped by the Draupne Fm. and sealed in the hanging wall by Cromer Knoll unit B.

After spill point injection of CO2, the CO2 will follow the highest elevation and migrate upwards below the Draupne Fm. towards the Øygarden fault hanging wall.

6.3 Limitations

The research conducted in this thesis leads to uncertainties due to the seismic resolution and limited well-data. The seismic cube does not cover the southern parts of the Øygarden fault in the study area, and I should therefore be careful to consider a Beta aquifer for the potential CO_2 storage sites suggested in section 6.2.

The seismic resolution is a limiting factor in subsurface interpretation as described in section 4.3. The resolution could give inaccurate data that can be essential for a seal analysis. As the units in my study area thin northwards, the point of where the units become absent could be inaccurate due to the units being too thin to be caught up on seismic.

The most accurate information about the subsea comes from well-data. Therefore, this should be used as much and effectively as possible. Unfortunately, well-data from my focus area was restricted, and information about the formations of the Cromer Knoll Gp. were not available. For this reason, there was no attempt to classify Cromer Knoll units A, B, and C into the Åsgard, Tuxen, Mime, Sola, Rødby formations, the Ran sandstone units, and the Svarte formation.

A restricting factor for my studies where the eastern boundary of the seismic cube because the data was cut west of the Øygarden fault in the southern parts of my study area. Previous studies proposed a Beta aquifer for Storage site 1 in the hanging wall of the Øygarden fault. The Beta storage site has been considered to have fault related containment risks, due to fractures in the hanging wall (Wu *et al.*, 2021; Gubbi, 2022).

The lithological sealing properties of the Cromer Knoll units A, B, and C in my studies are entirely based on their gamma-ray value. The gamma-ray is based on the unit's natural radioactivity (chapter 4.2). This means that naturally radioactive rocks with high permeability would be registered with a high gamma-ray value. This could for example occur if allochthonous shale fragments are transported to a location where permeable rocks already are deposited. Therefore, other well logs such as sonic and density should be used if there is available data.

6.4 Further Research

This study investigates the top seal variability for potential CO_2 storage sites along the Vette fault. As this study contains uncertainties due the seismic resolution and restricted well-data, more studies should be done in this area to reduce the risk of using it as a CO_2 aquifer.

- The Cromer Knoll Gp. varies greatly across the Vette and Tusse fault blocks and the group is also used as a juxtaposition seal for potential storage sites (Fig. 6.4). Therefore, an in-depth study on the lithology of the Cromer Knoll Gp. in these areas should be done to better establish the sealing properties.

- There has previously been done research on the Øygarden fault hanging wall (Gubbi, 2022), but more research should be done on the migration pathways from Storage site 2 to the potential Beta aquifer. Furthermore, the sealing variability for the Beta aquifer should be analyzed as it may have similar containment risks as the Storage site 1 beta aquifer.

- The spatial variation of The Cromer Knoll Gp. is significant across the northern Horda Platform. Therefore, detailed research using biostratigraphy would be useful to further identify lithological variations within the group. Little well data is available just north of well 32/4-1 T2 and 32/2-1. Detailed studies of the Cromer Knoll Gp. is therefore slim and should be further studied in this area.

- I would suggest that more research should be conducted on the aquifers of the potential CO_2 storage sites. The Sognefjord, Fensfjord, and Krossfjord formations of the Viking Gp. are the designated CO_2 aquifers on the northern Horda Platform (Wu *et al.*, 2021). Therefore, detailed analysis on how these formations vary spatially in porosity and permeability should be done. Mineral trapping is the most permanent trapping

mechanism, which is highly dependent on the mineral composition of the aquifer. Getting an understanding of the mineral composition would therefore help to determine the speed of mineralization.

- If the injection point is placed at the storage site, the CO_2 injection can weaken the cap rock. The injection point should therefore be placed at a lower elevation than the CO_2 storage sites. Further research could propose possible injection sites.

7 Conclusions

This thesis aims to better understand the spatial and temporal development of the Late Jurassic to Middle Cretaceous depositional systems and their influence on the top seal for potential future CO_2 storage sites on the northeastern Horda Platform. I hypothesize that the northward thinning of the seal and the increase in tectonic activity reduces the sealing capacities. Based on my results, I assess if the area of interest is sufficient for CO_2 storage.

The key objectives of this project are:

1. To establish detailed seismic stratigraphy for the uppermost Jurassic and Cretaceous successions, using a continuous coverage broadband survey tied to wells with key stratigraphic information and good stratigraphic control on the Horda Platform in the outlined area of interest.
2. To interpret key horizons, with a focus on key horizons in the Upper Jurassic and Lower Cretaceous in the area of interest.
3. To map the correlation of time and lithology in selected wells to establish an understanding of the development of unconformities.
4. Interpret key faults to understand the fault development in the area.

Objectives 1) and 2) are solved by creating well-ties with key stratigraphic information from the uppermost Jurassic to the middle Cretaceous. Objective 3) is met by selecting key transects in the E-W and N-S directions, creating wheeler diagrams, and interpreting the stratal terminations. Objective 4) is solved interpreting the main structural features in the area of interest. The Vette fault is further studied by creating fault diagrams and transects.

The main observations from my research objectives are:

- The interpreted horizons include the coverage of the Top Sognefjord Fm., Top Draupne Fm., Top Cromer Knoll Gp., and Top Shetland Gp. The Cromer Knoll Gp. is divided into units A, B, and C in a focus area for further investigation. The successions are thinning

towards the structural highs and are located at a deeper elevation towards the Lomre Terrace. Cromer Knoll units B, C, and the Shetland Gp. are truncated below the BQU in the southeastern part of the study area.

- Stratal terminations and thickness variations indicate several events of erosion. The Draupne Fm. has not received much erosion along the Vette fault, as the erosion is likely focused towards the Troll West high. Erosion in Cromer Knoll unit A is observed on the Vette fault footwall, as the Top of the unit is truncated below Cromer Knoll unit B. An erosion scar within unit B indicates erosional events during its deposition. Cromer Knoll unit C and the Shetland Gp. are conform with few stratal terminations except for the BQU, indicating little erosion.

- The interpreted faults are generally N-S oriented and western dipping. The master faults in the study area are thick-skinned listric normal faults and include the Svartalv, Tusse and Vette fault zones, and the Øygarden fault complex. The Vette fault has a general increase in throw northwards and an increase in throw with depth for the interpreted successions.

- The Vette fault diagrams and E.I. indicate that the fault was mostly active in the Middle to Late Jurassic, and that the faulting had a continuous decrease up to the Middle Cretaceous. The erosion observed on the Vette fault footwall is likely related to flexural uplift during faulting, as the truncations observed at the top of the units are more prominent for units A and B in relation to C.

My objectives are used to answer my research questions, and to confirm validity of my hypothesis:

- The Draupne Fm. is the primary seal for potential CO_2 storage sites on the northern Horda Platform. This formation has received a northward thinning in my focus area and becomes absent some places on the Vette fault footwall. Therefore, the Draupne Fm. will not be adequate and the Cromer Knoll Gp. becomes a direct seal for CO_2 storage along the Vette fault.

- The upwards gamma-ray decrease for the Cromer Knoll units indicate reduced sealing properties from Lower to Upper Cromer Knoll. Cromer Knoll units A and B have more

distinct thickness variations along the Vette fault and do not extend as far west and north as unit C. The thickness variations of the Cromer Knoll units are related to tectonic activities. Therefore, I will conclude that the northwards thinning and increase in tectonic activity reduces the top seal integrity of the Upper Jurassic to Lower Cretaceous successions on the northern Horda Platform.

- My research provides two potential CO_2 storage sites on the Vette fault footwall. These potential storage sites are selected based on their trapping mechanisms, which are: 1) The CO_2 aquifer is covered by a structural trap, preventing CO_2 migration. 2) The Vette fault has a potential juxtaposition seal, thus preventing CO_2 migration across the fault. There are more implications to CO_2 storage than what I conduct in this study. Therefore, I suggest more research regarding detailed top seal analysis, migration pathways, and aquifer integrity on the northern Horda Platform.

References

Anderson, E.M. (1905) *The dynamics of faulting*. Available at: https://doi.org/10.1144/transed.8.3.387.

Bachu, S., W.D. Gunter and E.H. Perkins, 1994: Aquifer disposal of CO2: hydrodynamic and mineral trapping, Energy Conversion and Management, 35(4), 269–279.

Badley, M.E. *et al.* (1988) 'The structural evolution of the northern Viking Graben and its bearing upon extensional modes of basin formation', *Journal of the Geological Society*, 145(3), pp. 455–472. Available at: https://doi.org/10.1144/gsjgs.145.3.0455.

Bauck, M.S., Faleide, J.I. and Fossen, H. (2021) 'The Måløy Slope: Source to sink fingerprints on the northernmost North Sea rift margin'.

Bell, R.E. *et al.* (2014) 'Strain migration during multiphase extension: Observations from the northern North Sea', *Tectonics*, 33(10), pp. 1936–1963. Available at: https://doi.org/10.1002/2014TC003551.

Bhattacharya, A.R. (2022) *Structural Geology*. Cham: Springer International Publishing (Springer Textbooks in Earth Sciences, Geography and Environment). Available at: https://doi.org/10.1007/978-3-030-80795-5.

Bjorlykke, K. and Nedkvitne, T. (1992) 'Diagenetic processes in the Brent Group (Middle Jurassic) reservoirs of the North Sea: an overview', p. 25.

Bullimore, S.A. and Helland-Hansen, W. (2009) 'Trajectory analysis of the lower Brent Group (Jurassic), Northern North Sea: contrasting depositional patterns during the advance of a major deltaic system', *Basin Research*, 21(5), pp. 559–572. Available at: https://doi.org/10.1111/j.1365-2117.2009.00410.x.

Catuneanu, O. (2002) 'Sequence stratigraphy of clastic systems: concepts, merits, and pitfalls', *Journal of African Earth Sciences*, 35(1), pp. 1–43. Available at: https://doi.org/10.1016/S0899-5362(02)00004-0.

Catuneanu, O. (2020) 'Sequence stratigraphy', in *Regional Geology and Tectonics: Principles of Geologic Analysis*. Elsevier, pp. 605–686. Available at: https://doi.org/10.1016/B978-0-444-64134-2.00021-3.

Chamock, M.A. *et al.* (2001) 'Sequence Stratigraphy of the Lower Jurassic Dunlin Group, Northern North Sea', in *Norwegian Petroleum Society Special Publications*. Elsevier, pp. 145–174. Available at: https://doi.org/10.1016/S0928-8937(01)80012-6.

Christiansson, P., Faleide, J.I. and Berge, A. (2000) 'Crustal structure in the northern North Sea: An integrated geophysical study', *Geological Society, London, Special Publications*, 167, pp. 15–40. Available at: https://doi.org/10.1144/GSL.SP.2000.167.01.02.

Christie-Blick, N. and Driscoll, N.W. (1995) 'Sequence Stratigraphy', *Annual Review of Earth and Planetary Sciences*, 23(1), pp. 451–478. Available at: https://doi.org/10.1146/annurev.ea.23.050195.002315.

CO2CRC 2008. Storage Capacity Estimation, Site Selection and Characterization for CO2 Storage Projects. CO2CRC Report RPT08–1001. Cooperative Research Centre for Greenhouse Gas Technology, Canberra, Australia.

Corfu, F., Andersen, T.B. and Gasser, D. (2014) 'The Scandinavian Caledonides: main features, conceptual advances and critical questions', *Geological Society, London, Special Publications,* 390(1), pp. 9–43. Available at: https://doi.org/10.1144/SP390.25.

Crameri, F. (2018). Scientific colour maps. Zenodo. http://doi.org/10.5281/zenodo.1243862

Davatzes, N.C. and Aydin, A. (no date) 'Distribution and Nature of Fault Architecture in a Layered Sandstone and Shale Sequence: An Example from the Moab Fault, Utah'.

Davies, R.J., Turner, J.D. and Underhill, J.R. (2001) 'Sequential dip-slip fault movement during rifting: a new model for the evolution of the Jurassic trilete North Sea rift system', *Petroleum Geoscience,* 7(4), pp. 371–388. Available at: https://doi.org/10.1144/petgeo.7.4.371.

Deegan, C. and Scull, B. (1977) ´A standard lithostratigraphic nomenclature for the central and the northern north sea´, Norwegian Petroleum Directorate Bulletin 1. Available: https://www.npd.no/globalassets/1-npd/publikasjoner/npd-bulletins/npd-bulletin-1-1977.pdf [Accessed 01.12.2022].

Doh, C.A. (1959) 'M. P. TIXIER R. P. ALGER', 216.

Dreyer, T. *et al.* (2005) 'From spit system to tide-dominated delta: integrated reservoir model of the Upper Jurassic Sognefjord Formation on the Troll West Field', *Geological Society, London, Petroleum Geology Conference Series*, 6(1), pp. 423–448. Available at: https://doi.org/10.1144/0060423.

Duffy, O.B. *et al.* (2015) 'Fault growth and interactions in a multiphase rift fault network: Horda Platform, Norwegian North Sea', *Journal of Structural Geology*, 80, pp. 99–119. Available at: https://doi.org/10.1016/j.jsg.2015.08.015.

Durmaz, T. (2018) 'The economics of CCS: Why have CCS technologies not had an international breakthrough?', *Renewable and Sustainable Energy Reviews*, 95, pp. 328–340. doi:10.1016/j.rser.2018.07.007.

Eaton, D.W., Milkereit, B. and Salisbury, M.H. (2003) *Hardrock Seismic Exploration*. SEG Books.

Eiken, O. *et al.* (2011) 'Lessons learned from 14 years of CCS operations: Sleipner, In Salah and Snøhvit', *Energy Procedia*, 4, pp. 5541–5548. doi:10.1016/j.egypro.2011.02.541.

Færseth, R.B. (1996) 'Interaction of Permo-Triassic and Jurassic extensional fault-blocks during the development of the northern North Sea', *Journal of the Geological Society*, 153(6), pp. 931–944. Available at: https://doi.org/10.1144/gsjgs.153.6.0931.

Færseth, R.B., Johnsen, E. and Sperrevik, S. (2007) 'Methodology for risking fault seal capacity: Implications of fault zone architecture', *AAPG Bulletin*, 91(9), pp. 1231–1246. doi:10.1306/03080706051.

Faleide, J.I., Bjørlykke, K. and Gabrielsen, R.H. (2015) 'Geology of the Norwegian Continental Shelf', in K. Bjørlykke (ed.) *Petroleum Geoscience: From Sedimentary Environments to Rock Physics*. Berlin, Heidelberg: Springer, pp. 603–637. Available at: https://doi.org/10.1007/978-3-642-34132-8_25.

Fawad, M., Rahman, M.J. and Mondol, N.H. (2021) 'Seismic reservoir characterization of potential CO2 storage reservoir sandstones in Smeaheia area, Northern North Sea', *Journal of Petroleum Science and Engineering*, 205, p. 108812. Available at: https://doi.org/10.1016/j.petrol.2021.108812.

Fazlikhani, H. *et al.* (2017) 'Basement structure and its influence on the structural configuration of the northern North Sea rift: Basement Shear Zones in the Northern North Sea', *Tectonics*, 36(6), pp. 1151–1177. Available at: https://doi.org/10.1002/2017TC004514.

Fossen, H. (1992) 'The role of extensional tectonics in the Caledonides of south Norway', *Journal of Structural Geology*, 14(8–9), pp. 1033–1046. Available at: https://doi.org/10.1016/0191-8141(92)90034-T.

Fossen, H. (2016) Structural geology. 2 ed. Cambridge: Cambridge University Press.

Gabrielsen, R.H. *et al.* (2001) 'The Cretaceous post-rift basin configuration of the northern North Sea', *Petroleum Geoscience*, 7(2), pp. 137–154. Available at: https://doi.org/10.1144/petgeo.7.2.137.

Gough, C. and Shackley, S. (2006) 'Towards a Multi-Criteria Methodology for Assessment of Geological Carbon Storage Options', *Climatic Change*, 74(1–3), pp. 141–174. doi:10.1007/s10584-006-0425-4.

Grunau, H.R. (1987) 'A Worldwide Look at the Cap-Rock Problem', *Journal of Petroleum Geology*, 10(3), pp. 245–265. doi:10.1111/j.1747-5457.1987.tb00945.x.

Gubbi, J. (2022) 'Structural Analysis of the Øygarden Fault Complex, on the northern North Sea Horda Platform'.

Gunter, W.D., E.H. Perkins and T.J. McCann, 1993: Aquifer disposal of CO2 -rich gases: reaction design for added capacity. Energy Conversion and Management, 34, 941–948.

Helland-Hansen, W. *et al.* (1992) 'Advance and retreat of the Brent delta: recent contributions to the depositional model', *Geological Society, London, Special Publications*, 61(1), pp. 109–127. Available at: https://doi.org/10.1144/GSL.SP.1992.061.01.07.

Holland, K. and Elmore, P. (2008) 'A review of heterogeneous sediments in coastal environments', *Earth-Science Reviews*, 89, pp. 116–134. Available at: https://doi.org/10.1016/j.earscirev.2008.03.003.

Høimyr, Ø., Kleppe, A. and Nystuen, J.P. (1993) 'Effects of heterogeneities in a braided stream channel sandbody on the simulation of oil recovery: a case study from the Lower Jurassic Statfjord Formation, Snorre Field, North Sea', *Geological Society, London, Special Publications*, 69(1), pp. 105–134. Available at: https://doi.org/10.1144/GSL.SP.1993.069.01.06.

IEA (2020), Key World Energy Statistics 2020, IEA, Paris https://www.iea.org/reports/key-world-energy-statistics-2020 (Accessed: 7 March 2022)

IPCC (2021), Climate Change 2021 The Physical Science Basis, Available at: https://www.ipcc.ch/report/ar6/wg1/downloads/report/IPCC_AR6_WGI_Full_Report_smaller.pdf (Accessed: 7 March 2022).

Isaksen, D., Tonstad, K. (1989) ´A revised Cretaceous and Tertiary lithostratigraphic nomenclature for the Norwegian North Sea´, Norwegian Petroleum Directorate Bulletin No 5, Available: https://www.npd.no/globalassets/1-npd/publikasjoner/npd-bulletins/npd-bulletin-5-1989.pdf [Accessed 30.11.2022].

Japsen, P. and Chalmers, J.A. (2000) 'Neogene uplift and tectonics around the North Atlantic: overview', *Global and Planetary Change*, 24(3–4), pp. 165–173. Available at: https://doi.org/10.1016/S0921-8181(00)00006-0.

Jr, J.C.S., Swift, G. and Hartline, R. (1962) 'A Review of Current Techniques in Gamma-Ray And Neutron Log Interpretation', *JOURNAL OF PETROLEUM TECHNOLOGY* [Preprint].

Kasa, S. (2000) 'Policy networks as barriers to green tax reform: The case of CO_2 -taxes in Norway', *Environmental Politics*, 9(4), pp. 104–122. doi:10.1080/09644010008414553.

Kyrkjebø, R., Gabrielsen, R.H. and Faleide, J.I. (2004) 'Unconformities related to the Jurassic–Cretaceous syn-rift–post-rift transition of the northern North Sea', *Journal of the Geological Society*, 161(1), pp. 1–17. Available at: https://doi.org/10.1144/0016-764903-051.

Langskip (2021) Langskip. Available at: https://langskip.regjeringen.no/langskip/artikkel/ (Accessed: 21 March 2022)

Lauritsen, H. *et al.* (2018) 'Assessing Potential Influence Of Nearby Hydrocarbon Production On CO2 Storage At Smeaheia', in. *Fifth CO2 Geological Storage Workshop*, Utrecht, Netherlands. doi:10.3997/2214-4609.201802970.

Løseth, H. *et al.* (2003) 'Gas and fluid injection triggering shallow mud mobilization in the Hordaland Group, North Sea', *Geological Society, London, Special Publications*, 216(1), pp. 139–157. Available at: https://doi.org/10.1144/GSL.SP.2003.216.01.10.

Marchetti, C. (1977) 'On geoengineering and the CO2 problem', *Climatic Change*, 1(1), pp. 59–68. doi:10.1007/BF00162777.

Milnes, A.G. *et al.* (1997) 'Contraction, extension and timing in the South Norwegian Caledonides: the Sognefjord transect', *Geological Society, London, Special Publications*, 121(1), pp. 123–148. Available at: https://doi.org/10.1144/GSL.SP.1997.121.01.06.

Mitchener, B.C. *et al.* (1992) 'Brent Group: sequence stratigraphy and regional implications', *Geological Society, London, Special Publications*, 61(1), pp. 45–80. Available at: https://doi.org/10.1144/GSL.SP.1992.061.01.05.

Mitchum, R.M. (1977) 'Seismic Stratigraphy and Global Changes of Sea Level, Part 11Glossary of Terms used in Seismic Stratigraphy[1]', in Payton, C. E., *Seismic Stratigraphy — Applications to Hydrocarbon Exploration*. American Association of Petroleum Geologists. Available at: https://doi.org/10.1306/M26490C13.

Morton, A. and Hurst, A. (1995) 'Correlation of sandstones using heavy minerals: an example from the Statfjord Formation of the Snorre Field, northern North Sea', *Geological Society, London, Special Publications*, 89(1), pp. 3–22. Available at: https://doi.org/10.1144/GSL.SP.1995.089.01.02.

Northern Lights (2021) How to store CO_2 with Northern Lights. Available at: https://northernlightsccs.com/how-to-store-co2-with-northern-lights/ (Accessed: 21 March 2022).

NPD Factpages 2002 Norwegian Petroleum Directorate Factpages [Online]. (Available at: https://factpages.npd.no/en/wellbore/PageView/Exploration/All/2918 (Accessed: 02 May 2023)

Odinsen, T. *et al.* (2000) 'Permo-Triassic and Jurassic extension in the northern North Sea: results from tectonostratigraphic forward modelling', *Geological Society, London, Special Publications*, 167(1), pp. 83–103. Available at: https://doi.org/10.1144/GSL.SP.2000.167.01.05.

Osmond, J.L. *et al.* (2022) 'Structural traps and seals for expanding CO2 storage in the northern Horda platform, North Sea', *AAPG Bulletin*, 106(9), pp. 1711–1752. Available at: https://doi.org/10.1306/03222221110.

Paris Agreement (2020), Norway's long-term low-emission strategy for 2050 Available at: https://unfccc.int/sites/default/files/resource/LTS1_Norway_Oct2020.pdf (Accessed: 7 March 2022).

P. A. Ziegler (2) (1975) 'Geologic Evolution of North Sea and Its Tectonic Framework', *AAPG Bulletin*, 59. Available at: https://doi.org/10.1306/83D91F2E-16C7-11D7-8645000102C1865D.

Platform, P. E. P. S. (2015) *Recommended Seismic Volume Attributes*. Available at: https://www.software.slb.com/-/media/software-media-items/software/documents/external/product-sheets/petrel_recommended_seismic_volume_attributes_2015_poster.pdf (Access: 16 February 2023).

Pritchard, D. W. (1967). "What is an estuary: physical viewpoint". In Lauf, G. H. (ed.). Estuaries. A.A.A.S. Publ. Vol. 83. Washington, DC. pp. 3–5. hdl:1969.3/24383

Rahman, M.J. *et al.* (2022) 'Top seal assessment of Drake Formation shales for CO2 storage in the Horda Platform area, offshore Norway', *International Journal of Greenhouse Gas Control*, 119, p. 103700. Available at: https://doi.org/10.1016/j.ijggc.2022.103700.

Richards, P.C. (1992) 'An introduction to the Brent Group: a literature review', *Geological Society, London, Special Publications*, 61(1), pp. 15–26. Available at: https://doi.org/10.1144/GSL.SP.1992.061.01.03.

Roberts, A.M. *et al.* (1993) 'Mesozoic extension in the North Sea: constraints from flexural backstripping, forward modelling and fault populations', *Geological Society, London, Petroleum Geology Conference Series*, 4(1), pp. 1123–1136. Available at: https://doi.org/10.1144/0041123.

Sandal, L. (2020). Geoviden. Available at: https://issuu.com/geoviden/docs/geoviden_1_2020_book (Access: 28 March 2022).

Schiøler, P., Andsbjerg, J., Clausen, O.R., Dam, G., Dybkjær, K., Hamberg, L., Heilmann-Clausen, C., Johannessen, E.P., Kristensen, L.E., Prince, I., Rasmussen, J.A., 2007. Lithostratigraphy: Rogaland Group, formations: Våle and Lista. Geological Survey of Denmark and Greenland Bulletin 12, 24–46.. doi:10.34194/geusb.v12.4934

Seranne, M. and Seguret, M. (1987) 'The Devonian basins of western Norway: tectonics and kinematics of an extending crust', *Geological Society, London, Special Publications*, 28(1), pp. 537–548. Available at: https://doi.org/10.1144/GSL.SP.1987.028.01.35.

Sheriff, R.E. (1975) 'Factors Affecting Seismic Amplitudes*', *Geophysical Prospecting*, 23(1), pp. 125–138. Available at: https://doi.org/10.1111/j.1365-2478.1975.tb00685.x.

Sheriff, R.E. (1980) *Seismic Stratigraphy*. Dordrecht: Springer Netherlands. Available at: https://doi.org/10.1007/978-94-011-6395-8.

SSB (2021) Emission factors used in the estimations of emissions from combustion. Available at: https://www.ssb.no/natur-og-miljo/forurensning-og-klima/statistikk/utslipp-til-luft/_/attachment/download/3febd5e6-66e7-4b7a-8b99-0ece784065ab:afd96d235ef7d964c3734f4709f8545110acaecc/emission-factors.pdf (Accessed: 5 April 2022)

Sundal, A. *et al.* (2016) 'The Lower Jurassic Johansen Formation, northern North Sea – Depositional model and reservoir characterization for CO2 storage', *Marine and Petroleum Geology*, 77, pp. 1376–1401. Available at: https://doi.org/10.1016/j.marpetgeo.2016.01.021.

Tangen, G. *et al.* (2021) 'IMPACT OF INNOVATIONS FROM THE NORWEGIAN CCS RESEARCH CENTRE (NCCS)', p. 6.

Ter Voorde, M. *et al.* (2000) 'Repeated lithosphere extension in the northern Viking Graben: a coupled or a decoupled rheology?', *Geological Society, London, Special Publications*, 167(1), pp. 59–81. Available at: https://doi.org/10.1144/GSL.SP.2000.167.01.04.

Tihomir Marjanac and Ronald J. Steel (1997) 'Dunlin Group Sequence Stratigraphy in the Northern North Sea: A Model for Cook Sandstone Deposition', *AAPG Bulletin*, 81 (1997). Available at: https://doi.org/10.1306/522B4307-1727-11D7-8645000102C1865D.

Urban S. Allan (2) (1989) 'Model for Hydrocarbon Migration and Entrapment Within Faulted Structures', *AAPG Bulletin*, 73. Available at: https://doi.org/10.1306/44B4A271-170A-11D7-8645000102C1865D.

Vail, P.R. and Mitchum, R.M. (1977) 'Seismic Stratigraphy and Global Changes of Sea Level, Part 1Overview[1]', in Payton, C. E., *Seismic Stratigraphy — Applications to Hydrocarbon*

Exploration. American Association of Petroleum Geologists. Available at: https://doi.org/10.1306/M26490C3.

Watts, N. L. (1987) 'Theoretical aspects of cap-rock and fault seals for single- and two-phase hydrocarbon columns'Catuneanu, O. (2020) 'Sequence stratigraphy', in *Regional Geology and Tectonics: Principles of Geologic Analysis*. Elsevier, pp. 605–686. Available at: https://doi.org/10.1016/B978-0-444-64134-2.00021-3.

Weissel, J.K. and Karner, G.D. (no date) 'Flexural Uplift of Riff Flanks Due to Mechanical Unloading of the Lithosphere During Extension'.

Whipp, P.S. *et al.* (2014) 'Normal fault array evolution above a reactivated rift fabric; a subsurface example from the northern Horda Platform, Norwegian North Sea', *Basin Research*, 26(4), pp. 523–549. Available at: https://doi.org/10.1111/bre.12050.

Wilgus, C.K. *et al.* (eds) (1988) *Sea-Level Changes: An Integrated Approach*. SEPM (Society for Sedimentary Geology). Available at: https://doi.org/10.2110/pec.88.42.

Wu, L. *et al.* (2021) 'Significance of fault seal in assessing CO_2 storage capacity and containment risks – an example from the Horda Platform, northern North Sea', *Petroleum Geoscience*, 27(3), pp. petgeo2020-102. Available at: https://doi.org/10.1144/petgeo2020-102.

Ziegler, P.A. (1992) 'Geodynamics of rifting and implications for hydrocarbon habitat'.